Charm Mixing ($D^0 \to K\pi$) With 9 fb^{-1}

Paul Karchin, Mark Mattson
Wayne State University, Detroit, MI
Satyajit Behari
Fermilab, Batavia, IL
Paolo Maestro
University of Siena and INFN-Pisa, Italy

CDF/ANAL/BOTTOM/CDFR/10914
Version 2.0

April 1, 2013

Abstract

We present a measurement of $R(t)$, the time-dependent ratio of the branching fraction for the rare decay $D^0 \to K^+\pi^-$ to that for the Cabibbo-favored decay $D^0 \to K^-\pi^+$. The decay $D^{*+} \to D^0\pi^+$ is used to identify whether the D^0 decay is rare or Cabibbo-favored. The rare decay is due to the combination of a doubly Cabibbo-suppressed diagram and a possible contribution from $D^0 - \bar{D}^0$ mixing. If R changes with decay time, this is evidence for charm mixing.

The data is recorded using the Two Track Trigger with 9.6 fb^{-1} marked good for B physics using the silicon tracker and COT. There are reconstructed signals of 7.6 million Cabibbo-favored D^0 decays and 33 thousand rare decays. We present a method to extract the branching ratio in bins of decay time and fit it to obtain the mixing parameters R_D, y', and x'^2. The fit takes into account promptly produced D^*, and non-prompt D^* resulting from beauty particle decay.

The best fit for the mixing parameters, assuming no CP violation, is $R_d = 3.69 \pm 0.33 (\times 10^{-3})$, $y' = 2.27 \pm 3.90 (\times 10^{-3})$, and $x'^2 = 0.13 \pm 0.16 (\times 10^{-3})$. The no-mixing hypothesis ($y' = x'^2 = 0$) is excluded with a significance equivalent to 6.1 Gaussian standard deviations.

Contents

List of Figures

List of Tables

1 Introduction

This note describes the analysis method to measure the mixing parameters for neutral charm meson oscillation, using all available data from Run II (up to period 38). Earlier stages of the analysis are described in the following notes:

- Note 7116 [1], the initial time-independent measurement with data set 0d (0.35 fb^{-1}). The analysis was blessed and resulted in a publication [2].
- Note 8879 [3], the initial time-dependent measurement with data sets 0d/0h/0i (1.5 fb^{-1}). The analysis was blessed and resulted in a publication [4].
- Note 9806 [5], an update of the time-dependent measurement using data up to period 21.

This document describes the method and reviews information from the previous studies. The blinded analysis method was blessed for the 1.5 fb^{-1} result.

1.1 Brief Theoretical Overview

Since the discovery of the charm quark in 1974, physicists have been searching for the mixing (or oscillation) of neutral charm mesons between particle and anti-particle states. The analogue process was discovered for kaons in 1962 and for B_d mesons in 1987. Charm mixing is so small that the first evidence was not seen until almost twenty years later, in 2006.

In the standard model, the decay $D^0 \to K^+\pi^-$ proceeds through a doubly Cabibbo-suppressed (DCS) tree diagram (see Fig. 1) and possibly through a "mixing" process in which the D^0 changes into a $\overline{D}^0$. (In this section, discussion of a decay reaction implicitly includes the charge conjugate process, unless otherwise noted.) The DCS decay rate depends on CKM factors as well as the magnitude of SU(3) flavor symmetry violation. Mixing may occur through two distinct types of second-order weak processes. In the first, shown in Fig. 2, the D^0 decays into a virtual ("long-range") intermediate state such as $\pi^+\pi^-$, which subsequently decays into a $\overline{D}^0$. The second type, shown in Fig. 3, is a short range process, with either a "box" or "penguin" topology. Short range mixing is negligible in the SM. However, exotic weakly interacting particles could enhance the short range mixing and provide a signature of new physics. Long-range processes can be much larger than short-range perturbative contributions, but are model-dependent. An observation of mixing can be due to a combination of long-range standard-model processes and exotic ones.

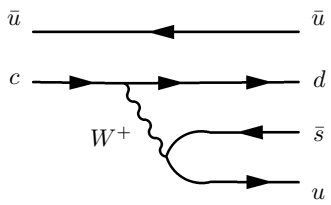

Figure 1: Feynman diagram for doubly- Cabibbo- suppressed decay.

1.2 Method Using $K^+\pi^-$ and $K^-\pi^+$ Decays of the D^0

The experimental method used here exploits the decay chain $D^{*+} \to D^0\pi^+$. The pion from the D^{*+} decay is called the *tagging* pion because its charge identifies the initial state of the neutral D meson

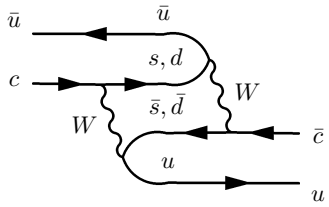

Figure 2: D^0 mixing through a virtual "long-range" intermediate state.

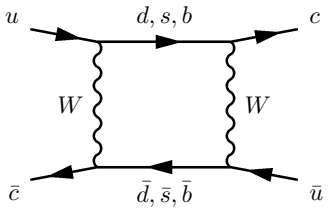

Figure 3: Highly suppressed standard model short-range D^0 mixing via a box diagram.

as particle (D^0) or anti-particle ($\overline{D}^0$). The subsequent decay $D^0 \to K^-\pi^+$ is Cabibbo-favored (CF) and experimentally well established. We can also have a D^0 decay into $K^+\pi^-$, either by doubly Cabibbo-suppressed decay (DCS), or by mixing. For mixing, the D^0 oscillates to $\overline{D^0}$, and the $\overline{D^0}$ has a CF decay.

For this decay mode, the literature refers to "right-sign" (RS) and "wrong-sign" (WS) decays. For CF decays, the pions from the D^* and D^0 decays have the same charge, and are called right sign. For DCS and mixing decays, the pions have opposite charges, and are grouped as wrong sign.

The D^* tagging pion is also called the *slow pion* because its laboratory momentum is much less than that of the D^0 or $\overline{D}^0$. This kinematic property is a result of the small Q-value (145.4 MeV) of the D^{*+} decay. In the subsequent discussion, the term *right sign* will denote the Cabibbo favored decay, $D^0 \to K^-\pi^+$.

1.3 D^0 Decay Time Dependence

Based on the current values for the charm mixing parameters, determined by the HFAG group from the available data for various D^0 decay modes, we expect the neutral charm meson to decay well before the time of one oscillation, in sharp contrast to B and K mixing. We can still look for variations in the time-dependence. The ratio $R(t)$ of wrong-sign to right-sign decay rates can be expressed [6] as a simple quadratic function of proper time t under the assumption of CP conservation and small values for the parameters x and y.The parameter R_D is the time-integrated rate of the direct DCS decay relative to the CF decay. The parameter x is defined in terms of the mass difference ΔM between the heavy and light mass eigenstates and the parameter y involves the mass width difference $\Delta\Gamma$ between these eigenstates according to,

$$x = \Delta M/\Gamma \quad \text{and} \quad y = \Delta\Gamma/2\Gamma$$

where Γ is the average mass width of the mass eigenstates. Under the assumptions stated above,

$$R(t) = R_D + \sqrt{R_D}y't + \frac{x'^2 + y'^2}{4}t^2. \tag{1}$$

The parameters x' and y' are linear combinations of x and y according to the relations,

$$x' = x\cos\delta + y\sin\delta \quad \text{and} \quad y' = -x\sin\delta + y\cos\delta$$

where δ is a strong interaction phase. While we can't measure the charm mixing parameters directly, we can get information about the amplitude ($x'^2 + y'^2 = x^2 + y^2$). This can be used to exclude the no-mixing hypothesis ($x = y = 0$).

1.4 Experimental Status

The initial CDF analysis resulted in a measurement [2] of R_B, the ratio of branching fractions of wrong-sign and right-sign decays,

$$R_{\mathcal{B}} = \mathcal{B}(D^0 \to K^+\pi^-)/\mathcal{B}(D^0 \to K^-\pi^+) \tag{2}$$

This ratio is given by the ratio of the time-integrals of the corresponding decay rates, yielding,

$$R_{\mathcal{B}} = R_D + \sqrt{R_D}y' + \frac{x'^2 + y'^2}{2}. \tag{3}$$

Thus $R_{\mathcal{B}}$ was sensitive to the three physics parameters R_D, x' and y', but does not provide a separate measure of them. Previous time-dependent measurements have been reported for R_D and had set limits on x'^2 and y'. At the time, experimental results were only precise enough to set upper limits.

At the Moriond Conference on March 13, 2007, the Belle [7] and BaBar [8] collaborations reported evidence for $D^0 - \overline{D}^0$ mixing, using different techniques. The results were published [9, 10].

BaBar saw a direct mixing signal using the same decay chain as studied here. So far, for this decay chain, Belle has reported only limits for x'^2 and y'. Thus, the BaBar evidence remained unconfirmed until the CDF publication with the time-dependent result [4].

It is also worth noting that the evidence for D^0 - $\bar{D}^0$ mixing presented by Belle is based on two methods, both different than the one discussed here for CDF and BaBar. One of the Belle methods is a comparison of the decay time distributions for D^0 to CP-eigenstates K^+K^- and $\pi^+\pi^-$ with the decay time distribution for D^0 to the CP-mixed state $K^-\pi^+$. They measure a non-zero value of y and hence indirect evidence of mixing.

The other method used by Belle is a time-dependent measurement of the Dalitz decay $D^0 \to K^0_s\pi^+\pi^-$ [11]. They report a preliminary non-zero value for x and a value for y consistent with zero. The non-zero value for x constitutes direct evidence for mixing. BaBar confirmed Belle's results [12] shortly after CDF provided the first confirmation of either experiments results.

Based on measurements up to 2008, $D-\overline{D}$ mixing was well-established by combining results from all charm meson decays including earlier results by CLEO [13] and FOCUS [14]. A fit by the HFAG group [15] excluded the no-mixing hypothesis at the 10σ level even though no single result had reached the level of observation (5σ). The situation changed in late 2012 when the LHCb collaboration reported a measurement of $D^0 - \overline{D}^0$ mixing in the $K^+\pi^-$ channel that excluded the no-mixing hypothesis with a significance corresponding to 9.1σ. The result was published in early 2013 [16].

The recent experimental measurements of $D^0 - \overline{D}^0$ mixing in the $K^+\pi^-$ channel are summarized in Table 1.

1.5 General Features of Analysis Method

An advantagious feature of this analysis is that both RS and WS D^0 decays originate from a D^* and have a $K\pi$ final state. Thus, the WS and RS decay chains involve particles of identical type. Events with WS and RS decays are recorded with the same trigger.

The CF RS signal is large and virtually background-free, as is presented later in this note. This allows the determination of many properties of the WS events, which are much fewer in number.

Experiment	R_D (10^{-3})	y' $(10^{-}3)$	x'^2 (10^{-3})	Mixing significance
Belle (2007)	3.64 ± 0.17	$0.6 \pm 4.0 \pm 3.9$	$0.18 \pm 0.21 \pm 0.23$	2.0
BaBar (2007)	3.03 ± 0.19	9.7 ± 5.4	-0.22 ± 0.37	3.9
CDF (2007)	3.04 ± 0.55	8.5 ± 7.6	-0.12 ± 0.35	3.8
LHCb (2013)	3.52 ± 0.15	7.2 ± 2.4	-0.09 ± 0.13	9.1

Table 1: Recent measurements of $D^0 - \overline{D}^0$ mixing in the $K^+\pi^-$ channel.

These properties include the signal shapes in M and ΔM, and the shape of the impact parameter distribution of the D^0s originating from prompt production, and non-promptly, from decay of beauty particles. The determination of these shapes is described in detail in this note.

The D^*s and their decay products for both WS and RS decays have identical kinematic (4-momentum) distributions. Only their decay time distributions are different. Thus, the detector acceptance and efficiency for WS and RS decays are identical.

Since in this analysis we assume that there is no CP-violation in mixing, the charge-conjugate decays are included in both WS and RS samples. This greatly reduces the sensitivity of the mixing analysis to possible differences between D^{*+} and D^{*-} production. The systematic uncertainty due to differences in the detector efficiencies for D^{*+} and D^{*-} decay chains is found to be negligible, as discussed in this note.

The mixing parameters are determined from the time-dependence of the ratio of WS to RS decays. Detector acceptance and efficiency cancel in the ratio, thus removing sensitivity to their uncertainties.

The analysis follows a primarily data-driven approach. Important quantities affecting the mixing analysis, such as shapes of mass and impact parameter distributions, are determined from the RS signal. The full detector simulation has only one critical use: to determine the decay time distribution of D^0s originating from beauty particle decays. Other uses of simulation provided checks and validation of the analysis method. A full detector simulation (see http://www-cdf.fnal.gov/ dicanto/internal/bmc.html) was used to study the expected mass distribution of partially reconstructed charm decays and to compare it with the observed background. Simulations of mass distributions (commonly refered to as toy simulations) were used to validate the overall analysis method and to assess the effect of alternative shapes for signal and background in mass distributions.

2 Data Sample

This section describes the data being used for this analysis, including selection and cuts applied. Basically, what was done before the first mass plots were made.

For convenience, we want to define a few quantities which will be used later.

- Transverse decay length significance for a particle is defined as

$$L_{xy} = \frac{\vec{r} \cdot \vec{P_T}}{P_T}$$

  where **r** is the distance between the primary and D^0 vertex and P_T is the transverse momentum vector of the D^0. In our analysis we sometimes use transverse decay length significance L_{xy}/σ_{xy}, where σ_{xy} is the uncertainty on L_{xy}.

- Transverse impact parameter for a particle is the distance of closest approach from the primary vertex in the transverse plane and is defined as

$$d_0 = \frac{\hat{z} \cdot (\vec{r} \times \vec{P_T})}{P_T}$$

  where $\hat{z}$ is the unit vector along z-axis.

- Mass difference (ΔM) is the difference in the mass between the D^* candidate and the D^0 and π^* candidates

$$\Delta M = M_{K\pi\pi^*} - M_{K\pi} - M_{\pi^*}$$

  The use of π^* is to distinguish between the soft momentum pion used to form the D^* candidate, and the trigger track pion used to form the D^0 candidate. The mass difference is used instead of the D^* mass because many of the detector uncertainties will cancel when subtracting the D^0 mass, resulting in a narrower mass (difference) peak.

2.1 CDF Detector

The detector components relevant to this analysis are the silicon vertex detector (SVX), Intermediate Silicon Layer (ISL), silicon Layer zero (L00), and the drift chamber (COT) surrounded by a superconducting magnet producing a magnetic field of 1.4 T. These components together provide the physics quantities required to reconstruct wrong sign and right sign events. The other detector parts, like the silicon vertex tracker (SVT), Extremely fast tracker (XFT), and Cherenkov luminosity counter (CLC), were used during online data taking, but do not directly affect how we reconstruct the events.

2.2 Data Sets

Table 2 lists the "hadronic" data sets we are using from the Bstntuple area. For comparison with other CDF analyses, we will quote an integrated luminosity of 9.3 fb^{-1} for this data set, which is the value quoted by the analysis for CPV asymmetries with charmless bottom hadrons [17]. The initial time-independent result used period 0 data only. The previous blessed result (CDF note 8879) used data up to period 10. The previous CDF note (9806) went to period 21.

The two track trigger is described in other CDF notes, but key points will be repeated here. The data were collected by a three-level trigger system, aimed at selecting detached heavy flavor decays with at least two decay tracks. At level 1, COT tracks are reconstructed in the transverse plane by a hardware processor (XFT). Two opposite-charge particles are required, with reconstructed transverse momenta $p_T(1), p_T(2) > 2GeV/c$, the scalar sum $p_T(1) + p_T(2) > 5.5GeV/c$, and an azimuthal

Data set	Periods	Run range	Dates	Name
hadr-80/xbhdid	0	138425-186598	2002.02.09-2004.08.22	x0d
cdfpbnt/xbhdih	1-4	190697-203799	2004.12.16-2005.09.04	x0h
cdfpbnt/xbhdii	5-10	203819-233111	2005.09.05-2007.01.30	x0i
cdfpbnt/xbhdij	11-13	233133-246231	2007.01.30-2007.05.13	x0j
cdfpbnt/xbhdik	14-17	252836-261005	2007.11.04-2008.04.16	x0k
cdfpbnt/xbhdfm	18-28	261119-289197	2008.04.18-2010.02.25	x0m
cdfpbnt/xbhdfp	29-38	289273-312510	2010.02.25-2011.09.30	x0p

Table 2: Bstntuple "hadronic" data sets and corresponding date ranges.

opening-angle $\Delta\varphi < 135°$. At level 2, the silicon vertex trigger (SVT) [18] combines XFT tracks with SVX hits to measure the impact parameter d_0 (distance of closest approach to the beam line) of each track with 45 μm resolution. The requirement of two tracks with $0.1 < d_0 < 1.0$ mm reduces the light-quark background by two orders of magnitude while preserving about half of the signal. A tighter opening-angle requirement, $20° < \Delta\varphi < 135°$, preferentially selects twobody B decays over multibody decays with 97% efficiency and further reduces background. Each track pair is then used to form a heavy flavor candidate, which is required to have an impact parameter $d_0(B) < 140\mu$m and to have travelled a distance $L_{xy} > 200\mu$m in the transverse plane. At level 3, an array of computers confirms the selection with a full event reconstruction.

For the blessing of the 1.5/fb result the B-Group agreed with us that the trigger (and specifically "volunteers") will not affect our WS/RS ratio, except for K+/K- and pi+/pi- detector efficiency (which we include as a systematic error calculation later) and any volunteers that involve the third track (soft pion) passing the trigger. We will later impose a cut on the soft track p_T to remove this possibility. (We don't have the full conversation handy, but do have an e-mail by Kevin Pitts where he mentions, "Provided that the kinematics of the RS and WS decays are identical, I don't immediately see another way in which volunteers can bias your analysis.") This is largely due to our signals including the charge conjugate decay, the identical kinematics of RS and WS D^*, and using the ratio.

2.3 Ntuples

To speed up processing, we are using the BStNtuple files [18]. These are the B-Physics ntuples built from the production StNtuples, with an emphasis on quantities used in heavy flavor physics analyses. The BStNtuple files provide a common track reconstruction and vertexing for all heavy flavor analyses, but we still need to make our own ntuple files with quantities specific to this analysis. The procedures to generate the local tuples are listed on an internal CDF web page (MarkMattson/analysis).

We select the "$B \to \pi\pi$" block. This makes a vertex from the oppositely charged TTT trigger tracks. The events in this block are required to have the decay vertex with $L_{xy}/\sigma_{xy} > 4$, but there is no mass selection. All available D^0s will be in the BStNtuple files, after changing the two tracks to be $K\pi$. For the two tracks that form the B candidate, we try both $K\pi$ and πK particle assignments for the tracks. If the two-track mass is within the range 1.78-1.95 GeV/c^2 for either interpretation, that candidate is accepted as a possible D^0. The "pion" track block is used to get extra pions, which are combined with the D^0 candidate to form a D^* candidate. The mass difference ($\Delta m = m_{K\pi\pi^*} - m_{K\pi} - m_{\pi^*}$) can be anywhere from 0 - 2 GeV, for a D^0 and any random pion in the event. We only retain candidates with $\Delta m < 40$ MeV, which will retain all possible D^* decays, and provide enough sideband events to observe the background distribution. These mass windows are deliberately wide, in case we wanted to make changes after the ntuples were processed. In practice, we only look at (RS or WS) $K\pi$ mass from 1.80 - 1.92 GeV, and ΔM below 30 MeV.

At the time we started this analysis, the BStNtuple had reconstructions for D^0 and D^*, which we could not use as the selections were for RS D^*, which are biased against WS D^*. It was pointed out

that the $B \to \pi\pi$ block would contain all the D^0 that we were looking for, and could be used to make the RS and WS D^*. We use "v80" tuples. The good run list (v31) selection was applied after the ntuples were written to disk.

Table 3 lists the approximate number of RS D^0 found in each data set, using a simple time-integrated $K\pi$ fit. This is not used in the analysis, but was part of the checks that the code was running correctly.

Data set	Luminosity (fb^{-1})	D^0 (millions)
x0d	0.38	1.5
x0h	0.39	1.7
x0i	0.87	3.0
x0j	0.40	1.6
x0k	0.50	1.4
x0m	3.19	5.1
x0p	3.14	2.5

Table 3: Approximate D^0 yield per data set, from the BStNtuples. The luminosity is the online value for "all good". Since this analysis does not use the calorimeter or the muon detectors, this is only to set a scale for the size of the sets.

Fig. 4 shows the p_T and d_0 of the trigger tracks, and L_{xy} of the D^0.

2.4 Signals and Backgrounds

Before describing the additional selection cuts used for this analysis, it is useful to give an overview of the classes of events that will be important for this analysis:

- Prompt D^* (signal) - RS or WS D^* that are produced at the primary vertex. The D^* signal peaks at 5.85 MeV in the mass difference, and 1.8645 GeV for $K\pi$ mass (PDG values).
- "B-decay" D^* (signal) - D^* that are produced at a secondary vertex. We expect these to come from B-decays. These are still potentially good D^*, but will have the wrong decay length (unless the primary vertex is not used). On the order of 10% of the RS D^* are from B decays. These candidates will have a different impact parameter (d_0) distribution compared to prompt D^*.
- D^0 plus random pion - A correctly reconstructed D^0 combined with an unassociated pion to get a fake D^* tag. This will form a D^0 peak in the $K\pi$ fits, but have a broad distribution for the mass difference.
- D^0 misidentification - A real D^0 decay where the kaon and pion assignments are swapped (double particle misidentification). The mass distribution in the $K\pi$ plot is about 10x wider than for correctly reconstructed D^0.
- Single misidentification - A real $D^0 \to KK$ or $\pi\pi$ decay which has one of the tracks misidentified, to form a $K\pi$ candidate. Those candidates will have a $K\pi$ mass that is low for both RS and WS interpretations, or high for both.
- Other charm decays - Other D^0 decay modes that might fall in our $K\pi$ mass window.
- Combinatorial background - Candidates formed from a random selection of tracks, which happens to pass our selection criteria. This is a well understood phenomena in any physics analysis. The mass plots from this background are featureless (beyond statistical fluctuations), and the $K\pi$ distribution can be modeled by a linear or simple polynomial fit.

Figure 5 shows candidates plotted with both RS and WS interpretations. The real RS D^0s, which appear as a broad distribution along the WS axis, dominate the plot. The plot also has

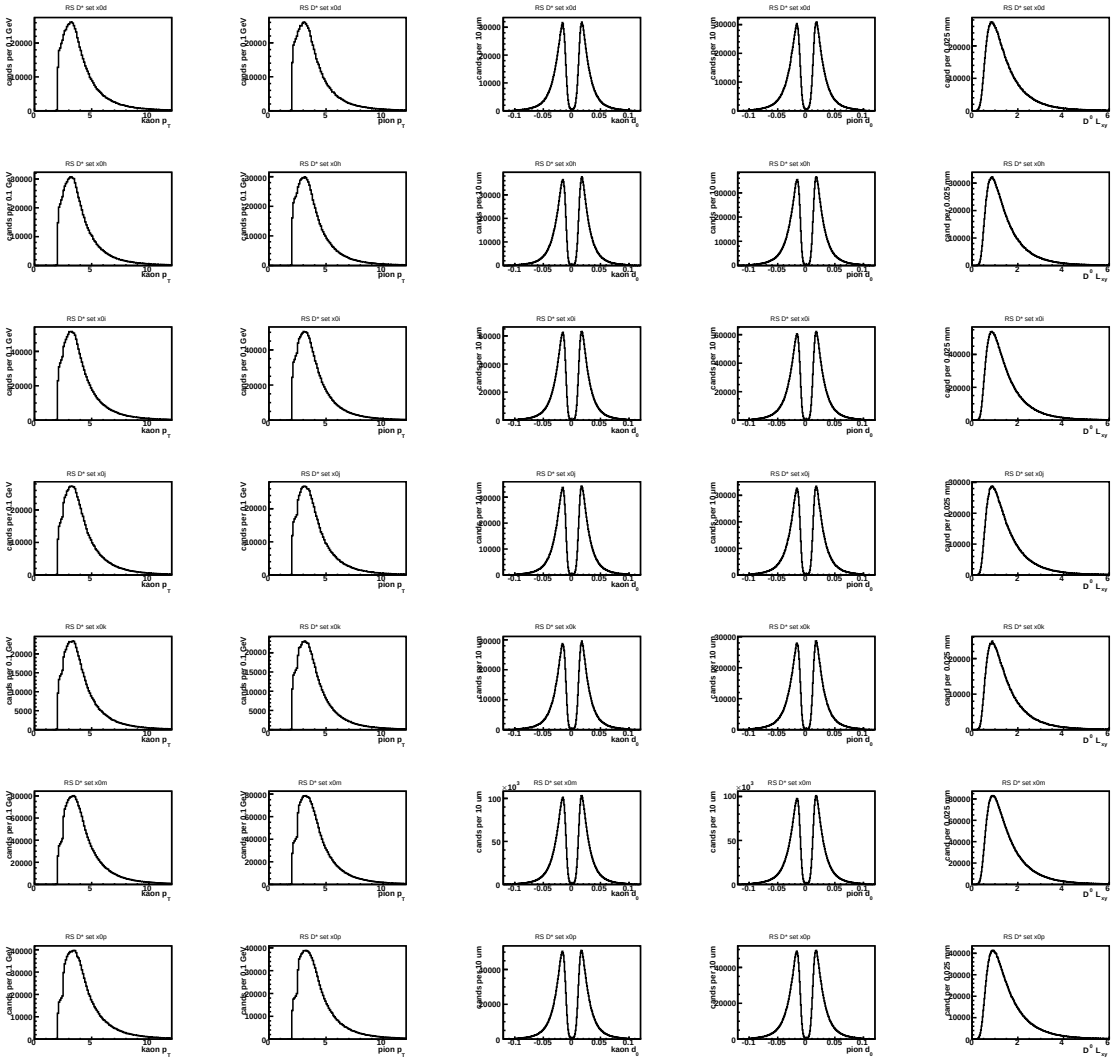

Figure 4: Variables from the BStNtuples
The p_T and d_0 of the trigger tracks, and L_{xy} of the D^0, from the post-processed BStNtuple output. A cut on the (RS) $K\pi$ mass and the mass difference, consistent with being a D*, is used to reduce background. Left to right: kaon p_T, pion p_T, kaon d_0, pion d_0, and L_{xy}. Top to bottom: set x0d, x0h, x0i, x0j, x0k, x0m, x0p. (The PDF figures can be zoomed in, to be read.)

clustering of events in the high mass (upper right) and low mass (lower left) regions. These are due to $D^0 \to KK, \pi\pi$ events. When transforming the data candidates into those mass plots, peaks at the D^0 mass are clearly shown, as seen in figure 6. These candidates are distinct from both the RS and WS $K\pi$ signal. Excluding these events is the primary reason for restricting the $K\pi$ mass range to 1.80-1.92 GeV. An additional complication below 1.80 GeV are charm decays involving π^0, which adds more complications in attempts to fit in that region.

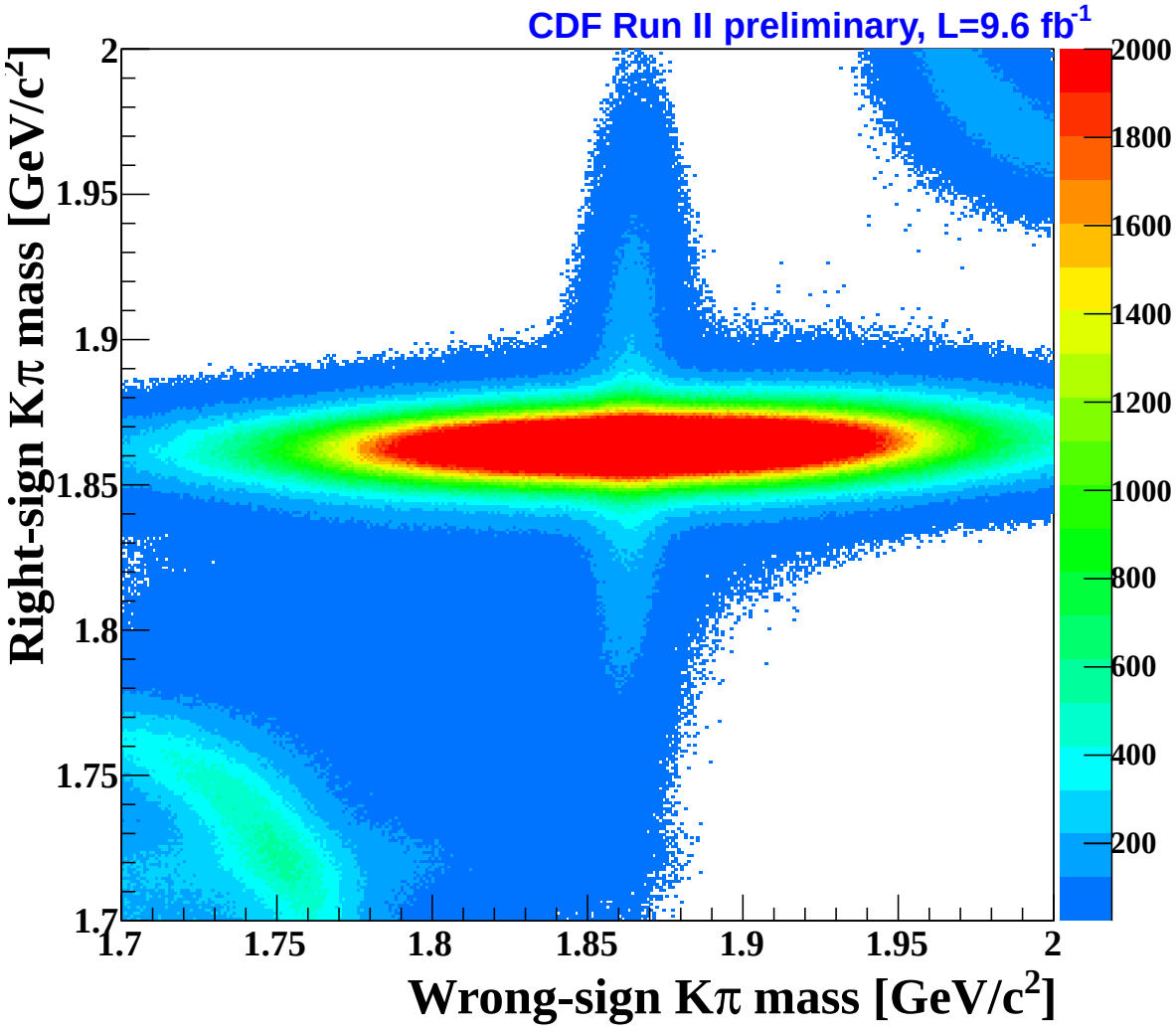

Figure 5: Candidates from the full data set are plotted with both RS and WS interpretations. The PDG D^0 mass of 1.8645 GeV. A cut requiring a good (WS) D* tag is used to reduce background. The extra events (above background) in the lower left corner are consistent with the decay $D^0 \to KK$, while extra events in the upper right corner are consistent with the decay $D^0 \to \pi\pi$.

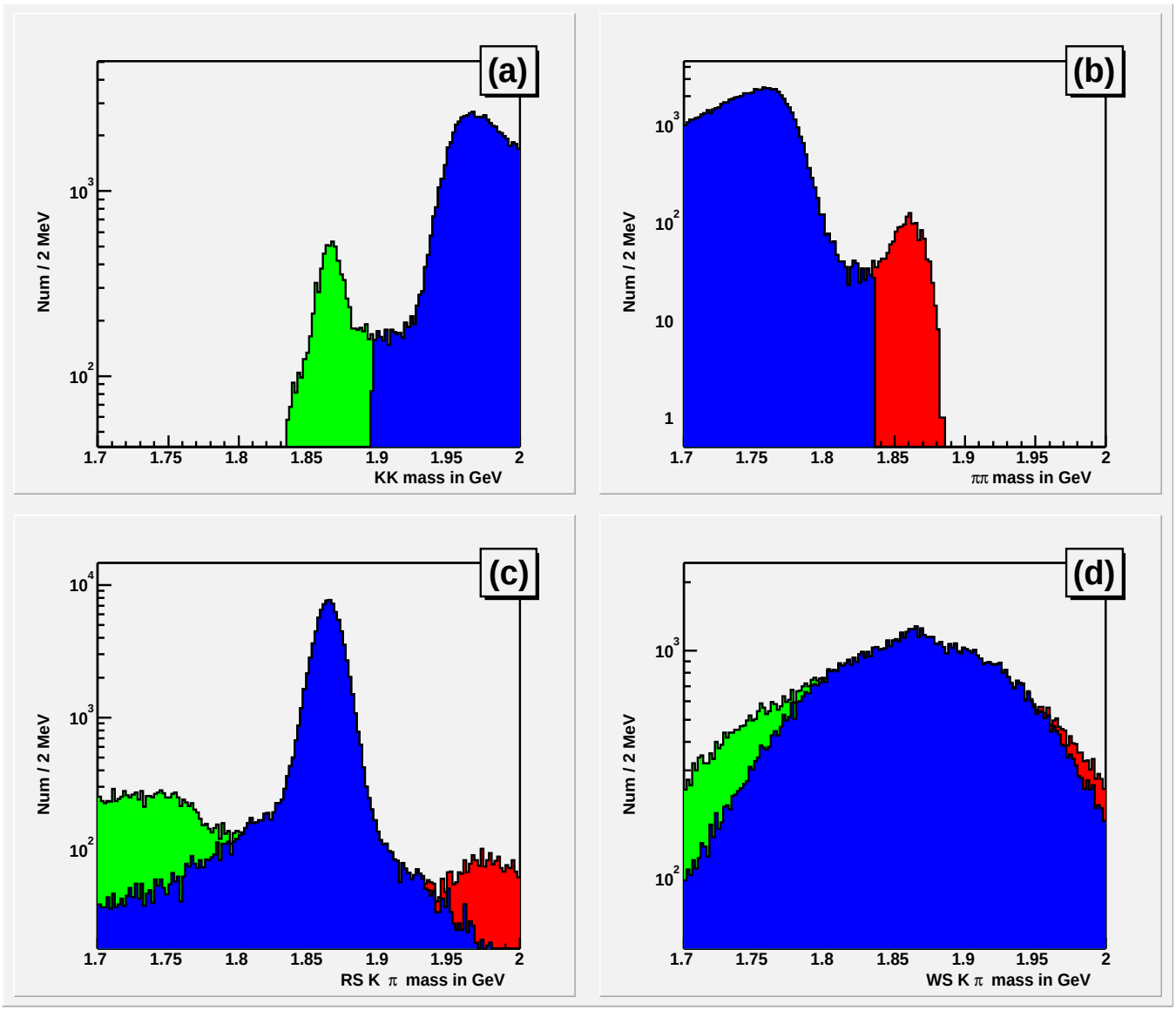

Figure 6: Data events from a 60 pb^{-1} subsample have their invariant mass recalculated, assigning the tracks as KK (a) or $\pi\pi$ (b). Events within 30 MeV of the D^0 mass in (a) are colored green. Events within 30 MeV of the D^0 mass in (b) are colored red. All others are colored blue. Those events are then shown as cumulative distributions for RS $K\pi$ candidates (c) and WS $K\pi$ candidates (d).

2.5 Basic Selection Cuts

We apply some modest selection cuts, to reduce the combinatoric background slightly. Since they affect RS and WS events equally, there is no systematic effect on the ratio. There will be selections to distinguish RS and WS interpretations, but that will be described in the next section. These cuts were optimized from the earliest sample, as described in CDF note 7116.

The last round of cut optimization used our analysis method to get the time-integrated number of D^*, as described in the next chapter. We want to improve the significance of the number of WS D^* to the uncertainty on that number, which will behave like $S/\sqrt{S+B}$. We used the number of RS D^*, and scaled it by $R_D \approx 1/250$ to give the estimate of the number of WS D^*. We use the WS D^* fit uncertainty, but do not look at the value of the number of WS D^*, to keep the procedure "blinded". Since that fit uncertainty is approximately $\sqrt{S+B}$, a script computes B (without revealing the value of S), then substitutes the scaled RS signal S' to get the blinded uncertainty $\sqrt{S'+B}$. The expected WS significance $S'/\sqrt{S'+B}$ is plotted for a range of cut variables and values, and we look for any improvements. The original procedure is described in CDF note 7116, and updated for the time-integrated result.

The cuts have not been modified since that time. Projecting from the local ntuples into histograms for this cut study took hours when we only had the 0d set. Such a study now would probably take days to run the code, independent of the time required for someone to look through several dozen pages of cut variables. A recent effort was made to use a neural network, as described in CDF note 9806, but the improvement was slight enough that we decided to retain these simple cuts.

Fig. 7 shows an example of the cut optimization that was done for the previous ($1.5/fb$) result. Cuts on most of the variables in our local ntuples do not improve the WS D* significance over what comes from the BStNtuples. Fig. 8 shows the one variable that had a clear improvement, the impact parameter of the soft pion. Another variable, Z_0 of the soft pion, does not show a clear maximum value, but the background distribution had long tails, extending well past where most of the signal and background events are distributed. A soft cut for this variable was chosen to exclude these "outliers".

These are the basic selection cuts we use:

- The two tracks that form the D^0 must have dE/dX information.
- The pion coming from the D^* vertex must have (unsigned) d_0 less than 600 microns.
- The reconstructed D^0 candidate must have an (unsigned) impact parameter d_0 less than 500 microns.
- The pion coming from the D^* vertex must have a point of closest approach to the primary vertex less than 1.5 cm along the Z axis.
- The pion coming from the D^* vertex must have p_T less than 2 GeV, and greater than 0.4 GeV. The first cut is to prevent the D^* pion from being a trigger track. The latter cut is to remove soft tracks of dubious quality.

The expected WS significance is best for impact parameter of the D^0 less than about 100 μm. However, that cut also reduces the number of D^* coming from B-decays. We actually need enough of those events, at impact parameter values up to 500 μm, to get a reasonable measurement of how many of those events are in our data sample. Thus, we do not cut on this variable, but rather use the distribution in the analysis as described later.

There was some question about how "spectators" would affect our result. From an e-mail exchange with Kevin Pitts, the only contribution that might affect our result is if the soft pion (from the D^*) were swapped with the pion from the D^0. We imposed the p_T cut on the soft pion, which makes it impossible for both of the pions to pass trigger requirements. This affected less than 1% of the events.

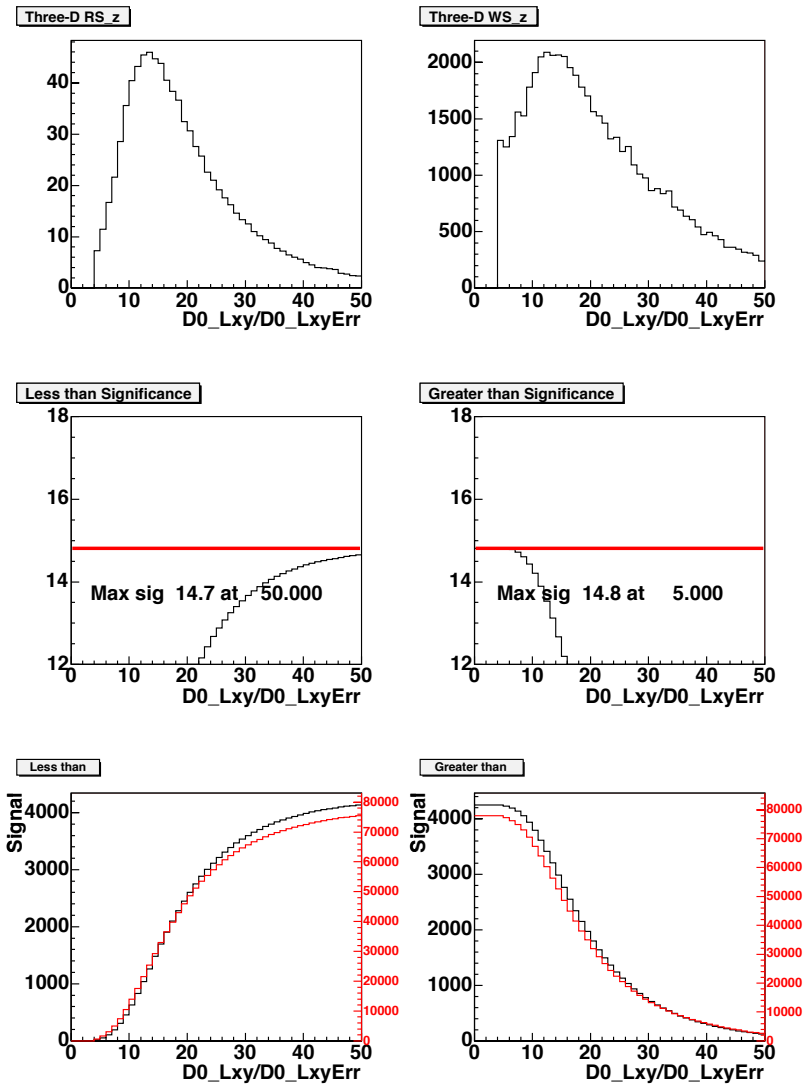

Figure 7: The upper left plot is an illustrative distribution, using sideband subtracted event near the D^0 mass. The upper right plot uses events from the sidebands. The middle left plot shows the expected WS signal/background significance, keeping events less than a particular cut value. The middle right plot shows the expected WS signal/background significance, keeping events greater than a particular cut value. The red line shows the WS significance if no cut on this variable is applied. The bottom plots show the expected signal S' (in black) and background B (in red) for the possible cut values.

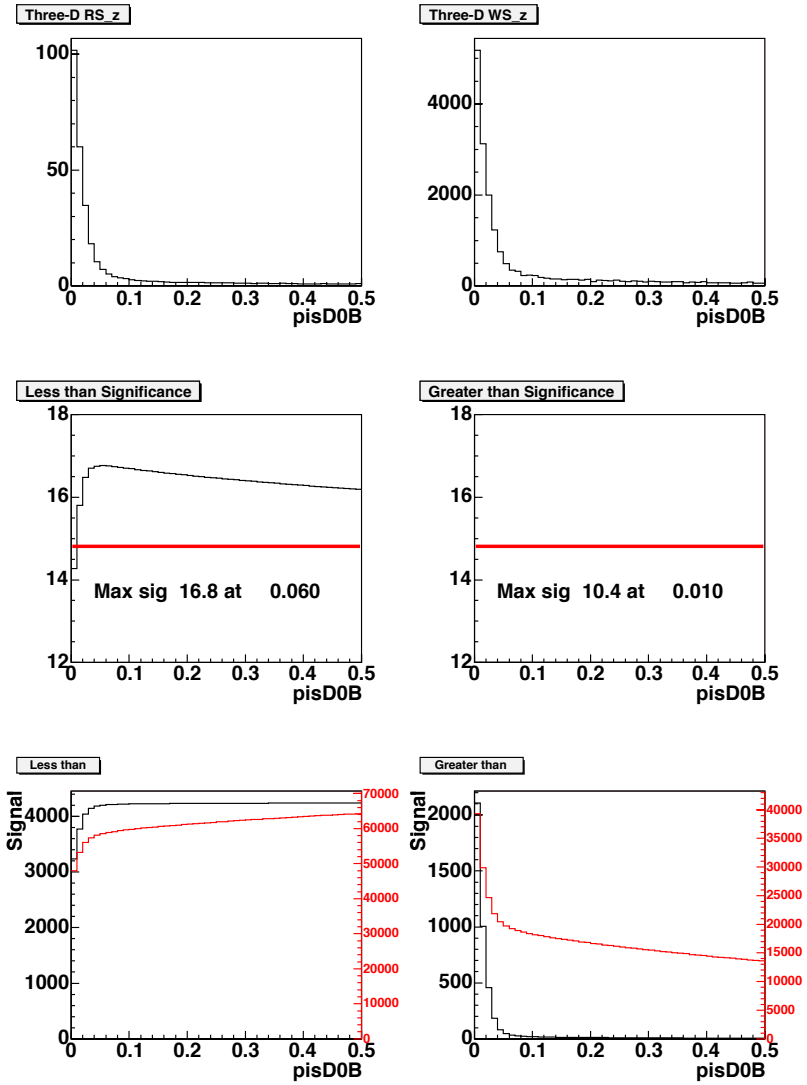

Figure 8: The upper left plot is an illustrative distribution, using sideband subtracted event near the D^0 mass. The upper right plot uses events from the sidebands. The middle left plot shows the expected WS signal/background significance, keeping events less than a particular cut value. The middle right plot shows the expected WS signal/background significance, keeping events greater than a particular cut value. The red line shows the WS significance if no cut on this variable is applied. The bottom plots show the expected signal S' (in black) and background B (in red) for the possible cut values.

We investigated using a dE/dX cut on the soft pion. While we cannot distinguish π from K at low momentum, we could exclude protons and hyperons. However, this cut was not used, as the current blessed dE/dX calibrations have not been established at low momentum. The background reduction was small, but might be worth exploring in the future (along with using the time-of-flight particle ID).

2.6 Selection Cuts to distinguish RS and WS

Every D^* candidate has both a RS and WS interpretation (by switching the K and π particle assignments). The mis-assigned interpretation has a $K\pi$ distribution much wider than a correctly reconstructed D^0. However, given the value of R_D, there are approximately 250 times as many RS D^* as WS D^*, which means that any real WS signal will be sitting on top of background from mis-assigned RS events.

To reduce mis-assigned background, we use what we refer to as "opposite assignment" mass cuts. When looking at WS $M_{K\pi}$, we remove candidates consistent with a RS $M_{K\pi}$ consistent with a D^0, $|M_{K\pi} - M_{D^0}| < 20MeV$. This cut is illustrated in Fig. 9. WS D^0 are similarly removed when looking at the RS $M_{K\pi}$ distribution, to have the same systematic effect for both interpretations. The improvement by making this cut is illustrated in Fig. 10 and Fig. 8.

To make sure that we understand the WS plot, we constructed a toy model. A particle with the D^0 mass decays to a kaon and a pion in the rest frame, with the track directions known. The daughter tracks are boosted to the lab frame. The kaon and pion assignments are swapped, and the new invariant mass is calculated. The difference in mass is shown in Figure 12. The kaon and pion will be boosted differently, when transforming from rest to lab frame. The largest difference in mass will occur when the kaon decays parallel or anti-parallel to the direction of the D^0 momentum. In Fig. 13, a scatter plot of the data is shown, with the toy model prediction drawn in red. The data is dominated by RS decays. At any particular decay angle of the kaon, the mass distribution is determined by the detector resolution. It is the sum over all decay angles which causes the integrated RS D^0s to have a broad distribution when reflected into the WS mass plot.

We also use dE/dX, which refers to the ionization energy loss as particles pass through the COT. (The details of how dE/dX is done are too complicated for this note, but are described in other papers[19, 20].) Rather than using particle identification for each track, we look at which two track interpretation ($K^-\pi^+$ or π^-K^+) is more likely, and only keep that interpretation.

The dE/dX variable which is expressed as $dE/dX = \log(dedx_{measured}/dedx_{predicted})$. For a correct hypothesis, the $Z = (dE/dX)/\sigma_{dE/dX}$ distribution is a unit gaussian centered at zero. For an incorrect hypothesis, the distribution is shifted away from zero. This is illustrated in Fig. 14. With $Z_{K(\pi)}(1)$ being the dE/dX value for the first track with a kaon (pion) hypothesis, and $Z_{\pi(K)}(2)$ being the dE/dX value for the second track with a pion(kaon) hypothesis, we compare $(Z_K^2(1) + Z_\pi^2(2))$ to $(Z_\pi^2(1) + Z_K^2(2))$ and only accept the more probable hypothesis (the one closer to zero).

We only accept the lower of those two interpretations, so each D^* candidate will only show up in either the RS or the WS plots. It is possible (in the future) to make a different selection, such as keeping both interpretations (if both PID values are small) or excluding both interpretations (if both are large).

The mass cut to remove mis-assigned background was optimized simultaneously with the dE/dX PID cut, as both cuts reduce the same background source. The mass cut is more effective than the PID cut (separately), but the combined effect is better. The optimal mass cut would be wider (30 MeV) if we did not use PID. This optimization was done for the time-integrated result, and has not changed since then.

The blinded (scaled RS signal) technique that was used to optimize the "basic" selections is also used here. The dE/dX cut variable is required to be less than (greater than) a given cut value,

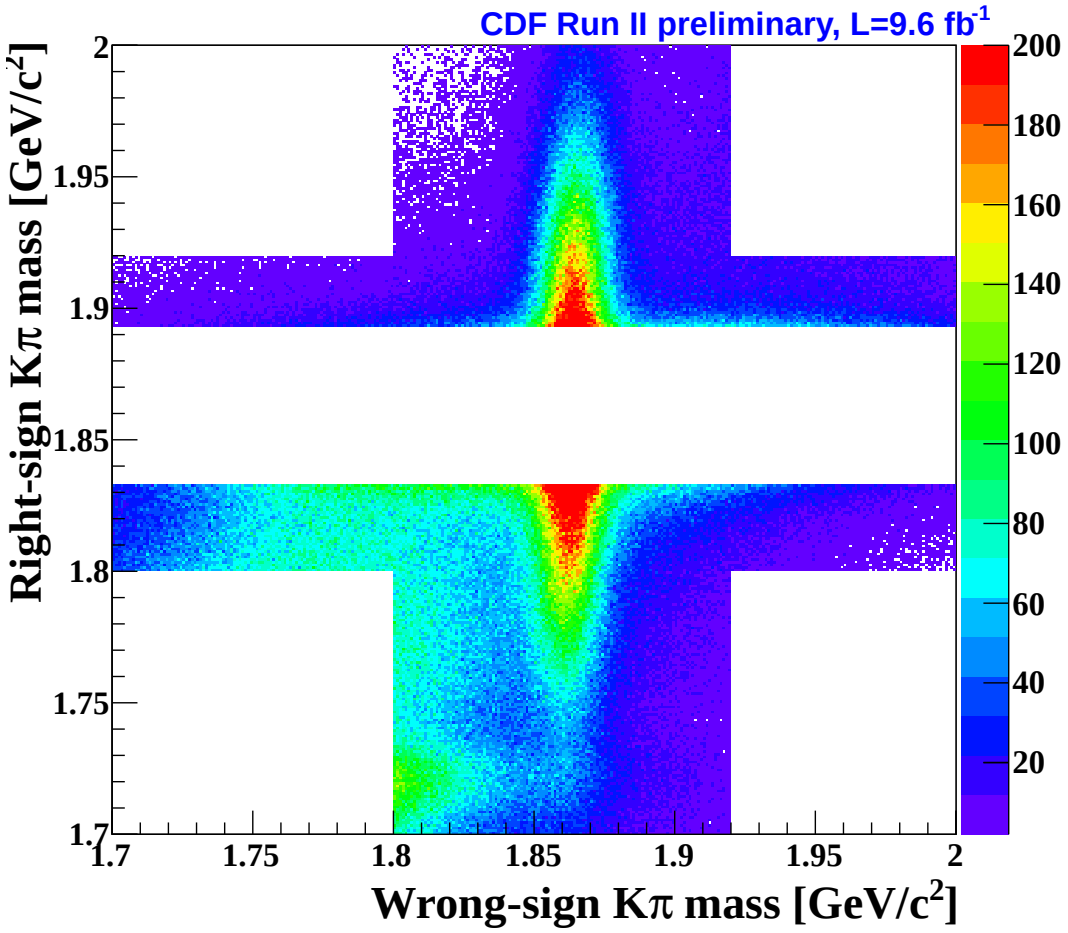

Figure 9: Plot to illustrate the mass cut to exclude RS D^0 that are mis-assigned as WS background. By removing the horizontal white band, the vertical band showing possible WS D^0 is visible.

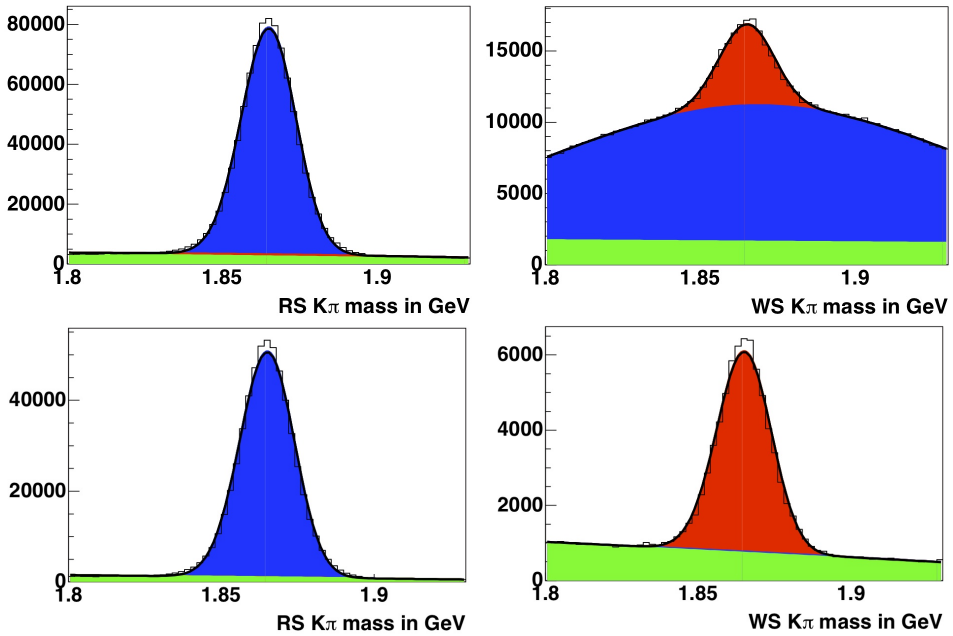

Figure 10: Plots from CDF note 8879, to illustrate the effect of the opposite assignment mass cut. The top two plots are before appying the cut, the bottom plots are after the cut. The left plots shows the RS $M_{K\pi}$ distribution, the right plots shows the WS $M_{K\pi}$ distribution The blue events are consistent with being correctly reconstructed as RS, the red events consistent with WS, and green is the combinatoric background level. The red events will be a combination of WS D^* and fake WS D^* candidates that are formed by a real D^0 and a random pion from the primary vertex. These plots are not used in the analysis, and were only generated to show visually the effectiveness of the opposite assignment mass cut.

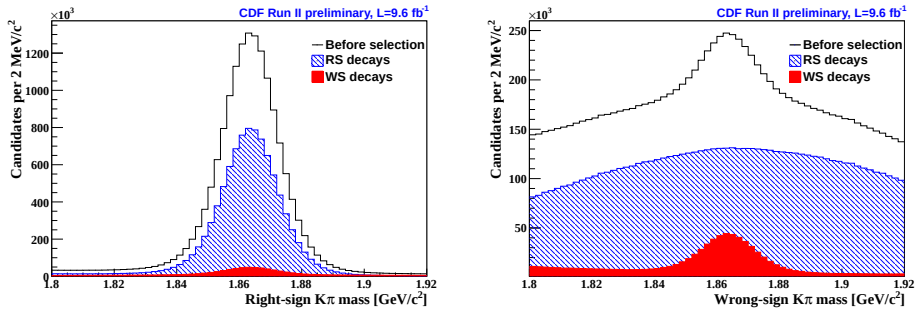

Figure 11: The plots from before applying OAM cuts, with the full data set. The left plots shows the RS $M_{K\pi}$ distribution, the right plots shows the WS $M_{K\pi}$ distribution The blue events are consistent with being correctly reconstructed as RS, and the red events consistent with WS. The red events will be a combination of WS D^* and fake WS D^* candidates that are formed by a real D^0 and a random pion from the primary vertex. These plots are not used in the analysis, and were only generated to show visually the effectiveness of the opposite assignment mass cut.

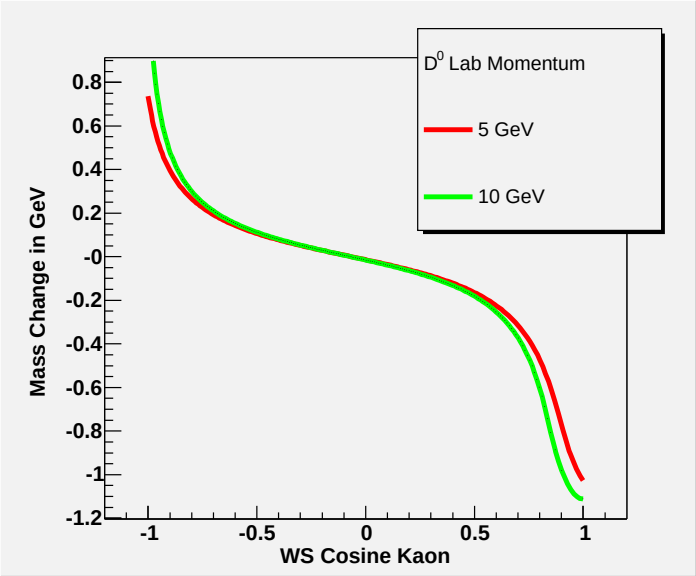

Figure 12: Change in two-particle mass when kaon and pion tracks from a simulated RS D^0 have their mass assignments switched. The cosine kaon is the cosine of the angle of the WS kaon in the rest frame of the WS D^0, with respect to the D^0 direction. The red curve is a D^0 with 5 GeV of momentum in the lab frame, the green curve is a 10 GeV D^0.

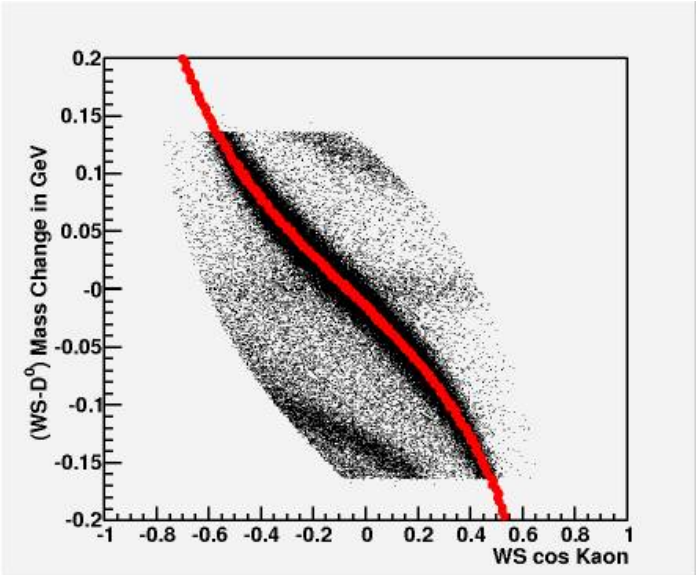

Figure 13: Scatter plot of WS mass (in GeV) with the mean fit D^0 mass subtracted versus cosine kaon. The $K\pi$ mass is limited to the range from 1.7 to 2.0 GeV. The cosine kaon is the cosine of the angle of the WS kaon in the rest frame of the WS D^0, with respect to the D^0 direction. The red line uses the same model as fig. 12, with 7 GeV momentum.

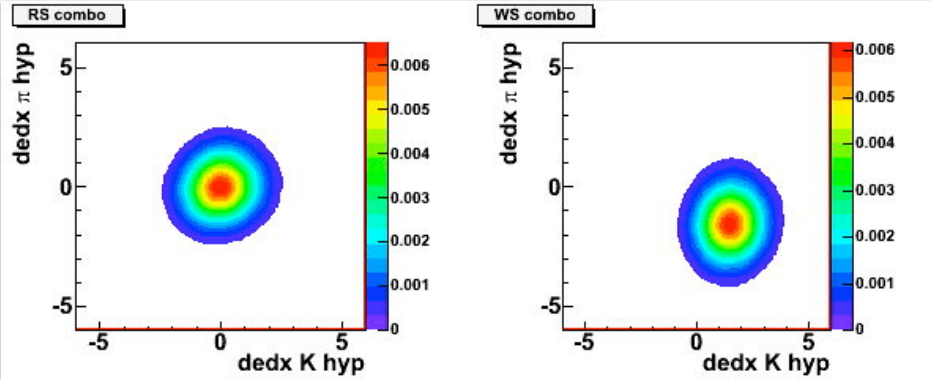

Figure 14: dE/dX distributions for events consistent with RS D^0 and D^* mass, from the $1.5/fb$ result. The left plot is the RS interpretation for the track assignments. The right plot is the WS interpretation, swapping the K and π tracks. This is not directly used in the analysis, and is for illustrative purposes only.

for the RS (WS) distributions. (A negative value means the RS interpretation is favored over the WS interpretation.) The opposite assignment mass cut is then chosen, to find the expected WS significance. The mass cut value was changed, until a maximum significance is found.

Table 4 summarizes the results of the cut optimization. While there is some overlap between the two cuts, a combination of OAM and dE/dX cuts is stronger than either of them alone. The OAM cut value is set at 20 MeV, and the dE/dX cut at 0. These are convenient, round numbers that are very close to the maximum significance. An advantage of having the dE/dX cut at zero, is that an event that passes the RS cut will fail the WS cut, and vice versa. Any other cut value will have events that could pass both the RS and WS dE/dX cuts, or fail both cuts.

dE/dX Cut Value	Max Significance	OAM Cut Value
-3.0	14.1	19
-2.5	14.5	19
-2.0	14.7	20
-1.5	14.9	20
-1.0	15.0	20
-0.5	15.1	22
0	15.1	22
+0.5	15.0	22
+1.0	14.9	23
+1.5	14.8	23
+2.0	14.7	25
+2.5	14.6	25
No dE/dX	13.0	28 MeV

Table 4: The blinded yield technique is used to get the WS signal significance for dE/dX and OAM cut values. The dE/dX cut is fixed at a value, while the OAM cut is scanned (in steps of 1 MeV) to find value with the highest significance. The dE/dX cut is then changed by half a unit, and the procedure repeated.

For a systematic study discussed later, we will need to compute the number of RS D^* that show up as mis-assigned background in the WS mass plots. This will require knowing the efficiency of the opposite mass and (dE/dX) PID cuts we applied. (The other selection cuts have the same efficiency for both RS and WS events, so won't affect our measurement.)

Suppose that we start with N_{D^*}, the number of RS D^* before we apply the opposite mass and PID cuts. The number of RS D^* that we measure will be

$$N_{RS} = N_{D^*} f_k(RS \to RS) f_p(RS \to RS)$$

where $f_k(RS \to RS)$ is the efficiency for RS D^* to pass the mass cut to make it to the RS plots, and $f_p(RS \to RS)$ is the efficiency for RS D^* to pass the PID cut to make it to the RS plots. The number of mis-assigned background events will be

$$N_{MRS} = N_{D^*} f_k(RS \to WS) f_p(RS \to WS)$$

where $(RS \to WS)$ are the cut efficiencies for a RS D^* to make it to the WS plots. Combining the two gives:

$$N_{MRS} = N_{RS} \frac{f_k(RS \to WS)}{f_k(RS \to RS)} \frac{f_p(RS \to WS)}{f_p(RS \to RS)}, \tag{4}$$

We measured $12.93 \times 10^6 \pm 4.57 \times 10^4 D^*$ before the PID cut, and $10.97 \times 10^6 \pm 4.20 \times 10^3 D^*$ after the PID cut (using fitting techniques described in the next chapter). Using the formula for the efficiency uncertainty [21], we have $f_p(RS \to RS) = 84.86 \pm 0.13\%$ and $f_p(RS \to WS) = (1 - f_p(RS \to RS))$.

To get the "failure rate" of the OAM cut, we fit the D^0 signal peak, and calculate how much of the fit function is more than 20 MeV away from D^0 mass. The fit function parameter uncertainties are used to get the uncertainty on the number of events outside the OAM cut. After the PID and opposite assignment mass cuts are applied, we measured $8.481 \times 10^6 \pm 3.61 \times 10^4 D^*$. These give us $f_k(RS \to RS) = 77.30 \pm 0.17\%$ and $f_k(RS \to WS) = 3.58 \pm 0.02\%$.

This means we can expect $N_{MRS} \approx N_{RS}/118$.

2.7 Multiple candidates per event

For simplicity, we remove events with multiple D* candidates. After the basic selection cuts, opposite assignment mass cut, and dE/dX were applied, any event with more than one D^* candidate (RS or WS) was excluded.

The events with multiple D^* candidates are, almost exclusively, a single D^0 candidate with more than one soft pion available to form a D^* candidate. This is not surprising, considering how many tracks are coming from the primary vertex. Combining a random pion with a D^0 will form a D^* candidate with a mass difference between 0 (no opening angle) and about 2 GeV (opposite directions). That is one reason why requiring the D^* makes such a clean D^0 signal, as the mass difference width of the signal peak is very small compared to the phase space from D^0 plus random pion.

We would expect those candidates to add to the background, but not affect the prompt D^* signal. At the November 3, 2009 BMLCPV meeting, we showed that the number of multiple candidate events is consistent with a model assuming that each event has a 6.5 % chance of having a 2nd candidate (with 6.5 % of those events having a third candidate), and that the extra candidate was equally likely to be from π^+ or π^-.

Another option, that was considered but not used, is to tighten selections that would reduce the likelihood of multiple D^* candidates, like reducing the mass difference window to less than 30 MeV. This will reduce the number of multiple candidate events, but no studies have been done yet to find an optimal value. (Making the mass difference window smaller will increase the uncertainty on the fit for the background.)

3 D^* Signal Estimation

Our goal is to determine the WS/RS ratio versus decay time $R(t_i)$, in time bins t_i, to extract the three mixing parameters in Eq. 1. We use what we call the "yield" technique. This is basically a 2-dimensional (binned) histogram fit, with a difference. We fit slices of "x" (for example), and use the results of those fits to make a 1-D histogram for the "y" variable. For example, when fitting the D^* mass peak, we will use the D^0 yield versus mass difference distribution. We are using the fact that $M_{K\pi}$ and ΔM are independent variables. We can get the number of D^0 by fitting the $M_{K\pi}$ distribution for a particular range of ΔM. By making multiple fits for the D^0 at different values of ΔM, we get the D^0 yield versus ΔM. The amplitude of the D^0 signal is allowed to be independent for every $M_{K\pi}$ fit. The advantage of this technique, compared to an unbinned likelihood fit, is that we don't need to know the distribution of non-D^0 events (like combinatoric background) versus ΔM.

Right-Sign (RS) and Wrong-Sign (WS) candidates are handled in separate binned fits. The following fits are done in succession, with the signal (and uncertainty) from the previous fit being used as the yield distribution for the next fit.

- Number of candidates vs. $K\pi$ mass: The result is the number of D^0.
- Number of D^0 vs. Δ mass difference: The result is the number of D^*.
- Number of D^* vs. impact parameter d_0: This information will be used to distinguish prompt D^* (produced at the primary vertex) versus D^* produced in secondary (beauty) decays.
- Ratio of WS to RS prompt D^*s vs. proper decay time: The fit for this distribution will provide the estimate of the charm mixing parameters.

We use the mass models developed for the ACP analysis of $D \to hh'$ decays (CDF-note 10296). For a detailed description of the fit functions see also A. Di Canto, Ph.D. thesis, University of Pisa [Fermilab-Thesis-2011-29], 2011.

3.1 Kπ Mass

The Kπ invariant mass distribution is fit to a probability density function (p.d.f.)

$$P^{K\pi} = N_{sgn}\, P^{K\pi}_{sgn} + N_{bkg}\, P^{K\pi}_{bkg}$$

given by the sum of a normalized signal component $P^{K\pi}_{sgn}$ and normalized background component $P^{K\pi}_{bkg}$ with event yields N_{sgn} for the signal and N_{bkg} for the background. The signal function $P^{K\pi}_{sgn}$ is composed of the sum of two normalized gaussians

$$G\left(M|\mu,\sigma\right) = \frac{1}{\sqrt{2\pi}\sigma}\, e^{-\frac{(M-\mu)^2}{2\sigma^2}}$$

which parameterize the bulk of the distribution, and a function

$$F_T\left(M|\mu,\alpha,\beta\right) = \frac{1}{A_T}\, e^{\alpha(M-\mu)} \frac{2}{\sqrt{\pi}} \int_{\beta(M-\mu)}^{+\infty} e^{-t^2} \mathrm{d}t$$

which describes a tail at lower masses due to final state soft photon emission or energy loss in the detector. The factor A_T is for normalization. The parameters α and β are fixed to values 13.2 and 57.4, respectively, as determined from simulated events. The signal p.d.f. is then written as

$$\begin{aligned} P^{K\pi}_{sgn}\left(M\right) &= f_T F_T\left(M|\mu_1,\alpha,\beta\right) \\ &\quad + \left(1-f_T\right)\left[f_1 G\left(M|\mu_1,\sigma_1\right) + \left(1-f_1\right) G\left(M|\mu_2,\sigma_2\right)\right] \end{aligned} \tag{5}$$

The relative contribution of the tail, f_T, is fixed to the value 0.0277 as determined from simulation.

The background is modelled by an exponential function

$$P_{bkg}^{K\pi}(M|s) = \frac{1}{A_E} e^{-sM} \tag{6}$$

where s is the slope parameter and A_E is the normalization factor.

Five Kπ signal shape parameters, μ_1, σ_1, μ_2, σ_2, and f_1, are determined for each of twenty time bins using the RS ΔM-integrated data for each time bin. Each Kπ mass histogram has range 1.800 - 1.920 GeV/c^2 with 2 MeV/c^2 wide bins, and is fit using a χ^2 technique with the function of Eq. 3.1. In each fit, the free parameters are the five shape parameters, the signal and background yields, and background slope s. For histograms with a large number of entries (> 10) in each bin, the χ^2 fit gives essentially identical results as a binned-likelihood fit. However, the χ^2 fit is much faster. For histograms which have bins with less than 10 events, a binned likelihood fit is performed, which properly takes into account the statistical fluctuations for small numbers of events.

The RS signal in each of the 1200 Kπ mass distributions (20 time bins and 60 ΔM bins) is determined using the five shape parameters for that time bin and leaving the signal and background amplitudes and the background slope as free parameters.

The WS signal in each of the 1200 Kπ mass distributions is determined using the five shape parameters for that time bin (determined from the RS data) and leaving the signal and background yields and the background slope as free parameters.

The quality of the fits to the 2400 distributions of $M_{K\pi}$ are illustrated by the χ^2/dof values, shown in Fig. 15. The distribution of χ^2/dof peaks just above one for both the RS and WS cases. For some of the RS $M_{K\pi}$ distributions corresponding to bins of ΔM near the D^* peak, the number of events in the signal peak is large and the χ^2/dof values are somewhat high. This is a well-known effect and does not degrade the accuracy of the fit parameters. The 2400 fits are not shown here, but are available from the authors. With 4 plots to a page, they require over 600 pages to display and take up a file size of several hundred MB. However, to illustrate the fits, we show, in Appendix B, the ΔM-summed RS and WS $M_{K\pi}$ distributions and fits for the 20 time bins.

The signal yields obtained from the 2400 $K\pi$ fits are used to build 20 RS and 20 WS 60-bin ΔM distributions which are fit according to the method described next.

3.2 ΔM

The ΔM distribution is fit to the sum of two p.d.f.'s, for signal and background,

$$P^{\Delta M} = N_{sgn}\, P_{sgn}^{\Delta M} + N_{bkg}\, P_{bkg}^{\Delta m} \tag{7}$$

where N_{sgn} and N_{bkg} are the signal and background yields, respectively. The signal is described by the sum of two normalized gaussians $G(\Delta M|\mu,\sigma)$ for the central bulk, plus a Johnson function

$$J(\Delta M|\mu,\sigma,\delta,\gamma) = \frac{1}{A_J} \frac{e^{-\frac{1}{2}\left[\gamma+\delta \sinh^{-1}\left(\frac{\Delta M-\mu}{\sigma}\right)\right]^2}}{\sqrt{1+\left(\frac{\Delta M-\mu}{\sigma}\right)^2}}$$

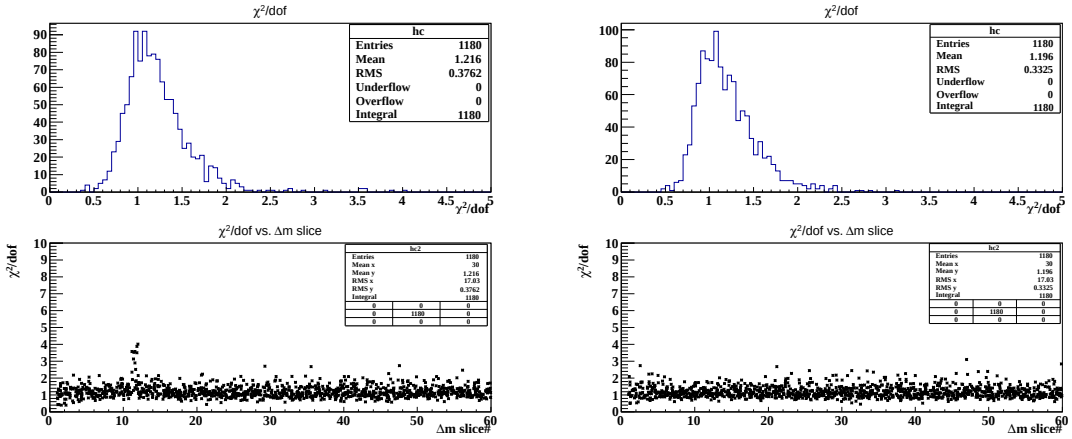

Figure 15: χ^2/dof distribution and individual values for the $M_{K\pi}$ fits. The left plots are for RS, the right plots for WS. Each set of RS or WS plots has 1200 entries (60 bins of ΔM, 20 bins of time).

that accomodates a possible asymmetric tail of the distribution. The signal p.d.f. is then written as

$$\begin{aligned} P_{sgn}^{\Delta m}(\Delta M) &= f_J J(\Delta M|\mu_J,\sigma_J,\delta_J,\gamma_J) \\ &\quad + (1-f_J)\left[f_{G1} G(\Delta M|\mu_{G1},\sigma_{G1}) + (1-f_{G1})\, G(\Delta M|\mu_{G2},\sigma_{G2})\right] \end{aligned} \tag{8}$$

where f_J is the relative fraction of the tail, and f_{G1} is the relative fraction between the two Gaussian components.

For the random pion background, we use an empirical function with a form developed from data by random association of a well-reconstructed D^0 meson from each event with a pion from another event. The functional form is,

$$P_{bkg}^{\Delta m}(\Delta M|b,c) = \frac{1}{A_B}(\Delta M)^b\ e^{-c(\Delta M)} \tag{9}$$

The signal shape parameters for the ΔM fit function are determined from the time-integrated RS yield distribution, shown in Fig. 16, histogrammed in 60 bins of ΔM in the range 0 to 30 Mev/c^2. The distribution is fit in the range 0 to 25.6 Mev/c^2 using the χ^2 method and the fit function with 14 free parameters: N_{sgn}, f_J, μ_J, σ_J, δ_J, γ_J, f_{G1}, $\mu_{G1(2)}$, $\sigma_{G1(2)}$ for signal (Eq.8), and N_{bkg}, b and c for bkg (Eq.9)).

The RS and WS ΔM distributions in each time interval are fit with the signal shape parameters fixed from the time-integrated RS fit described above. In the fits for each time interval, the free parameters are the signal and background yields and the background shape parameters b, and c. The 20 RS and 20 WS ΔM distributions and fits are shown in Appendix C. The quality of the fits are demonstrated by the distribution and individual values for χ^2/dof shown in Fig. 17. The χ^2/dof distributions for both RS and WS cases peak at about 1.5. The RS fits have somewhat high χ^2/dof for the smaller time intervals. However, inspection of the individual plots in Appendix C shows good qualitative behavior. The RS and WS signal yields for each time bin are reported in Table 5.

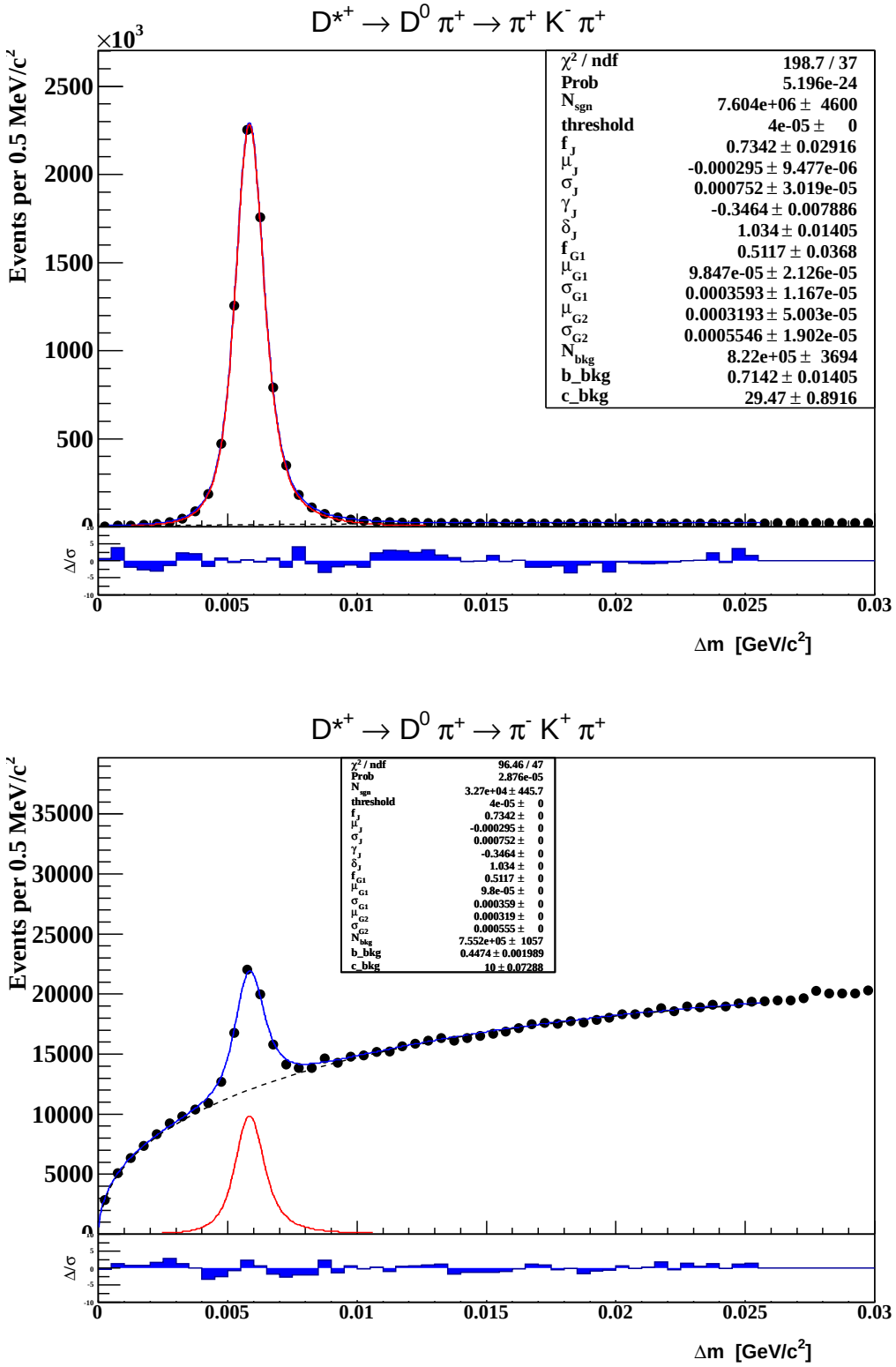

Figure 16: Time-integrated ΔM fits. The RS fit (top) is used to determine the signal shape parameters. A fit to the WS distribution (bottom) has the signal shape parameters fixed from the RS fit.

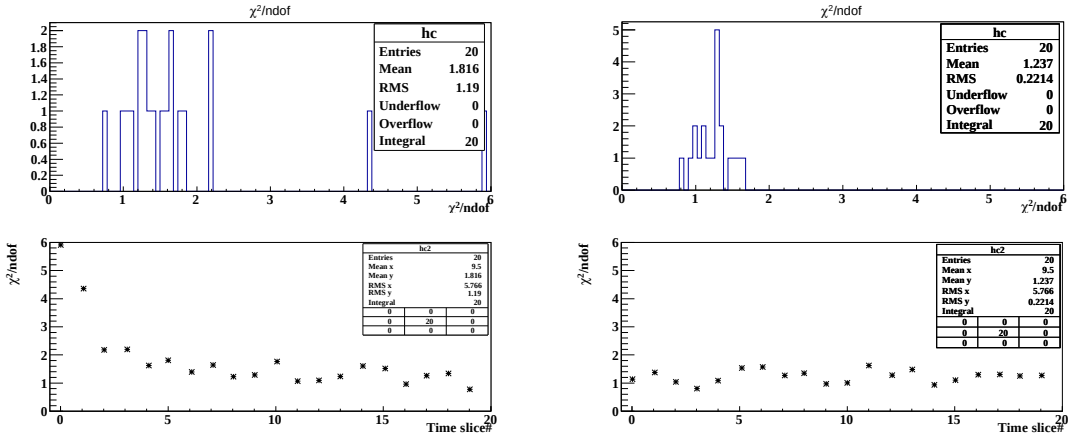

Figure 17: χ^2/dof distribution for the ΔM yield fits. The left plots are for the 20 RS fits, the right plots are for the 20 WS fits.

time-bin	ct (μm)	t/τ	RS yield	WS yield
0	110.89±6.96	0.90±0.06	73403.3±19.1	221.8±44.2
1	140.28±7.45	1.14±0.06	301466.9±588.6	1177.6±83.9
2	169.99±7.64	1.38±0.06	603463.1±831.6	2538.6±123.7
3	200.19±7.68	1.63±0.06	803461.6±960.4	3236.0±138.7
4	230.64±7.69	1.88±0.06	864037.3±996.6	3348.4±143.4
5	261.22±7.69	2.13±0.06	827503.1±972.9	3475.5±143.2
6	291.87±7.68	2.37±0.06	743630.1±925.1	3212.1±141.1
7	322.57±7.68	2.62±0.06	637117.0±857.5	2585.0±127.0
8	353.27±7.68	2.87±0.06	536238.6±793.0	2401.7±117.8
9	383.99±7.68	3.12±0.06	440929.1±711.6	1936.6±110.5
10	414.75±7.68	3.37±0.06	360404.2±646.1	1535.3±98.1
11	445.50±7.68	3.62±0.06	291219.5±579.3	1251.0±88.3
12	476.21±7.68	3.87±0.06	234127.5±522.0	1204.2±80.3
13	520.70±17.09	4.24±0.14	337352.3±630.0	1703.5±102.4
14	582.09±17.11	4.74±0.14	213116.8±504.6	1062.3±80.0
15	643.64±17.14	5.24±0.14	132881.6±394.6	776.4±67.3
16	705.08±17.08	5.74±0.14	82553.1±310.9	422.2±50.9
17	790.07±34.37	6.43±0.28	79358.1±307.9	464.4±54.0
18	912.66±34.25	7.43±0.28	26384.3±178.9	96.2±33.4
19	1073.83±66.75	8.74±0.54	11511.1±120.5	93.7±26.1

Table 5: Fitted yields for RS and WS $D^0 \to K\pi$ decays in each time interval.

4 Analysis of the WS/RS Yield Ratio versus Time $R(t)$

Based on the WS and RS signal yields shown in Table 5, $R(t)$ is determined from the distribution of the ratio of WS to RS signal yields in 20 time bins:

- 13 bins of a quarter D^0 lifetime width, for decay times from 0.75 - 4.0 D^0 lifetimes
- 4 bins of a half D^0 lifetime width, for decay times from 4.0 - 6.0 D^0 lifetimes
- 2 bins of a D^0 lifetime width, for decay times from 6.0 - 8.0 D^0 lifetimes
- 1 bin of two D^0 lifetimes width, for decay times from 8.0 - 10.0 D^0 lifetimes

Instead of using the bin center, we will be using the RS D^* time distribution, as shown in Fig. 18 to compute the event-weighted mean time for each bin. Table 6 shows the decay time and WS/RS ratio for the twenty time bins.

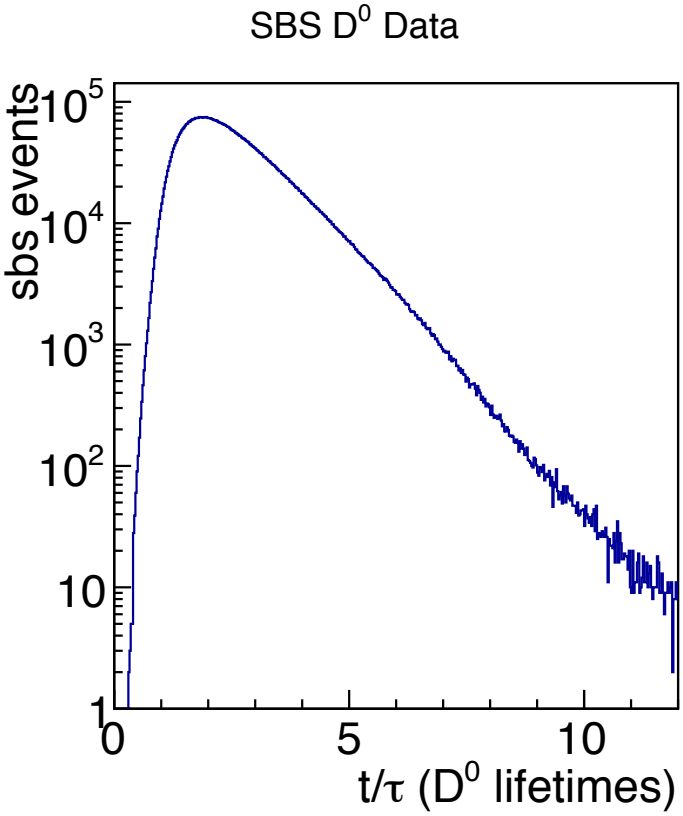

Figure 18: Distribution of RS D^*, using sideband subtraction for the $K\pi$ mass and a mass difference cut. The distribution shown includes events at shorter and longer decay times, that are not used for the analysis.

4.1 Functional Form for $R(t)$

Let the number of D^0 decays reconstructed in a given bin of proper time t be denoted by N^x (N^x_B) for promptly (non-promptly) produced D^0s where $x = WS$ or RS. Then the measured ratio R_m of

time-bin	**t/τ**	**WS/RS ratio $\times 10^{-3}$**
0	0.90±0.06	3.02± 0.60
1	1.14±0.06	3.91± 0.28
2	1.38±0.06	4.21± 0.20
3	1.63±0.06	4.03± 0.17
4	1.88±0.06	3.88± 0.17
5	2.13±0.06	4.20± 0.17
6	2.37±0.06	4.32±0.19
7	2.62±0.06	4.06±0.20
8	2.87±0.06	4.48± 0.22
9	3.12±0.06	4.39± 0.25
10	3.37±0.06	4.26± 0.27
11	3.62±0.06	4.30± 0.30
12	3.87±0.06	5.14± 0.34
13	4.24±0.14	5.05± 0.30
14	4.74±0.14	4.98± 0.38
15	5.24±0.14	5.84± 0.51
16	5.74±0.14	5.11± 0.62
17	6.43±0.28	5.85± 0.68
18	7.43±0.28	3.65± 1.27
19	8.74±0.54	8.14± 2.27

Table 6: Measured WS/RS ratio as a function of time. The error in the ratio is statistical only.

WS to RS decays for time bin t is given by,

$$R_m = \frac{N^{WS} + N_B^{WS}}{N^{RS} + N_B^{RS}} = \frac{N_B^{RS}}{N^{RS} + N_B^{RS}} \left(\frac{N^{RS}}{N^{RS}} \frac{N^{WS}}{N_B^{RS}} + \frac{N_B^{WS}}{N_B^{RS}} \right) = \frac{N_B^{RS}}{N^{RS} + N_B^{RS}} \left(\frac{N^{WS}}{N^{RS}} \frac{N^{RS}}{N_B^{RS}} + \frac{N_B^{WS}}{N_B^{RS}} \right). \tag{10}$$

It is convenient to define the variables

$$B^{RS} = \frac{N_B^{RS}}{N^{RS} + N_B^{RS}}, \qquad R = \frac{N^{WS}}{N^{RS}}, \qquad R_B = \frac{N_B^{WS}}{N_B^{RS}}, \qquad \Delta_B = f_B^{RS} \left(1 - \frac{R_B}{R} \right), \tag{11}$$

where f_B^{RS} is the fraction of non-prompt decays in the RS sample, R and R_B are the ratio of prompt D^0's and non-prompt D^0's, respectively, and Δ_B is a time-dependent factor which characterizes the non-prompt decays. Using the definitions of Eq. 11, Eq. 10 can be written as

$$R_m = f_B^{RS} \left(R \frac{N^{RS}}{N_B^{RS}} + R_B \right) =$$

$$= f_B^{RS} R \frac{N^{RS}}{N_B^{RS}} + f_B^{RS} R_B = \left(1 - f_B^{RS} \right) R + f_B^{RS} R_B =$$

$$= R \left[1 + f_B^{RS} \left(\frac{R_B}{R} - 1 \right) \right] = R \left[1 - \Delta_B \right] \tag{12}$$

The last term of Eq. 12 provides a convenient form for R_m which is used to fit the data.

The effect of the factor $\Delta_B(t)$ describing non-prompt decays is illustrated in the simplified case (not assumed in this analysis) where $R(t)$ is a monotonically increasing function of t. For non-prompt D^0 decays, the reconstructed proper decay time, t, overestimates the true proper time, t', according to $t \approx t_B + t' \geq t'$, where t_B is the B meson decay time. Then,

$$R(0) \leq R_B(t) = R(t') \leq R(t) \qquad \Longrightarrow \qquad \frac{R(0)}{R(t)} \leq \frac{R_B(t)}{R(t)} \leq 1 \quad \forall t \tag{13}$$

It follows that the factor $\Delta_B(t)$ is bounded from above:

$$0 \leq \Delta_B(t) \leq f_B^{RS}\left(1 - \frac{R(0)}{R(t)}\right) \tag{14}$$

and

$$R_m \leq R \leq \frac{R_m}{[1-\Delta_B]} \tag{15}$$

As will be shown, the fit to the data for R_m does indeed yield a function R which satisfies the bounds described above.

4.2 Determination of f_B^{RS} from the D^0 transverse impact parameter distribution

The fitting method for $R(t)$ requires knowledge of $f_B^{RS}(t)$, the fraction of non-prompt RS D^0 decays. This information is extracted from the distribution of transverse impact parameter d_0 of the D^0, with respect to the primary vertex. As shown in Fig. 19, the d_0 for a D^0 produced in a B decay, tends to be, on average, larger than for a D^0 produced promptly, from the primary vertex. It is also seen in the figure that the transverse distance from the primary vertex to the D^0 decay vertex tends to be, on average, larger for non-prompt decays than for prompt ones.

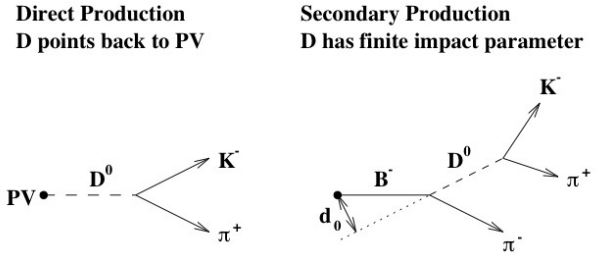

Figure 1: The impact parameter of direct and secondary charm in the $r - \phi$ plane.

Figure 19: Schematic representation of prompt and non-prompt D^0 production as seen in the transverse plane. In the non-prompt diagram, the D^0 is produced from $B \to D^* X$.

4.3 Impact parameter fit

The contributions of prompt and non-prompt D^0 decays are evident from the RS d_0 distribution, integrated over decay time, shown in Fig. 20. The d_0 distributions are obtained by selecting events with $4 < \Delta M < 8$ MeV/c^2 and $1.848 < M_{K\pi} < 1.880$ GeV/c^2 ($\pm 2\sigma$) and subtracting the sidebands (low-mass 1.808-1.824 GeV/c^2, high-mass 1.904-1.920 GeV/c^2). The peak at small times is due to the prompt component. The broad distribution extending to large times is due to the non-prompt component. The prompt and non-prompt components are each modelled with the sum of two gaussians. The widths and relative fraction of the two gaussians are free parameters. The fitted curve to the RS time-integrated d_0 distribution, shown in Fig. 20, shows a good quality of fit.

For each time bin, the RS d_0 distribution is fit using the method described above. In each case, the parameter values are found to be within $\pm 5\%$ of the values obtained from the time-integrated distribution. The parameter values are also consistent with the values obtained from simulation. The 20 RS d_0 distributions with fits are shown in Appendix D.

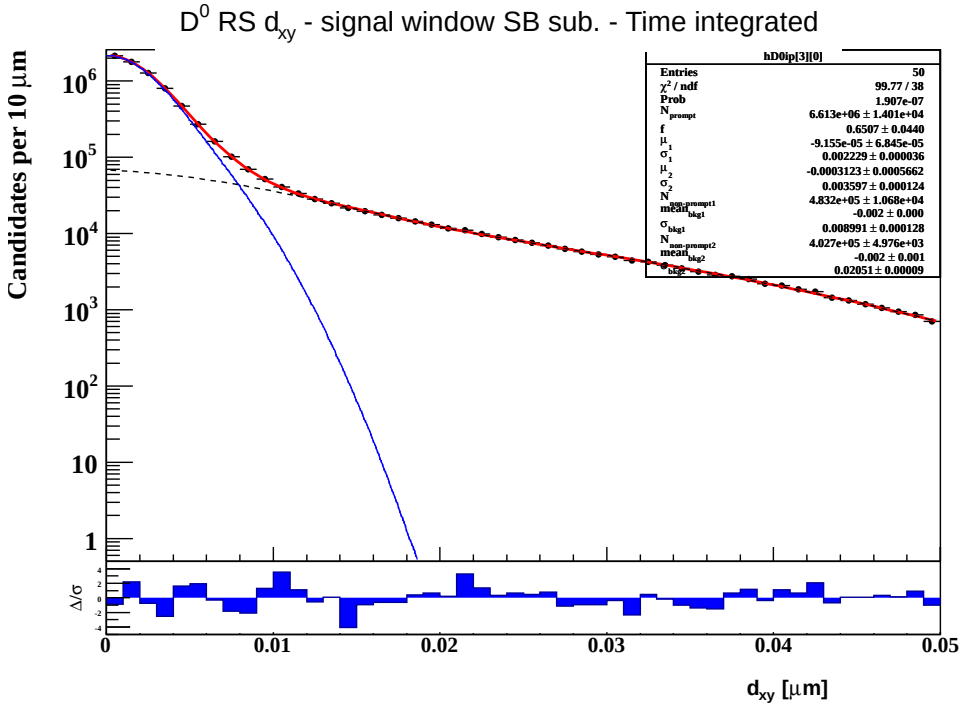

Figure 20: Time-integrated impact parameter distributions, d_0, for D^*s produced promptly and from secondary, non-prompt, decays.

The p.d.f. for the prompt d_0 distribution is denoted by $P(d_0)$ and $P_B(D_0)$ describes the non-prompt component. The fraction f_B^{RS} is determined in the region $d_0 < 60\mu$m, a selection cut which reduces the contribution of non-prompt decays.

$$f_B^{RS} = \frac{N_B^{RS}}{N^{RS} + N_B^{RS}} = \frac{\int_0^{+60\mu m} P_B(d_0)\, d(d_0)}{\int_0^{+60\mu m} P_B(d_0)\, d(d_0) + \int_0^{+60\mu m} P(d_0)\, d(d_0)} \tag{16}$$

The values of f_B^{RS} for the 20 time bins, obtained using this prescription, are given in Table 7 and plotted in Fig. 21. Note that f_B^{RS} is zero at 1 mean lifetime and increases to about 0.44 at 9 mean lifetimes. A polynomial with 5 parameters denoted by p_i, provides a good fit to $f_B^{RS}(t)$ as shown in Fig. 21. The fitted parameters are used in the subsequent fit to the data for R_m.

4.4 Fitting method for $R(t)$

The fraction $R(t)$ is determined from a fit to the data for R_m. According to equation 12,

$$R_m \;=\; R\,[1 - \Delta_B]\,. \tag{17}$$

Letting r_i denote the measured values of R_m for the 20 time bins, $i = 0, 19$, a fit χ^2 is defined by,

$$\chi^2 = \sum_{i=1}^{20} \left[\frac{r_i - R(t_i)\,(1 - \Delta_B(t_i))}{\sigma_i} \right]^2 + \sum_{k=0}^{4} \sum_{l=0}^{4} (p_k - \theta_k)\, V_{kl}^{-1}\, (p_l - \theta_l) + \sum_{i=1}^{20} \sum_{j=1}^{100} \left(\frac{h_{ij} - \tilde{h}_{ij}}{\Delta h_{ij}} \right)^2 \tag{18}$$

where σ_i are the errors on r_i. The second term in Eqn. 18 provides a Gaussian constraint to f_B^{RS} using the 5 parameters p_k (k=0,4) from the fit to f_B^{RS}, and the covariance matrix V_{kl} of the parameters p_k.

time-bin	f_B^{RS}
-1	0.054±0.002
0	0.002±0.006
1	0.002±0.005
2	0.015±0.004
3	0.030±0.010
4	0.046±0.012
5	0.057±0.011
6	0.074±0.011
7	0.082±0.011
8	0.084±0.009
9	0.121±0.028
10	0.101±0.009
11	0.102±0.009
12	0.112±0.017
13	0.120±0.006
14	0.130±0.008
15	0.162±0.011
16	0.189±0.017
17	0.235±0.010
18	0.288±0.039
19	0.438±0.068

Table 7: Estimate of the fractions f_B^{RS} of non-prompt decays in the RS sample from impact parameter fits in time bins 0-19. The first row (time bin -1) represents the time-integrated value.

The "nuisance" parameters θ_k are the values of p_k which result from the Gaussian constraint. The third term in Eqn. 18 is a Gaussian constraint using the matrix h_{ij} which describes the distribution of apparent decay time t resulting from a non-prompt D^0 decay with actual decay time t'. The third term and the matrix h_{ij} can be understood by using the definitions in equation 12, to write the first term as follows.

$$\chi^2 = \sum_{i=1}^{20} \left[\frac{r_i - R(t_i)\left(1 - f_B(t_i)\left(1 - \frac{R_B(t_i)}{R(t_i)}\right)\right)}{\sigma_i} \right]^2 + \sum_{k=0}^{4}\sum_{l=0}^{4} (p_k - \theta_k)\, V_{kl}^{-1}\, (p_l - \theta_l) + \sum_{i=1}^{20}\sum_{j=1}^{100} \left(\frac{h_{ij} - \tilde{h}_{ij}}{\Delta h_{ij}} \right)^2 \tag{19}$$

$$\chi^2 = \sum_{i=1}^{20} \left[\frac{r_i - R(t_i) + R(t_i) f_B(t_i) - R_B(t_i) f_B(t_i)}{\sigma_i} \right]^2 + \sum_{k=0}^{4}\sum_{l=0}^{4} (p_k - \theta_k)\, V_{kl}^{-1}\, (p_l - \theta_l) + \sum_{i=1}^{20}\sum_{j=1}^{100} \left(\frac{h_{ij} - \tilde{h}_{ij}}{\Delta h_{ij}} \right)^2 \tag{20}$$

The first term in equation 20 shows the explicit dependence on $R_B(t)$, the WS/RS signal ratio for non-prompt decays. The function $R_B(t)$ can be expressed as,

$$R_B\,(t_i) = \frac{\sum_{j=1}^{M} h_{ij} R(t'_j)}{\sum_{j=1}^{M} h_{ij}}. \tag{21}$$

The matrix h_{ij} is determined from a simulation of B decays to final states with a D^*. Each term h_{ij} gives the number of non-promptly produced D^0 decays with apparent decay time t_i, as measured from the primary vertex, that have generated decay time t'_j, j=1, ..., 100. In equation 20, $\tilde{h}_{ij}$ are "nuisance" parameters whose values are determined by the gaussian constraint. The terms $\Delta\, h_{ij}$ are the statistical errors on h_{ij} due to the number of simulated events. Of the 2000 $h_i j$ elements, 907 have non-zero counts in the simulation. The $h_i j$ are presented in detail in a later section.

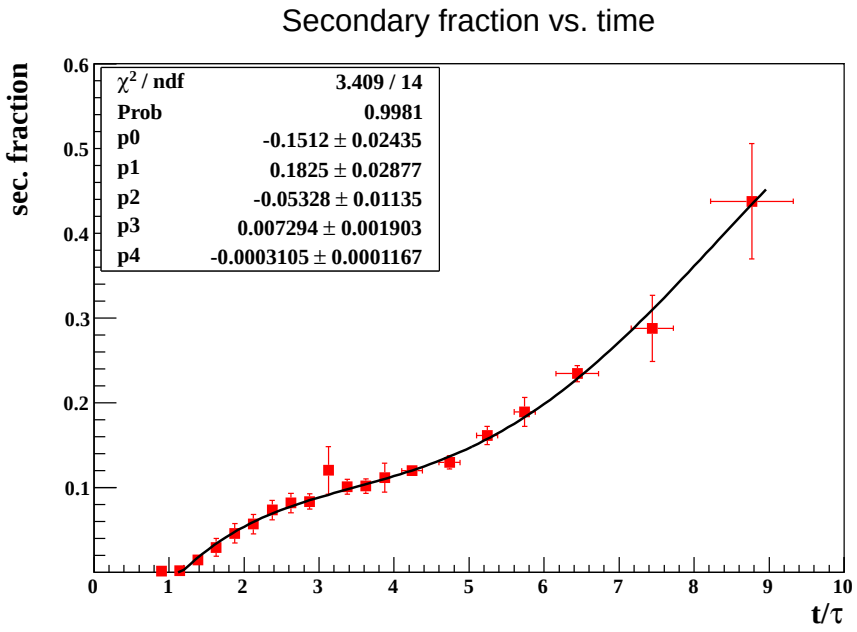

Figure 21: Fraction f_B^{RS} of D^*s coming from non-prompt decays as a function of decay time, for impact parameter $d_0 < 60\mu$m.

5 Studies, Systematics, and Result Interpretations

Fig. 22 shows the mixing fit compared to the data points.

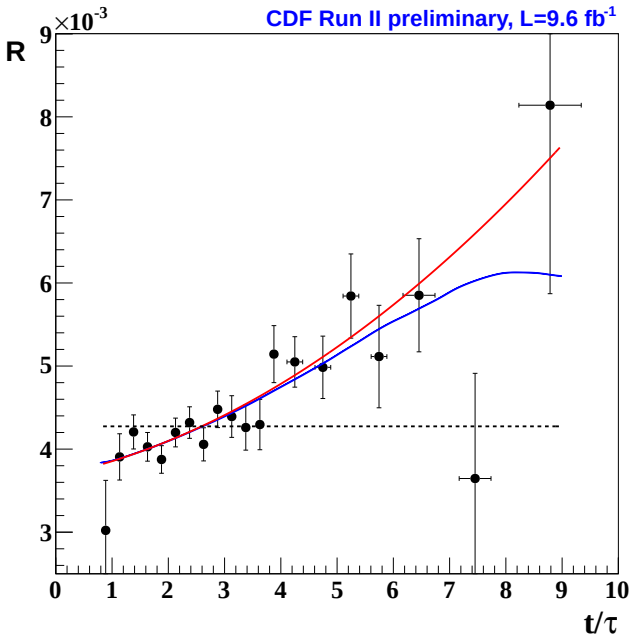

Figure 22: Fit of the WS/RS Ratio. The data points and error bars are listed in Table 6. The blue curve is the fit function described in the previous chapter. The red curve is the projection of the prompt time-behavior. The dashed line is the fit assuming no mixing.

This chapter describes the additional work done to verify the analysis method, determine systematic uncertainties, and ways to present the ratio fit results.

5.1 Monte Carlo

We are taking advantage of the full (Pythia) MC generated by Angelo DiCanto, Paola Garosi, and Paola Squillacioti. Some useful information is on the web page: http://www-cdf.fnal.gov/∼dicanto/internal/bmc.html. There are samples of $D*$ is allowed to decay to all (known) decay modes, and D^* produced from B decays. It is statistics limited (compared to data), but has the advantage of being run through detector simulation and written out in BStNtuple form. These samples was used during the investigation on partially reconstructed charm backgrounds in our $K\pi$ plots, and to make the h_{ij} matrix mentioned in the previous chapter to get the D^0 decay times from non-promptly produced D^*.

We also use two toy MC simulations. The simpler one takes the WS/RS data points, moves the points to an arbitrary value, and allows the points to vary within the Gaussian error bars. This toy MC is used for a p-value test of the no-mixing hypothesis.

The second toy MC generates simulated mass distributions. The results from our fits to data are used to estimate the amounts and distributions of all signals and backgrounds that were included in the fit. This template is then used to generate mass plots, which can be fed into our normal analysis code. The advantage of this toy is that mass or decay time distributions can be modified, to see the effect it has on the analysis fits. The disadvantage is that we need to be confident that the analysis is dividing the various signals and backgrounds properly, and that fit distributions are close enough to the real thing to be useful. This toy MC is used during studies of the systematic effects, and to

validate that the analysis code is working as expected.

5.2 Analysis Convergence

We made four toy MC samples, each with different mixing parameters. 100 experiments per sample were made, to make the study less sensitive to statistical effects. The 400 toy experiments were put through the analysis method, and the mixing parameter fits were compared to the original simulation values. Fig. 23 shows the mixing fit results for the first toy MC sample. Table. 8 has the comparison between the average fit results and the original mixing parameters put into the toy MC.

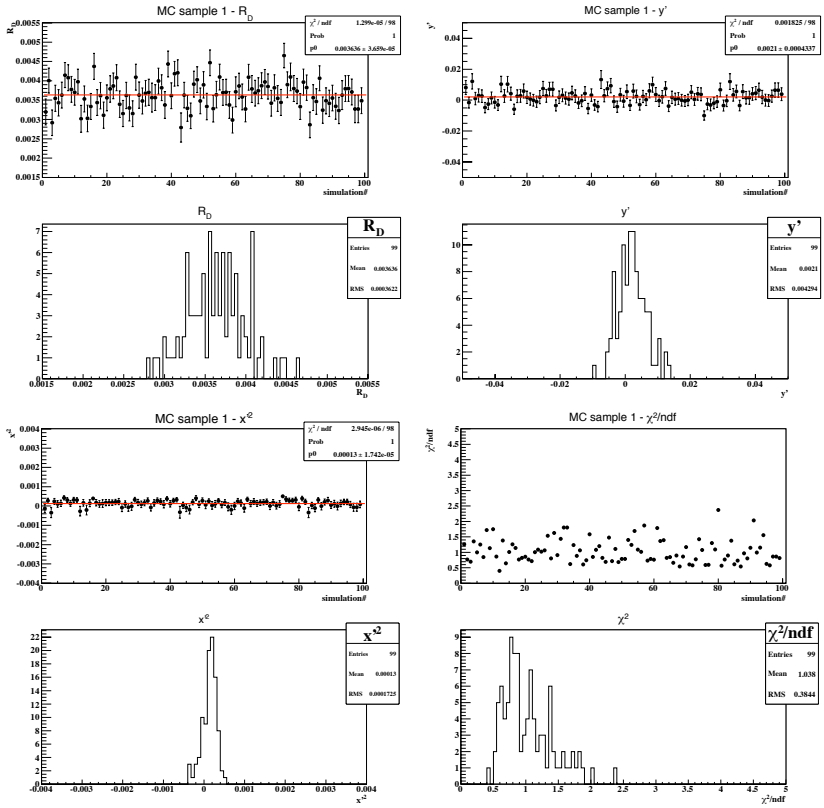

Figure 23: Analysis output from the 100 toy MC experiments made starting with $y' = 2.40 \times 10^{-3}$ and $x'^2 = 2.40 \times 10^{-3}$. The plots show the distributions of the analysis results for the three mixing parameters, and the mixing fit χ^2 per d.o.f.

5.3 Systematic Uncertainties

Before we fit the prompt WS/RS D* ratio versus decay time, we considered possible sources of systematic uncertainties. If any are found that are significant, they can be added (in quadrature) to the existing uncertainty for the number of RS and WS D^*, to the WS/RS ratio, or to the mixing parameters, depending on what is appropriate.

5.3.1 Signal Shapes

The true distribution of the D^0 and D^* signal shapes is complicated, but appears to be well matched by the signal functions we have chosen. The true signal distributions should be the same for RS and

Sample	$R_D(10^{-3})$	$y'(10^{-3})$	$x'^2(10^{-3})$	χ^2 / dof
1	3.636 ± 0.037	2.10 ± 0.43	0.130 ± 0.017	1.038
	3.67	2.40	0.13	
2	4.144 ± 0.033	-4.46 ± 0.36	0.403 ± 0.013	1.096
	4.160	-4.0	0.40	
3	3.143 ± 0.033	8.29 ± 0.46	-0.118 ± 0.022	1.049
	3.177	8.50	-0.12	
4	4.263 ± 0.038	-0.086 ± 0.40	-0.008 ± 0.015	1.034
	4.310	0.	0.	

Table 8: The mixing parameters obtained from running the analysis code on the toy MC samples. The first line for each sample is the average of the 100 results for that sample. The second line is the seed value for each toy MC sample. The uncertainty is on the average value. For comparison, each pseudo experiment has uncertainties on the mixing parameters around the following values: $R_D \pm 0.33 \times 10^{-3}$, $y' \pm 3.90 \times 10^{-3}$, and $x'^2 \pm 0.13 \times 10^{-3}$.

WS, since they have identical kinematics. We use the same signal shapes for RS and WS. If we wanted to report the RS or WS signal yield separately (like for a lifetime fit), we would need to account for the systematic uncertainty on the signal shapes, which we are fixing from the time-summed fits. However, we only use the WS to RS ratio. The systematic effect is a common multiplicative factor for both WS and RS, and will mostly cancel in the WS/RS ratio.

The fixed signal shapes were modified, to see the effect on the ratio for each time bin. One parameter at a time was shifted by $\pm 1\sigma$, while the other parameters were kept at their optimal value. Fig. 24 shows the table for the D^0 shape variation, while Fig. 25 shows the table for the D^* shape variation. Since the systematic effect is small compared to the existing statistical error, the effect will be negligible when added in quadrature to the existing errors.

bin	par2		par5		par6		par7		par8		total		stat
0	-0.04	-3.55	1.29	-4.42	-3.90	-2.39	0.05	-3.60	-3.99	1.47	**-9.05**	**1.96**	19.90
1	0.02	0.00	-0.55	0.53	-0.27	0.34	0.01	-0.02	-0.27	0.26	**-0.67**	**0.68**	7.10
2	-0.01	0.01	-0.39	0.30	-0.24	0.16	0.00	0.01	-0.21	0.13	**-0.50**	**0.36**	4.90
3	0.00	0.00	-0.47	0.47	-0.25	0.23	0.01	0.00	-0.26	0.23	**-0.59**	**0.57**	4.30
4	-0.01	0.02	-0.46	0.45	-0.24	0.25	0.00	0.02	-0.21	0.22	**-0.56**	**0.56**	4.30
5	-0.01	0.01	-0.38	0.39	-0.21	0.21	0.00	0.00	-0.18	0.17	**-0.47**	**0.47**	4.10
6	0.00	0.01	-0.42	0.47	-0.21	0.23	0.01	0.00	-0.22	0.24	**-0.52**	**0.57**	4.40
7	0.02	-0.02	-0.43	0.43	-0.26	0.24	0.02	-0.03	-0.21	0.19	**-0.55**	**0.53**	4.90
8	0.00	0.00	-0.47	0.49	-0.26	0.25	0.03	-0.03	-0.26	0.25	**-0.60**	**0.60**	4.90
9	-0.01	0.02	-0.39	0.41	-0.25	0.24	-0.02	0.03	-0.15	0.11	**-0.49**	**0.49**	5.70
10	-0.01	0.01	-0.47	0.48	-0.30	0.27	0.03	-0.01	-0.23	0.18	**-0.60**	**0.58**	6.40
11	-0.02	-0.01	-0.64	0.66	-0.33	0.36	-0.01	-0.02	-0.28	0.26	**-0.77**	**0.79**	7.10
12	-0.03	-0.03	-0.69	0.68	-0.39	0.42	-0.03	-0.02	-0.32	0.27	**-0.86**	**0.85**	6.70
13	-0.03	-0.01	-0.41	0.30	-0.29	0.14	-0.01	-0.01	-0.18	0.16	**-0.53**	**0.37**	6.00
14	0.05	-0.05	-0.65	0.70	-0.34	0.37	0.07	-0.05	-0.36	0.37	**-0.82**	**0.88**	7.50
15	0.00	-0.02	-1.09	1.21	-0.61	0.61	0.06	-0.06	-0.62	0.58	**-1.40**	**1.47**	8.70
16	0.07	-0.09	0.78	-0.88	-0.41	0.08	-0.01	0.03	-0.64	0.54	**-1.16**	**0.96**	12.10
17	0.07	-0.09	-1.20	1.24	-0.66	0.56	0.05	-0.06	-0.68	0.60	**-1.54**	**1.49**	11.60
18	0.00	0.32	0.69	2.77	-1.03	-2.49	0.21	0.00	-12.38	1.49	**-12.67**	**3.24**	34.70
19	2.75	3.12	-4.23	10.40	-1.35	7.28	2.87	3.19	-0.70	6.09	**-4.50**	**15.29**	27.90

Figure 24: D^0 signal shape variation, and the change in the WS/RS ratio for the twenty time bins. The difference between the WS/RS ratio and the reference value (unmodified signal shape) is expressed in the table in % with respect to the reference value.

bin	par2		par3		par4		par5		par6		par7		par8		par9		par10		par11		total		stat
0	0.25	-0.26	0.00	-0.01	1.39	-1.26	-0.09	0.13	-0.30	0.33	-0.74	0.74	0.78	-0.79	0.62	-0.56	0.89	-0.89	0.09	-0.05	-2.01	2.11	19.9
1	-0.56	0.61	0.15	-0.14	-0.68	0.72	-0.05	0.06	0.23	-0.22	0.22	-0.22	-0.08	0.10	-0.18	0.18	-0.17	0.22	-0.12	0.13	-0.99	1.06	7.1
2	-0.67	0.72	0.10	-0.09	-0.72	0.78	-0.02	0.02	0.30	-0.28	0.17	-0.17	0.04	-0.03	-0.11	0.11	-0.16	0.21	-0.17	0.17	-1.08	1.15	4.9
3	-0.47	0.51	0.05	-0.04	-0.83	0.87	0.00	0.00	0.30	-0.29	0.20	-0.19	-0.11	0.12	-0.11	0.11	-0.25	0.28	-0.11	0.11	-1.07	1.13	4.3
4	-0.57	0.61	0.07	-0.07	-0.67	0.71	0.00	0.01	0.26	-0.25	0.18	-0.18	0.01	0.00	-0.11	0.12	-0.19	0.24	-0.15	0.15	-0.97	1.04	4.3
5	-0.50	0.53	0.07	-0.07	-0.74	0.78	-0.01	0.02	0.27	-0.26	0.19	-0.19	-0.07	0.08	-0.11	0.12	-0.22	0.25	-0.12	0.12	-0.99	1.05	4.1
6	-0.52	0.55	0.01	0.00	-0.95	0.98	0.05	-0.04	0.37	-0.36	0.21	-0.21	-0.12	0.12	-0.11	0.11	-0.29	0.32	-0.12	0.12	-1.22	1.26	4.4
7	-0.57	0.61	0.09	-0.08	-0.76	0.79	-0.02	0.02	0.29	-0.28	0.18	-0.18	-0.04	0.04	-0.11	0.11	-0.18	0.22	-0.13	0.12	-1.04	1.09	4.9
8	-0.69	0.73	0.14	-0.13	-0.80	0.83	-0.05	0.06	0.30	-0.28	0.19	-0.19	-0.01	0.01	-0.12	0.12	-0.16	0.21	-0.15	0.15	-1.15	1.20	4.9
9	-0.53	0.56	0.05	-0.05	-0.80	0.83	0.00	0.00	0.31	-0.30	0.16	-0.16	-0.06	0.06	-0.10	0.09	-0.19	0.23	-0.12	0.12	-1.05	1.10	5.7
10	-0.56	0.59	0.04	-0.03	-0.84	0.90	0.01	-0.01	0.34	-0.32	0.14	-0.13	-0.02	0.03	-0.04	0.05	-0.18	0.24	-0.13	0.14	-1.09	1.17	6.4
11	-0.17	0.19	-0.06	0.06	-0.69	0.72	0.03	-0.03	0.25	-0.24	0.10	-0.10	-0.15	0.14	-0.01	0.00	-0.23	0.24	-0.04	0.04	-0.81	0.84	7.1
12	-0.54	0.56	0.04	-0.03	-0.99	0.99	0.03	-0.03	0.33	-0.33	0.29	-0.30	-0.19	0.21	-0.20	0.19	-0.36	0.40	-0.14	0.13	-1.30	1.32	6.7
13	-0.72	0.76	0.05	-0.04	-0.80	0.85	0.03	-0.02	0.36	-0.34	0.15	-0.14	0.08	-0.08	-0.06	0.07	-0.17	0.24	-0.20	0.20	-1.17	1.25	6.0
14	-0.49	0.52	0.05	-0.04	-0.72	0.76	0.00	-0.01	0.28	-0.28	0.13	-0.14	-0.06	0.06	-0.08	0.07	-0.16	0.19	-0.11	0.11	-0.95	1.00	7.5
15	-0.74	0.76	0.09	-0.09	-0.89	0.92	-0.02	0.01	0.34	-0.33	0.24	-0.25	0.02	0.00	-0.15	0.14	-0.27	0.32	-0.20	0.18	-1.29	1.33	8.7
16	-0.79	0.80	0.06	-0.09	-1.18	1.19	0.01	-0.03	0.39	-0.42	0.25	-0.28	-0.16	0.15	-0.18	0.16	-0.32	0.35	-0.18	0.16	-1.58	1.57	12.1
17	-0.87	0.90	0.16	-0.15	-0.62	0.65	-0.01	0.02	0.25	-0.24	0.20	-0.22	0.11	-0.10	-0.16	0.17	-0.14	0.21	-0.26	0.24	-1.18	1.23	11.6
18	-1.13	1.18	0.17	-0.26	-0.94	0.76	-0.09	-0.01	0.29	-0.32	0.19	-0.29	0.00	-0.09	-0.30	0.20	-0.18	0.20	-0.38	0.28	-1.64	1.51	34.7
19	0.52	-0.45	-0.43	0.44	-1.15	1.19	0.30	-0.19	0.42	-0.32	0.27	-0.26	-0.41	0.53	0.03	-0.03	-0.66	0.79	0.04	-0.04	-1.59	1.77	27.9

Figure 25: D^* signal shape variation, and the change in the WS/RS ratio for the twenty time bins. The difference between the WS/RS ratio and the reference value (unmodified signal shape) is expressed in the table in % with respect to the reference value.

5.3.2 $K\pi$ Background

We expect an effect due to uncertainty in the background shapes for the $K\pi$ plots. Since the signal-to-background ratio is different for WS and RS, the ratio could be affected as well. However, since the background parameters are floating for every $K\pi$ fit, the systematic uncertainty is should be smaller than if we had assumed a particular background shape a priori.

We made two studies to investigate partially reconstructed charm background. The first was for $D^+ \to K\pi\pi$. The first two tracks form the D^0 candidate, while the second pion is treated as the D^* tag. These events fall outside of the RS mass window, but swapping the K and π particle assignments can cause a mass shift which puts these events in the WS mass window. Fortunately, we can see a clear D^+ peak when we knew what to look for, as shown in Fig. 26. We obtain the number of D^+ background in bins of WS $K\pi$ mass, similar to our normal yield technique. The study showed 0.274% WS background, per RS $K\pi$. That background fit is well described by an exponential fit. Fig. 27 shows the WS and RS scatter plot, and the fit for the D^+ background.

The D^+ background will have a different lifetime distribution than the D^0. We measured the number of D^* for each time bin, as shown in Fig. 28, for use in the Toy MC. Fig. 29 shows the output of 400 Toy MC events, where we replace the appropriate amount of the (WS) combinatorial background (quadratic fit) with the exponential distributions of the D^+. We still see a shift of $|\Delta R/R| = 0.28\%$. The systematic bias might be zero, but to be conservative, we will add this value in quadrature to the current errors. The study of the individual time bins (to look for time-correlated systematic effects) is not completed, but the first impression is that this systematic effect is negligible.

While it is possible to impose a lower limit on the RS $K\pi$ mass that would eliminate this background, it would also cut away signal. (The WS signal has a wide distribution when plotted with RS $K\pi$ mass.) Depending on how hard a D^+ cut is applied, around 5% of the signal would be lost. Since the assigned systematic error for this background is small (and might actually be zero), we decide not to apply that cut.

The second was for D^0 that decay to modes other than $K\pi$. The used the full Pythia MC samples. We obtain the number of background events relative to the RS $D^0 \to K\pi$ (which is also in that MC). This MC sample had 1.39% RS background and 2.35% WS background, per RS $K\pi$. We also get the distributions for the RS and WS mass plots. Those background fits are well described by an exponential fit. Fig. 30 shows the WS and RS scatter plot, and the fit for the D^+ background.

Fig. 31 shows the output of 800 Toy MC events, where we replace the appropriate amount of

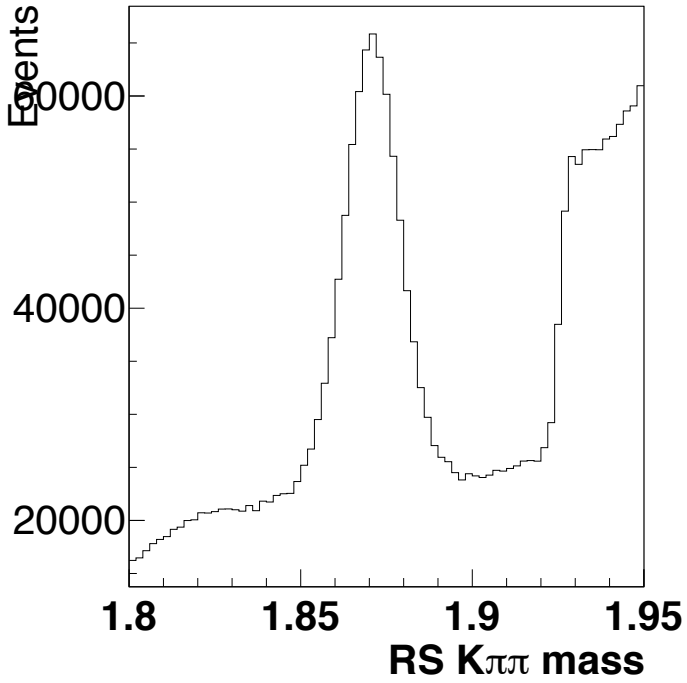

Figure 26: D^+ signal peak for the three-track RS mass plot. The climb in the background above 1.92 GeV is an artifact due to the event selection for this study, which is also related to the cross structure in the RS-WS scatter plot.

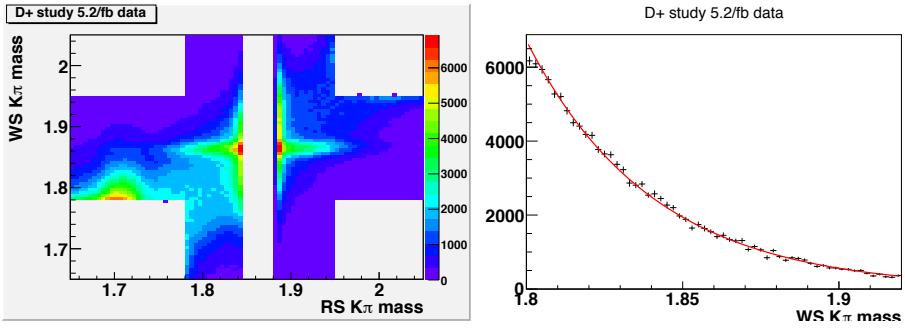

Figure 27: D^+ background in WS $K\pi$ mass plots. The left plot shows an excess of events at RS $m_{K\pi} = 1.7$ GeV, which can spill into the WS mass window used for the analysis. These events formed a clear mass peak when reconstructed as $D^+ \to K\pi\pi$. The right plot shows the D^+ versus WS $m_{K\pi}$ yield plot, with a red line for an exponential fit.

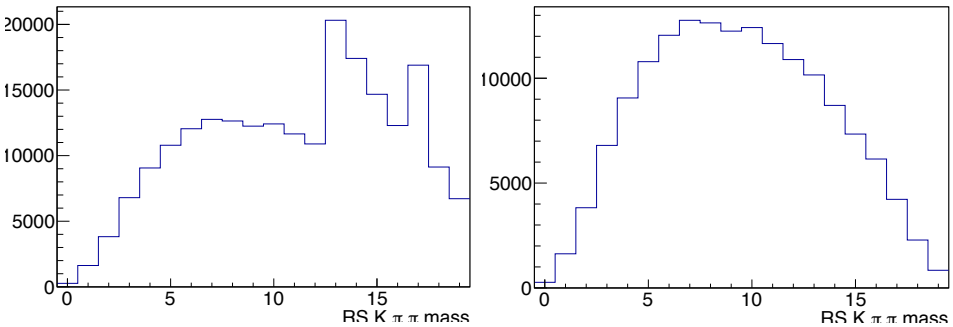

Figure 28: Fit number of D^+ for the twenty time bins used in the analysis. The left plot are the "raw" numbers per bin, the right plot is normalized for the varying width of the time bins.

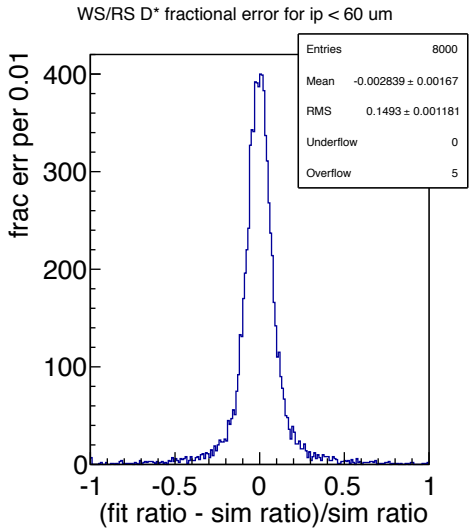

Figure 29: Generated 400 toy MC events, with entries for all 20 time bin ratios. The comparison is between the generated amount of signal in a particular simulation, and the analyzed value for that simulation. Based on the D^+ data studies, we replace an appropriate amount of the combinatorial background (quadratic fit) with the exponential distributions for $m_{K\pi}$.

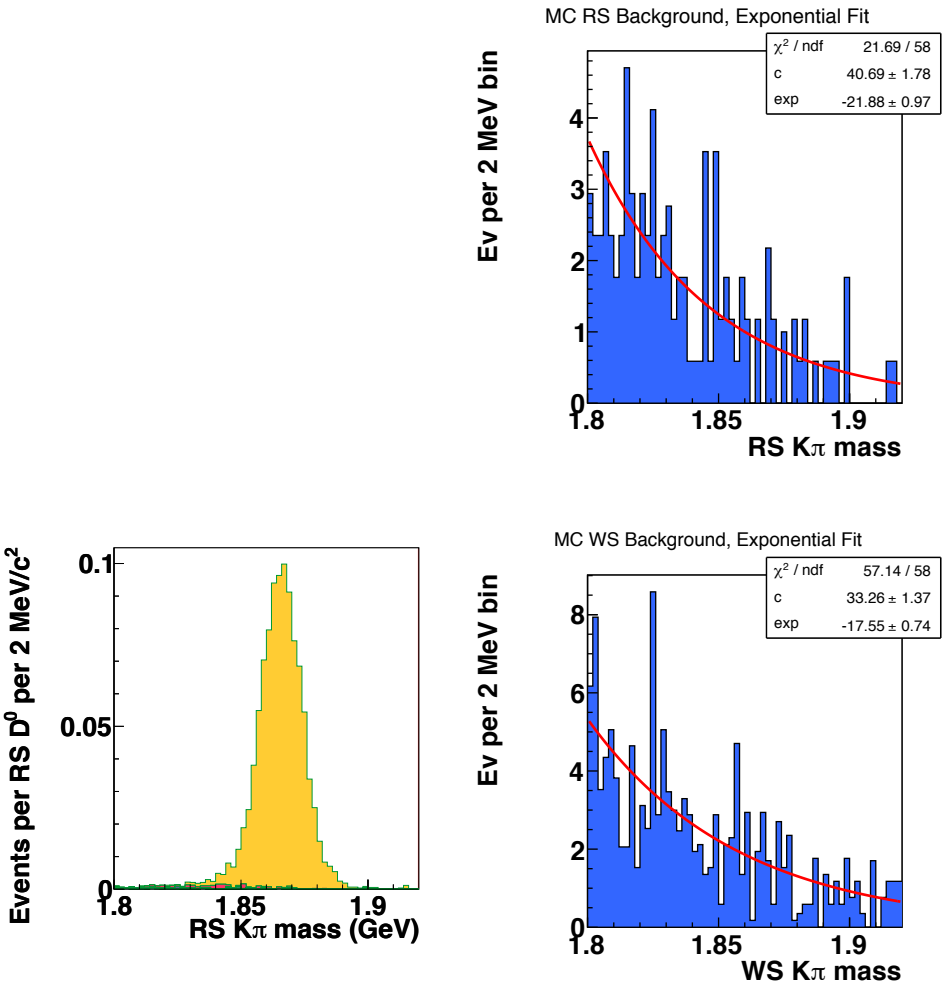

Figure 30: Partially reconstructed charm background from full MC. The left plot shows the RS D^0 signal (yellow) compared to the partially reconstructed charm background (all other colors, near the x-axis). The right plot shows the exponential fit to the RS and WS $K\pi$ background distributions.

the combinatorial background (quadratic fit) with the exponential distributions from the partially reconstructed charm studies. We still see a shift of $|\Delta R/R| = 0.09\%$, consistent with zero. To be conservative, we will add this value in quadrature to the current errors.

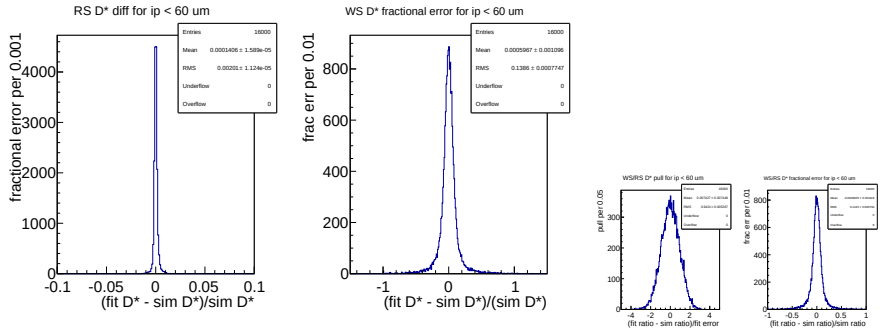

Figure 31: Generated 800 toy MC events, with entries for all 20 time bin ratios. The comparison is between the generated amount of signal in a particular simulation, and the analyzed value for that simulation. Based on the partially reconstructed charm studies, we replace an appropriate amount of the combinatorial background (quadratic fit) with the exponential distributions. The left plot is RS D^*, the middle plot is WS D^*, and the right plot is the ratio.

5.3.3 Secondary Fraction Fit

The RS d_0 fits were redone with a single Gaussian for the non-prompt distributions. The fits were poorer than our normal fits, but the single Gaussian fits are an alternate fit model to test how sensitive our analysis is to the impact parameter fits. Fig. 32 shows the change in the secondary fraction curve using the alternate fit model. The table in Fig. 33 shows a comparison of the mixing fit results between the normal and alternate secondary fraction curves. The difference between the mixing parameter values is less than 1% of the error for y', and about 6% of the error for x'^2.

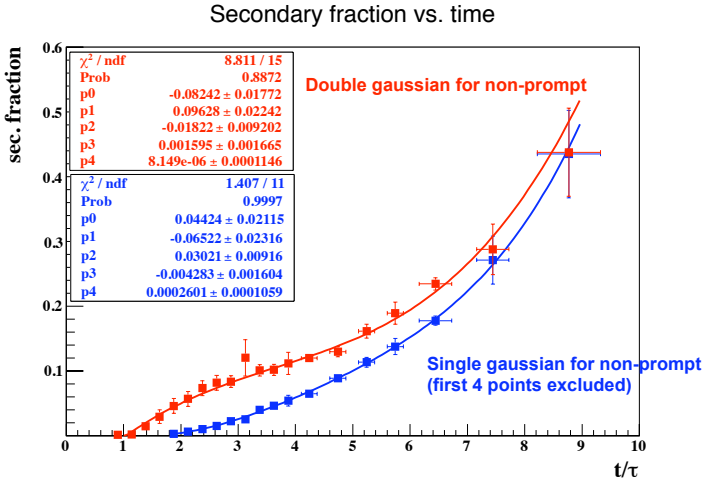

Figure 32: Comparison of the secondary fraction fit curve, between the normal fits with a double Gaussian for the non-prompt shape (red) and the alternate fit with a single Gaussian (blue).

	Non-prompt 2 gaus	Non-prompt 1 gaus
R_D	3.68±0.33	3.68±0.32
y'	2.39±3.90	2.41±3.71
x'^{2}	0.13±0.16	0.12±0.15
χ^2/ndf	17.15/17	17.19/17
$\Delta\chi^2$ (difference between no- mixing and best fits)	35.83	35.79
Significance from $\Delta\chi^2$	5.52 σ	5.52 σ

Figure 33: Comparison of the mixing fit results, using the normal fits with a double Gaussian for the non-prompt shape (middle column) and the alternate fit with a single Gaussian (right column).

5.3.4 Non-prompt MC Time Histograms

The MC decay time histograms used to get the behavior of non-prompt charm might be different than the actual distribution. We assume that the MC is accurate enough that the general shape of the distribution is correct, but the time scale might be off. To measure a systematic effect, the h_{ij} histograms were used with the x-axis time scale expanded or contracted by 10%. (The time at the center of each bin was multiplied by 1.1 or 0.9.) Table. 9 shows the change in the mixing parameters when the fitting function has the modified MC non-prompt times. The change in value is negligible compared to the parameter uncertainty.

Fit	$R_D(10^{-3})$	$y'(10^{-3})$	$x'^2(10^{-3})$	χ^2 / dof
Normal	3.68 ± 0.33	2.39 ± 3.90	0.13 ± 0.16	17.15 / 17
$t' \times 1.1$	3.67 ± 0.33	2.44 ± 3.85	0.12 ± 0.15	17.04 / 17
$t' \times 0.9$	3.68 ± 0.34	2.36 ± 3.94	0.13 ± 0.16	17.00 / 17

Table 9: Mixing parameters fits with modified MC non-prompt decay times.

5.3.5 Detector charged track asymmetries

In CDF note 6391 [22], they measure the charge asymmetry in the detector. This will result in a difference in the efficiency of finding the charged pions used to tag the D^*. On page 26, they quote the charge asymmetry as being $A = \frac{N_+ - N_-}{N_+ + N_-} = 1$ % (within errors). Angelo DiCanto updated this study with more data, and quotes $\Delta(\pi_s) = -2.078\%$ in his thesis.

The charged kaons and pions have different nuclear interactions. On page 75 of CDF note 8464 [23], the ratio of the efficiencies to reconstruct $K^+\pi^-/K^-\pi^+ = 1.0166$. Our measured WS/RS ratio is

$$R = (N_{D^{*+},D^0\to K^+\pi^-} + N_{D^{*-},D^0\to K^-\pi^+})/(N_{D^{*+},D^0\to K^-\pi^+} + N_{D^{*-},D^0\to K^+\pi^-})$$

If we assume that we started with equal numbers of mesons and anti-mesons, then

$$\Delta R/R = (1.0166 + 1.02)/(1 + (1.0166)(1.02)) - 1 = -0.016\%$$

This systematic is negligible compared to current errors. However, if we were to separate the D^{*+} and D^{*-} events, then these effects would no longer cancel in the ratio.

5.4 Comparison with Other Experiments

Table 10 shows the comparison of recent experiments. The mixing parameters are highly correlated, so some caution must be used when drawing conclusions about the significance of the differences between parameter values.

Experiment	R_B (10^{-3})	R_D (10^{-3})	y' (10^{-3})	x'^2 (10^{-3})	No-Mix Significance
Belle (2006)	3.77 ± 0.09	3.64 ± 0.17	0.6 ± 4.0	0.18 ± 0.22	2.0
BaBar (2007)	3.53 ± 0.09	3.03 ± 0.19	9.7 ± 5.4	-0.22 ± 0.37	3.9
CDF (2007)	4.15 ± 0.10	3.04 ± 0.55	8.5 ± 7.6	-0.12 ± 0.35	3.8
LHCb	4.25 ± 0.04	3.52 ± 0.15	7.2 ± 2.4	-0.09 ± 0.13	9.1
CDF (now)	4.27 ± 0.06	3.69 ± 0.33	2.27 ± 3.90	0.13 ± 0.16	6.1

Table 10: Mixing parameters from recent experiments. R_B refers to the fit of the data points, assuming no-mixing (no time dependence). R_D is the part of the three parameter mixing fit, giving the value of the WS/RS at time 0. The significance of excluding the no-mixing hypothesis is given in Gaussian sigma.

5.5 No-Mixing interpretation of the results

We can ask if the results are consistent with the hypothesis that there is no mixing. We will use three different measures. They are described in more detail in CDF note 8879. The different methods came up with approximately the same significance for no-mixing for the previous blessed result, so we use all three as a cross-check.

5.5.1 χ^2 difference

The fastest check we make is to use the difference in χ^2 between the no-mixing point and the best fit (or the best fit in the physically allowed region). While it is the easiest to determine, it does assume that the errors are Gaussian, which may not be valid for very small no-mixing probabilities.

If we have two fit functions which are similar, and differ by n additional parameters, we assume that the difference in χ^2 has a χ^2 distribution with n degrees of freedom. The statistical contribution to the χ^2 will be the same for both fits, and cancel in the difference, leaving the systematic difference of the two functions. For this analysis, the no-mixing fit is a constant, while the best fits is a 2nd order polynomial. The difference between those fits are the two additional parameters used in the best (mixing) fit. We can then compute the probability that a χ^2 distribution with 2 degrees of freedom will have a value the same or worse than the measure $\Delta\chi^2$.

The best no-mixing fit has $\chi^2 = 52.98$, while the best fit with mixing has $\chi^2 = 17.10$. $\Delta\chi^2 = 35.88$ for 2 degrees of freedom is at 5.53σ.

5.5.2 Bayesian contours

We calculate the Bayesian probability that a particular set of values for (y', x'^2) are consistent with our ratio plot. We use the χ^2 of the fit, integrate over the mixing parameter R_D (as a nuisance

parameter), and assume a prior uniform for y' and x'^2. We then generate contours containing the highest probability points, such that the region enclosed corresponds to n Gaussian σ

Fig. 34 shows the Bayesian contours for the most recent result. The highest probability contour that excludes the no mixing point is equivalent to 6.1σ.

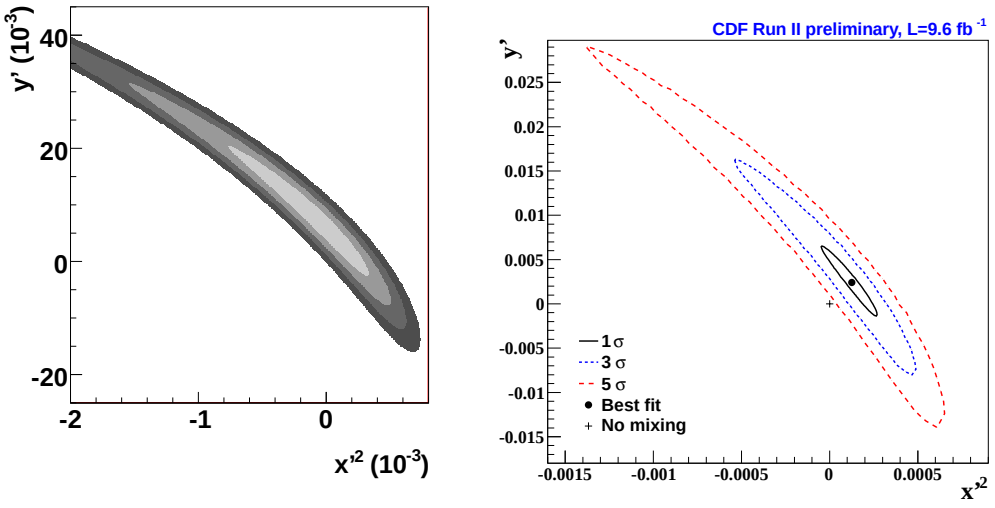

Figure 34: Bayesian contours from data, showing the posterior probabilities The left plot is from the previously published 1.5 fb^{-1} result, and shows the 1 through 4 Gaussian sigma contours. The right plot is from the full data set, and shows the 1, 3, and 5 sigma contours.

5.5.3 P-Value

During the process to write the previous paper [4], the Godparent committee approved a procedure to test the Frequentist p-value. A simple toy model is made of our final ratio plot for prompt D^*. The generated ratio points are assumed to have a Gaussian distribution, with the width equal to our data error bars, and a mean at the (best data fit) no-mixing value. For each toy model generated, we make mixing (quadratic) and no-mixing (constant value) fits. The difference in χ^2 between those fits is calculated. We then determine how many of those models have $\Delta\chi^2$ greater than or equal to what we observe with data.

Fig. 35 shows the distribution with almost 600 million simple toy MC experiments. There were only five experiments with $\Delta\chi^2$ greater than or equal 35.88, which is consistent with a no-mixing significance of 5.6σ.

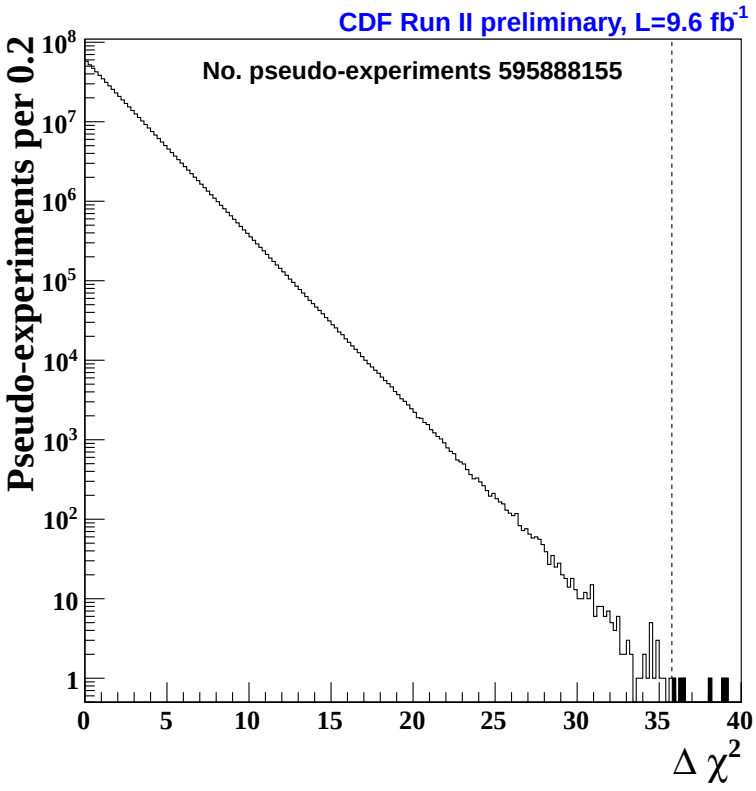

Figure 35: P-value test for no-mixing.

Appendices

A PR Plots

There are certain plots in this note that will be useful to be included in journal publications or conference talks. Those plots are listed here, with changes in the format making them more suitable for use outside of the collaboration.

At the time of this writing, these plots have not yet been blessed by the B-Group.

- Fit to RS D0 time-integrated and Dm-summed

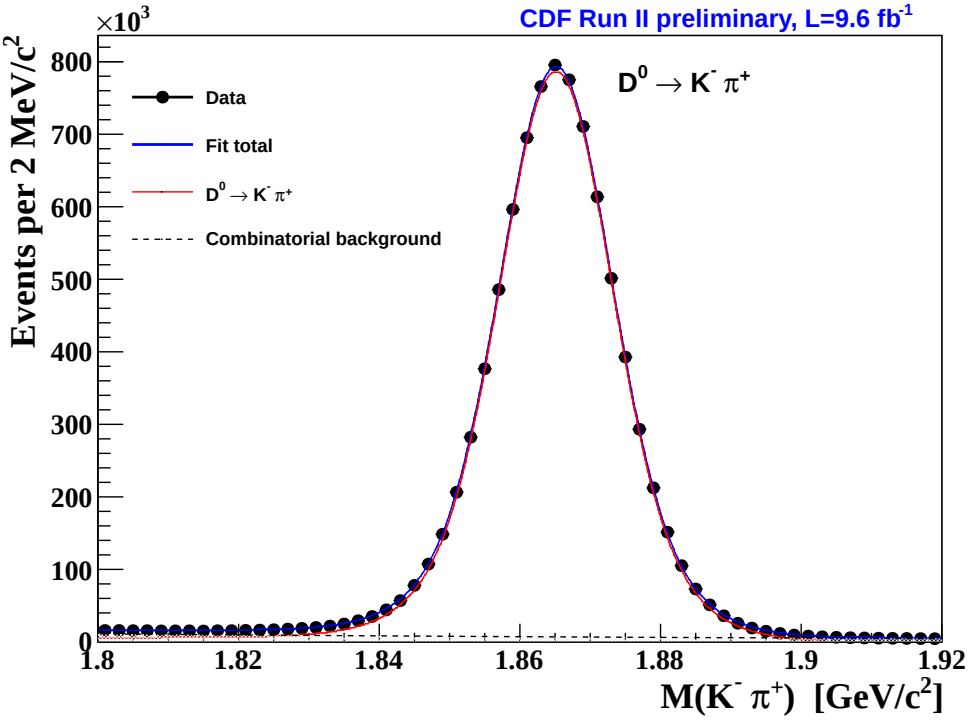

- Fit to WS D0 time-integrated and Dm-summed

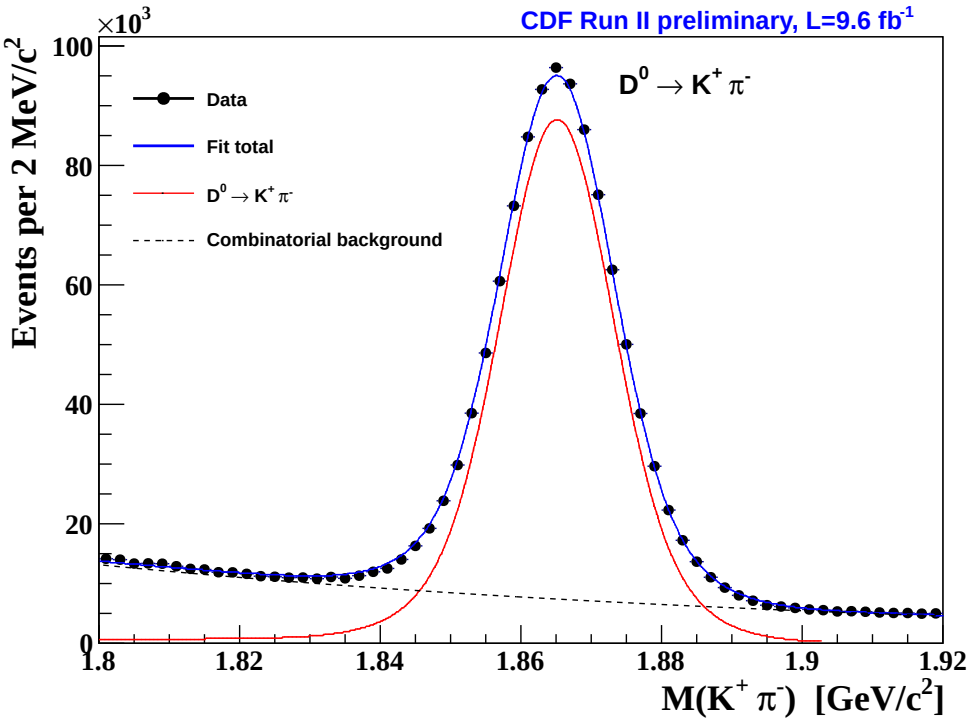

- Fit to DeltaM distribution for RS (time-integrated)

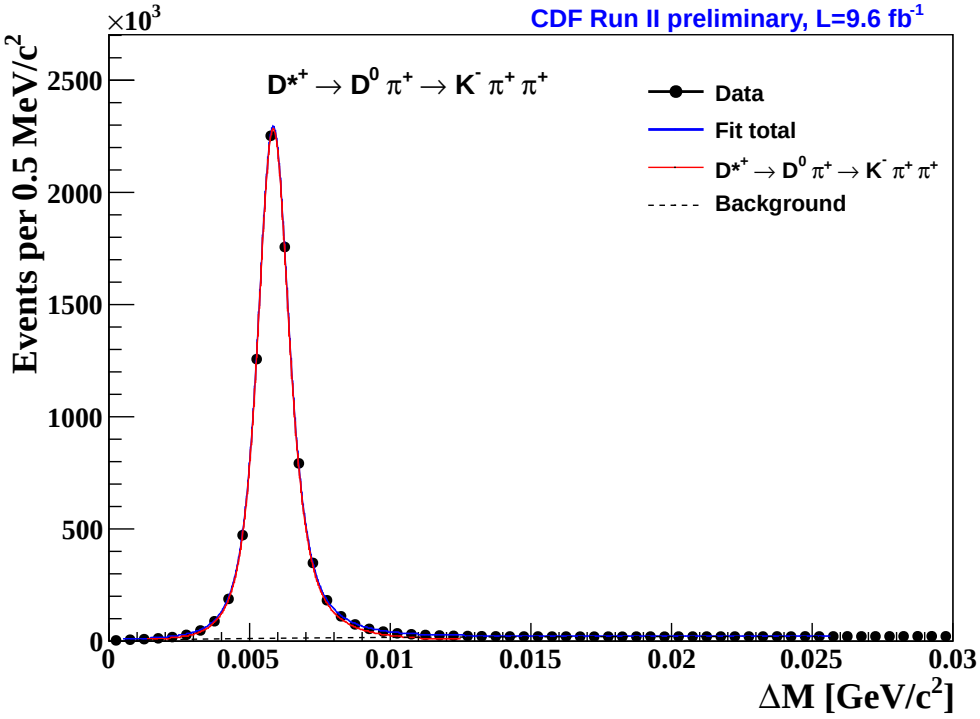

- Fit to DeltaM distribution for WS (time-integrated)

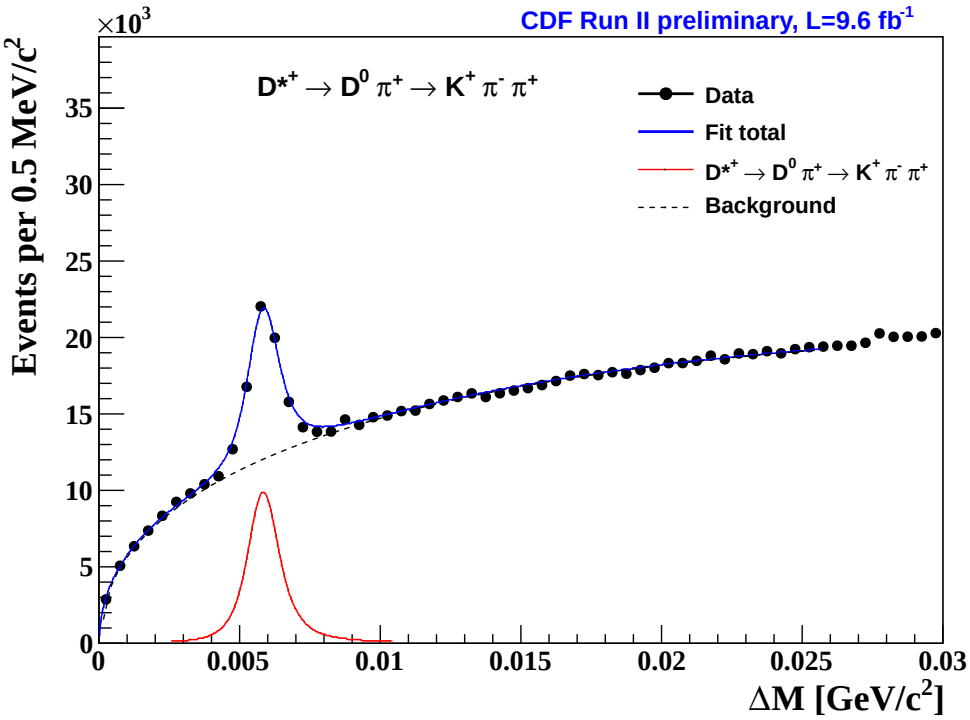

- Fit to the impact parameter distribution (time-integrated)

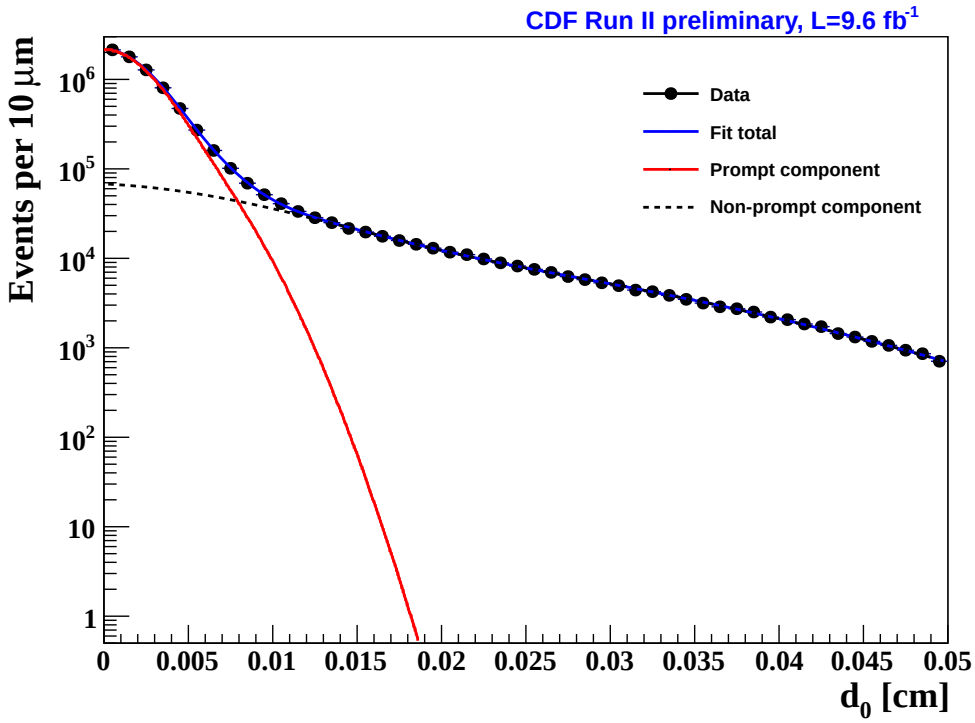

- Secondary fraction vs. time and parametrization

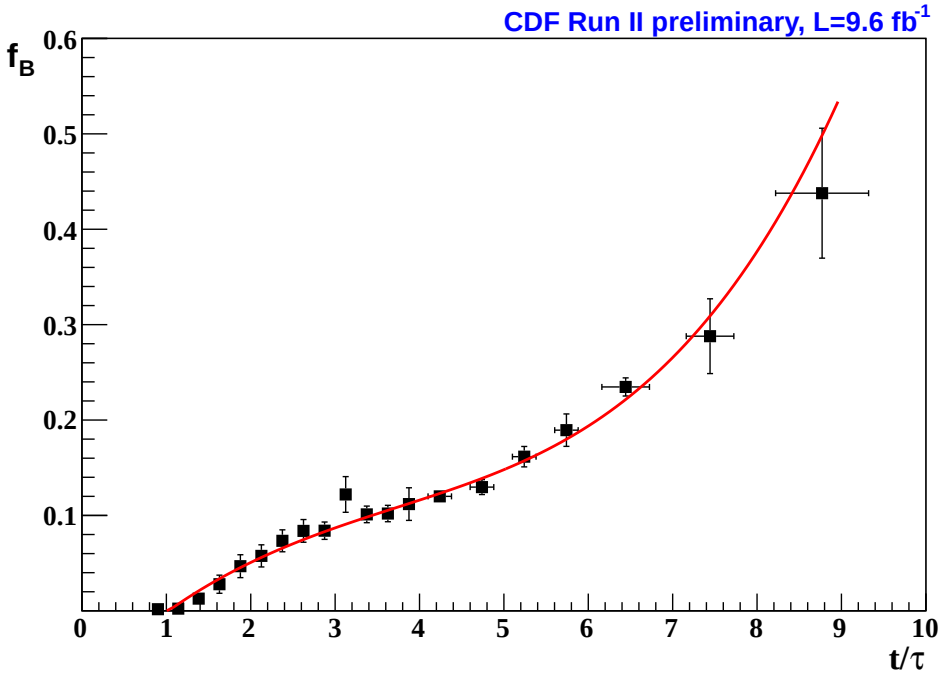

- Fit to WS/RS ratio vs. time (mixing and no-mix fits)

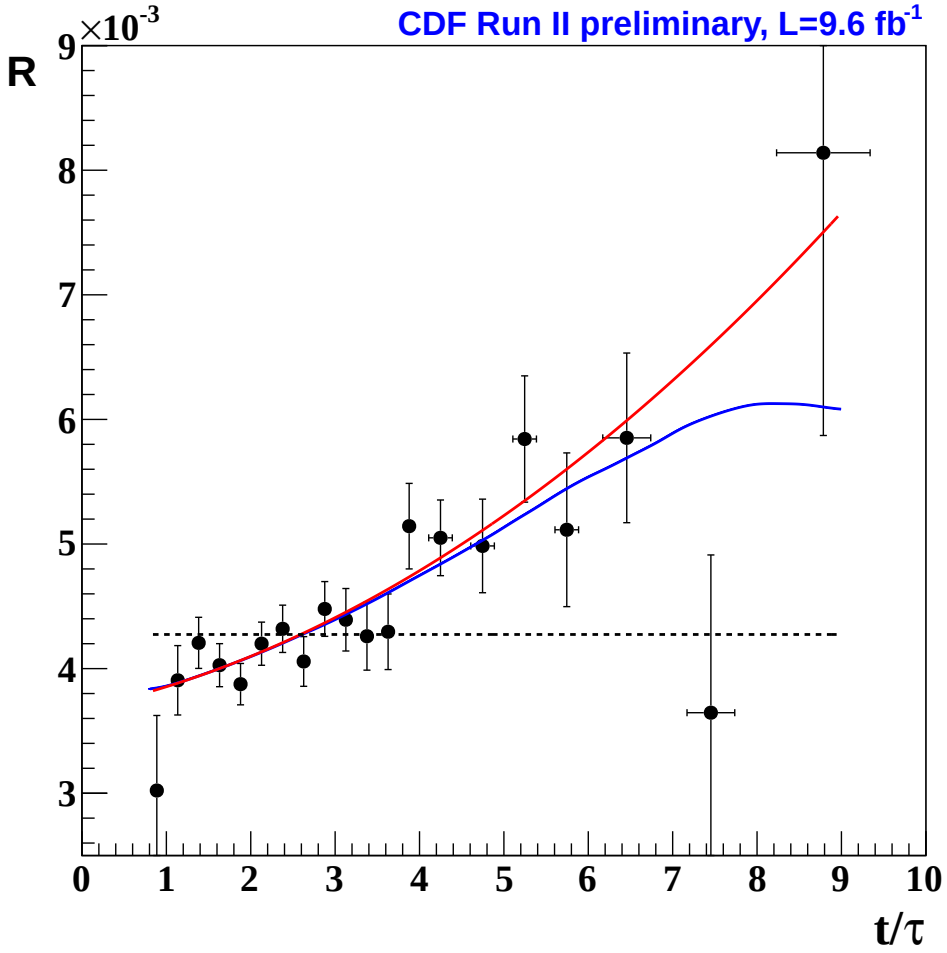

- Probability contour plot

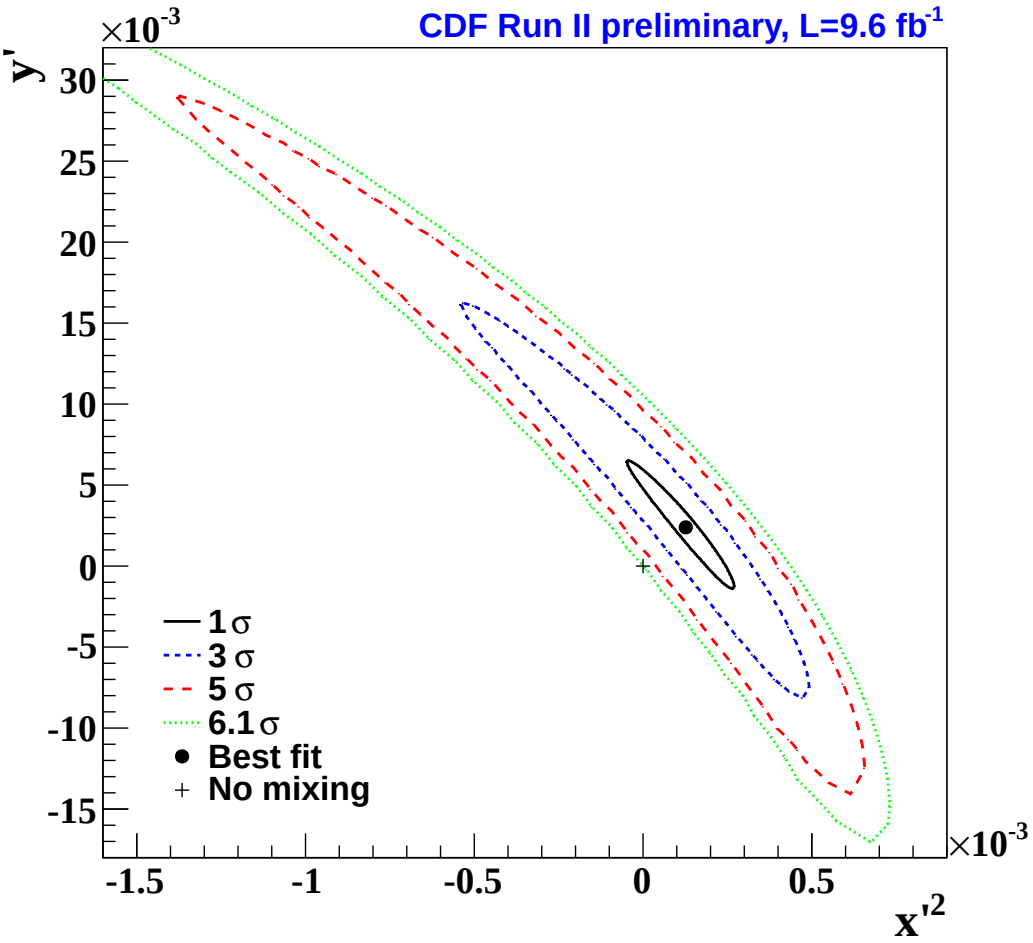

- Histograms of DeltaChi2 for simulated pseudo-experiments (p-value test)

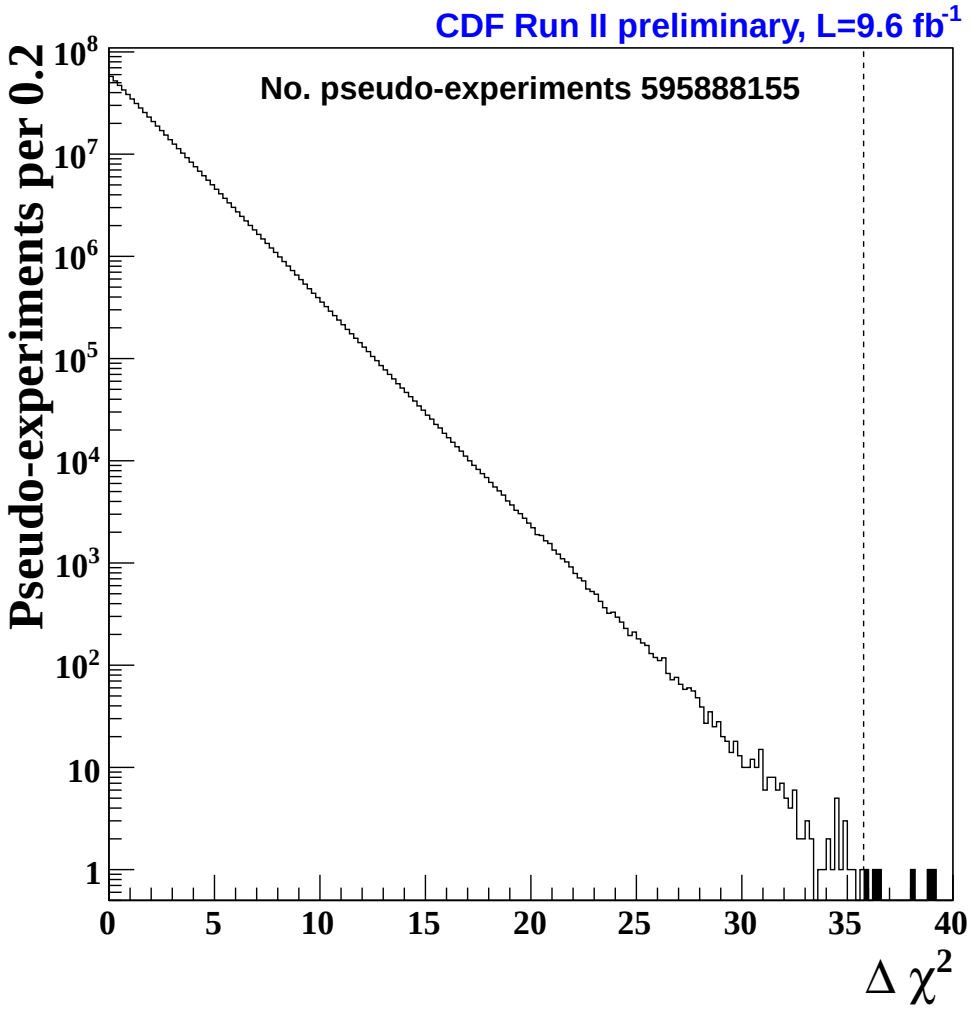

- Table for the final fitted parameters and correlation matrix

Fit type	χ^2/ndf	Parameter	Fitted values $\times 10^{-3}$	Correlation coefficient R_D	y'	x'^2
Mixing	17.17/17	R_D	3.68 ± 0.33	1	-0.966	0.891
		y'	2.39 ± 3.90		1	-0.971
		x'^2	0.13 ± 0.16			1
No-mixing	52.98/19	R_D	4.274 ± 0.058			

Table 1: Results of the time-dependent fit to the data. The uncertainties include statistical and systematic sources.

B Mass-Difference Integrated $M_{K\pi}$ Fit

This appendix shows the $M_{K\pi}$ fits for the twenty time bins (from 0 to 19).

For all plots, the events require $d_0 < 60\mu$m and $\Delta m < 30$ MeV (mass-difference summed). The plots on the left are RS, and the plots on the right are WS. The dark blue curve is the signal + background fit, the red curve is signal only.

For each time bin, the WS signal shape is required to be the same as the RS signal shape.

Appendix B: Mass-Difference Integrated $M_{K\pi}$ Distributions

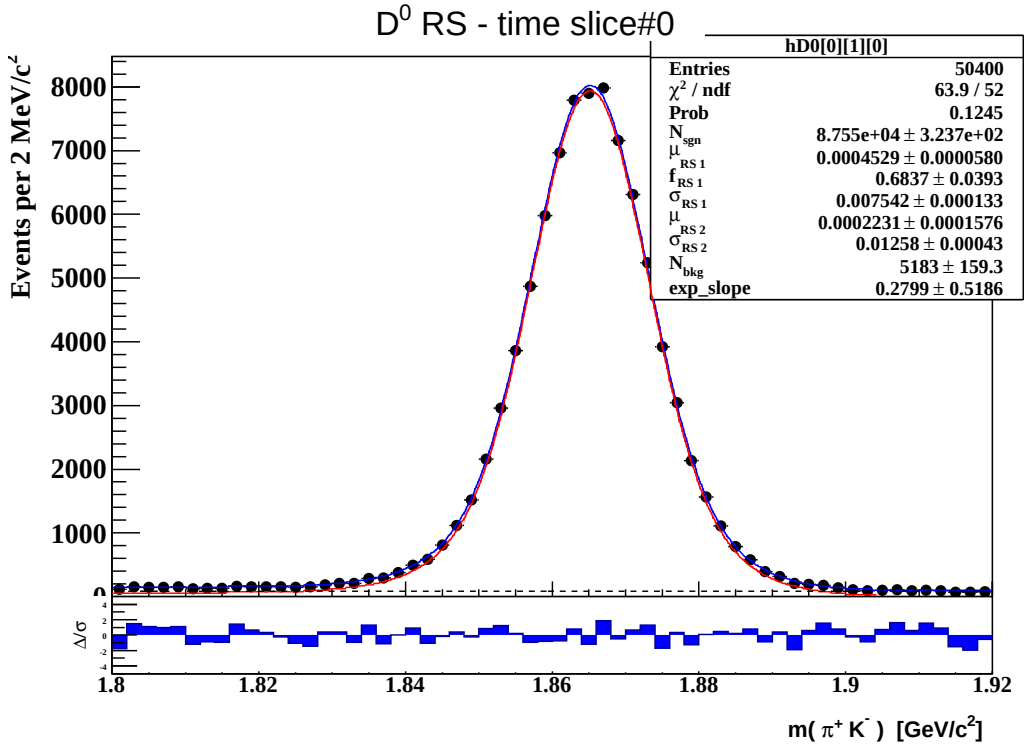

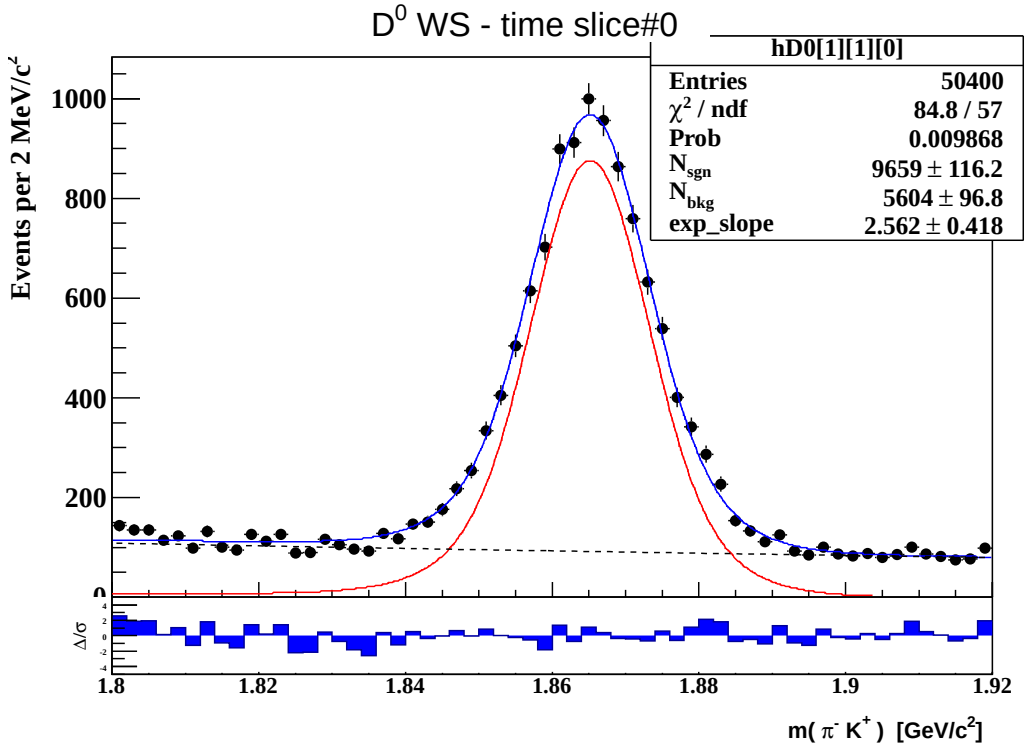

Appendix B: Mass-Difference Integrated $M_{K\pi}$ Distributions

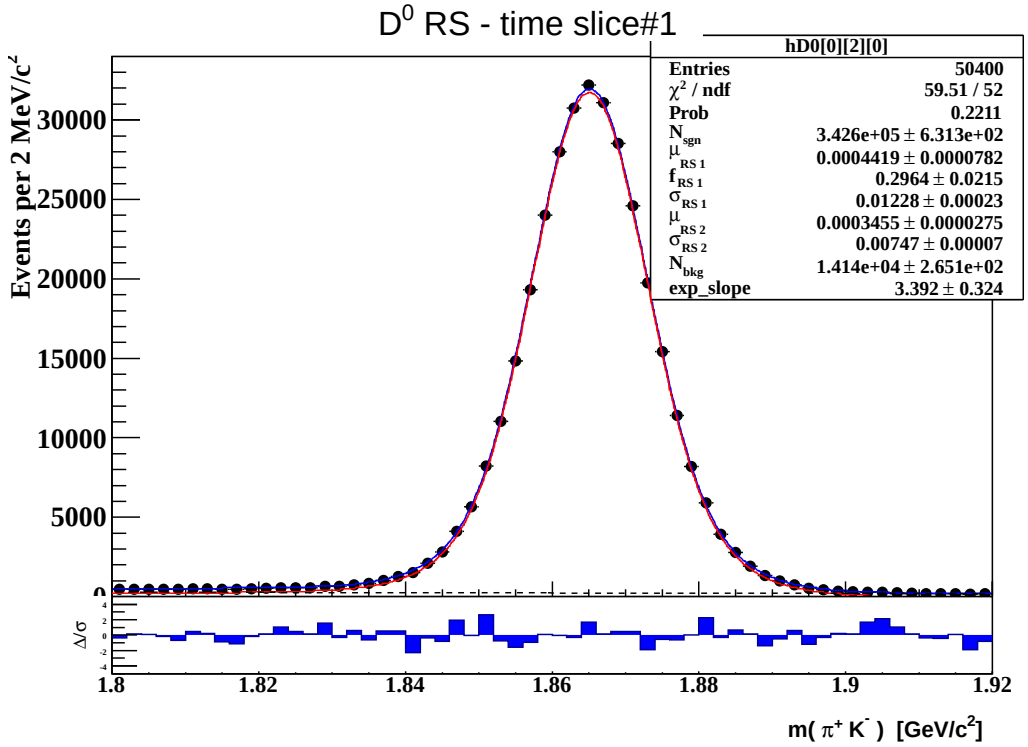

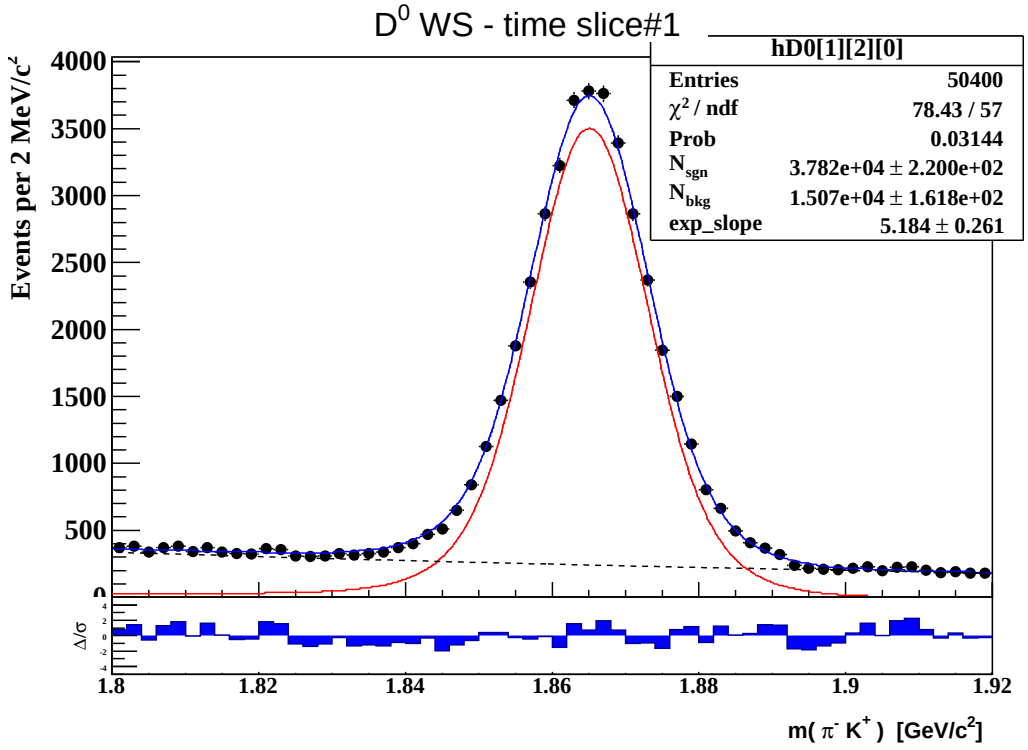

Appendix B: Mass-Difference Integrated $M_{K\pi}$ Distributions

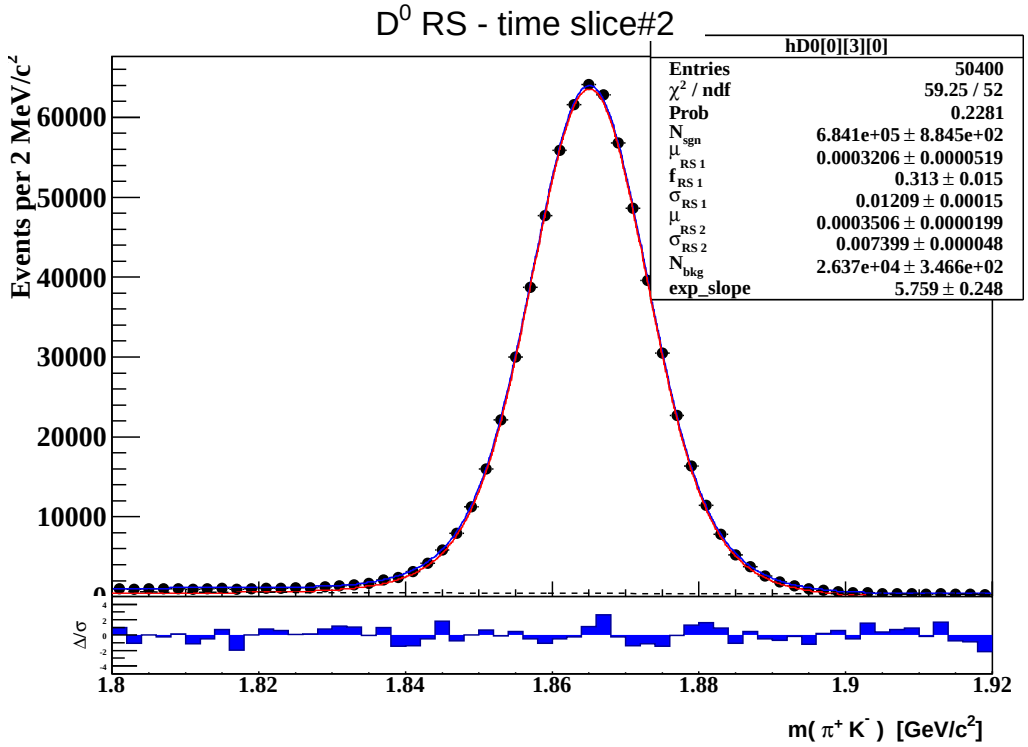

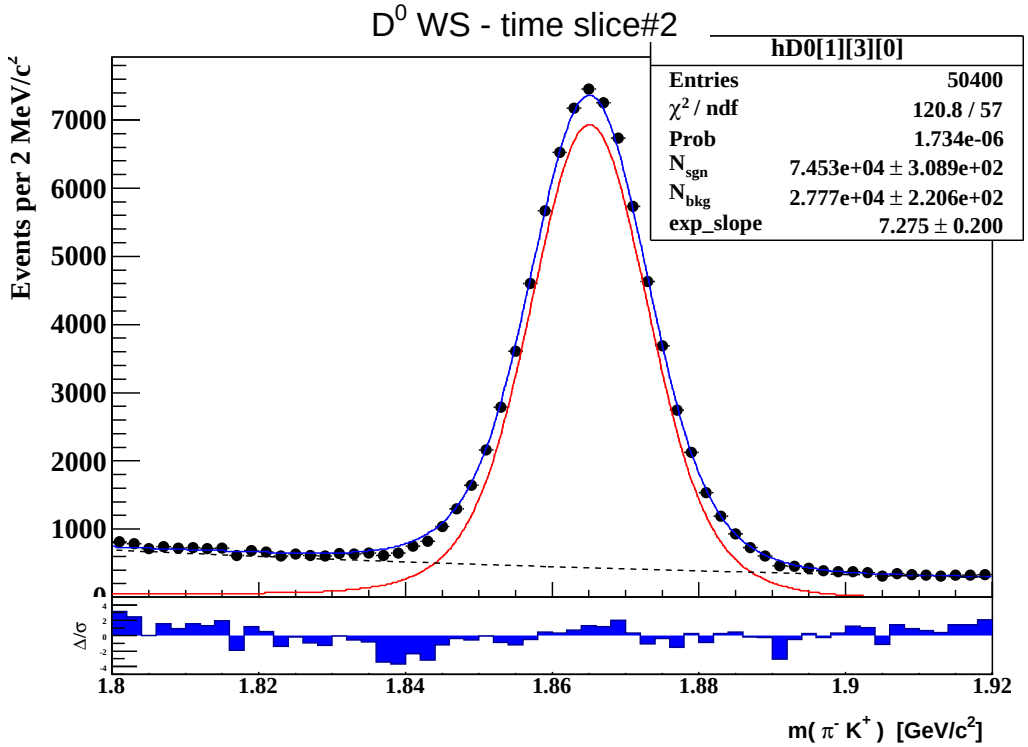

Appendix B: Mass-Difference Integrated $M_{K\pi}$ Distributions

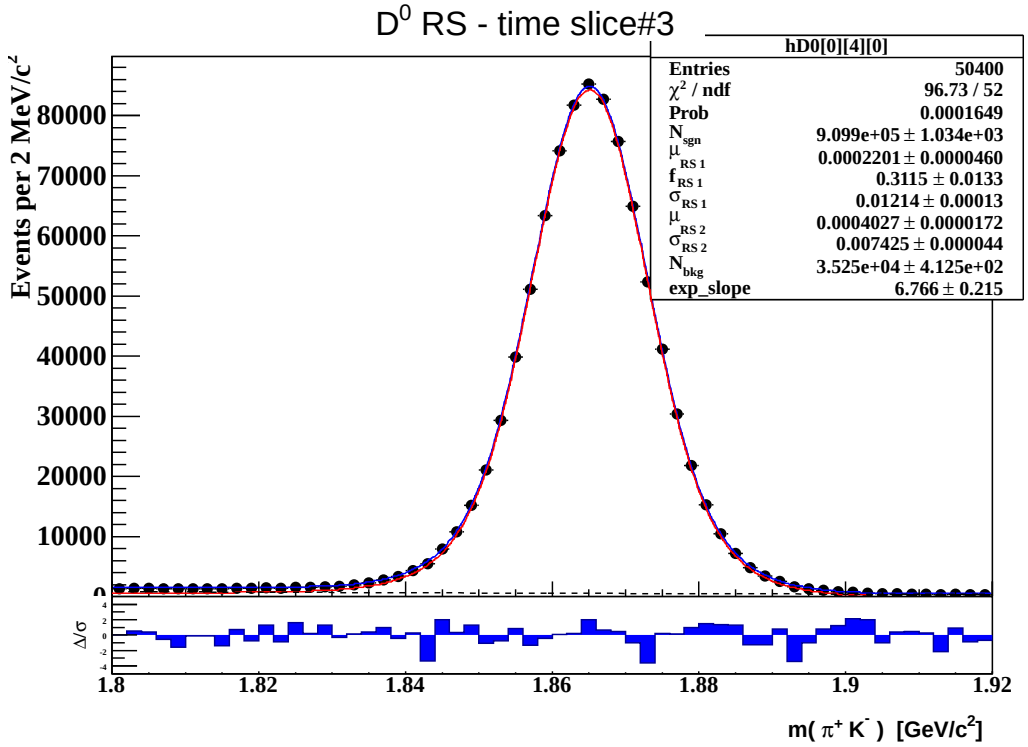

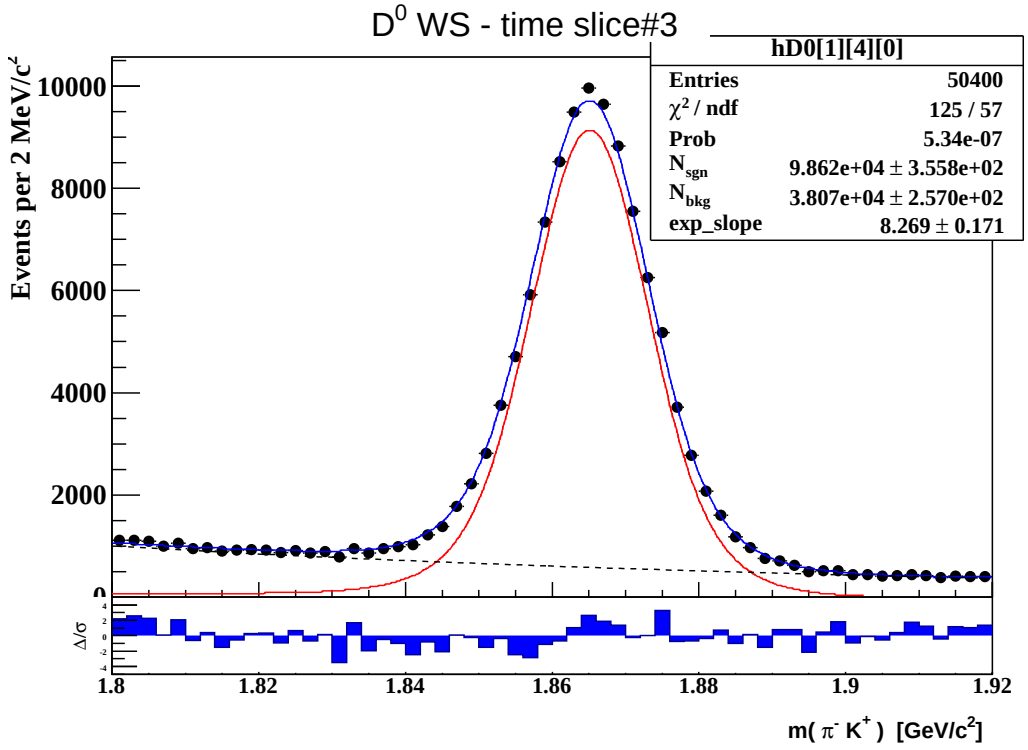

Appendix B: Mass-Difference Integrated $M_{K\pi}$ Distributions

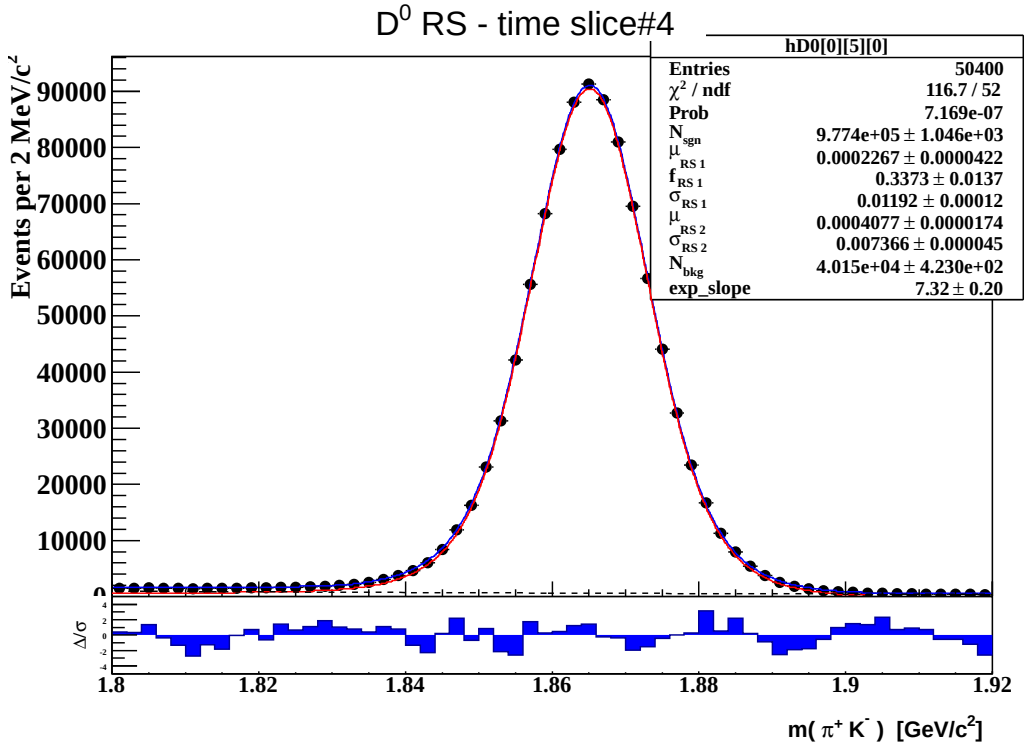

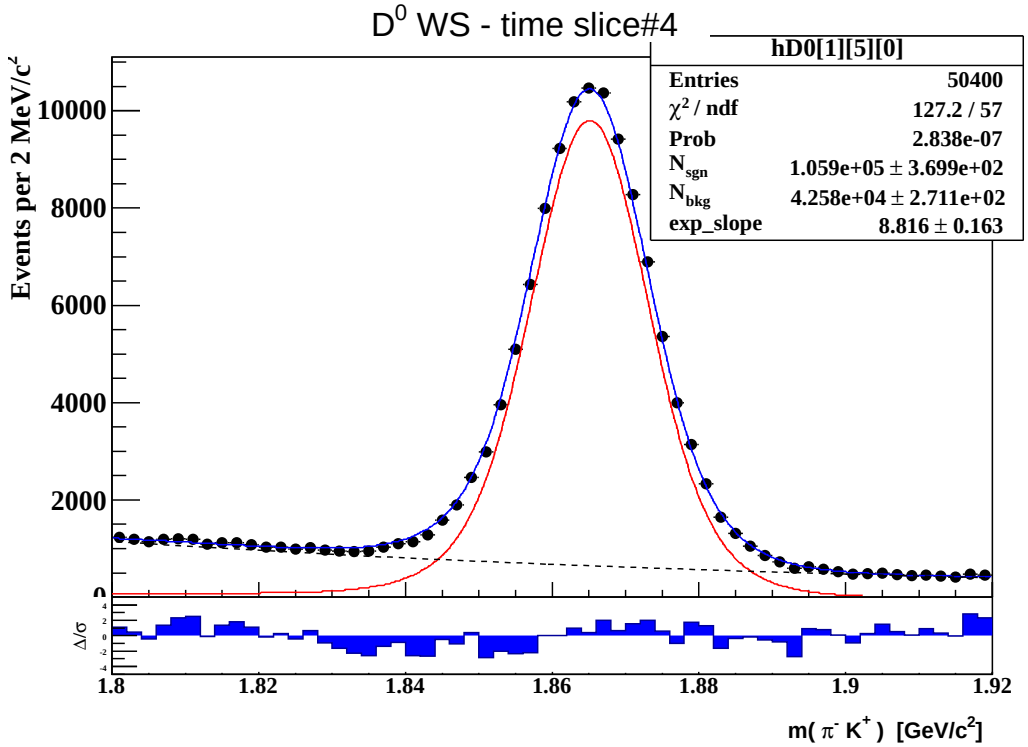

Appendix B: Mass-Difference Integrated $M_{K\pi}$ Distributions

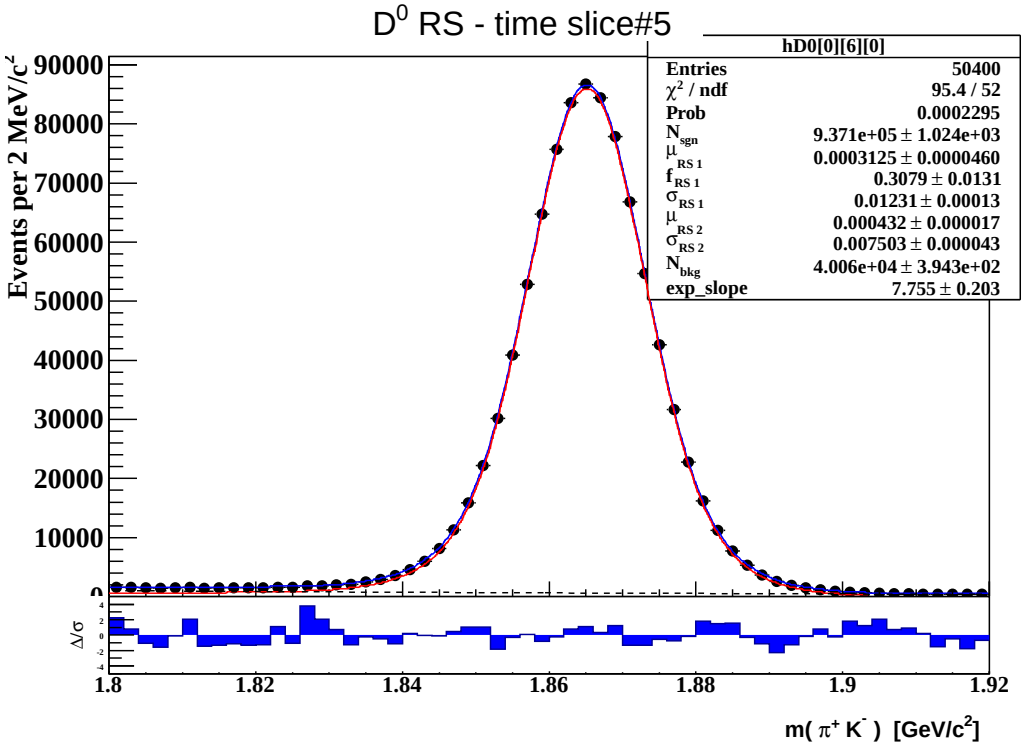

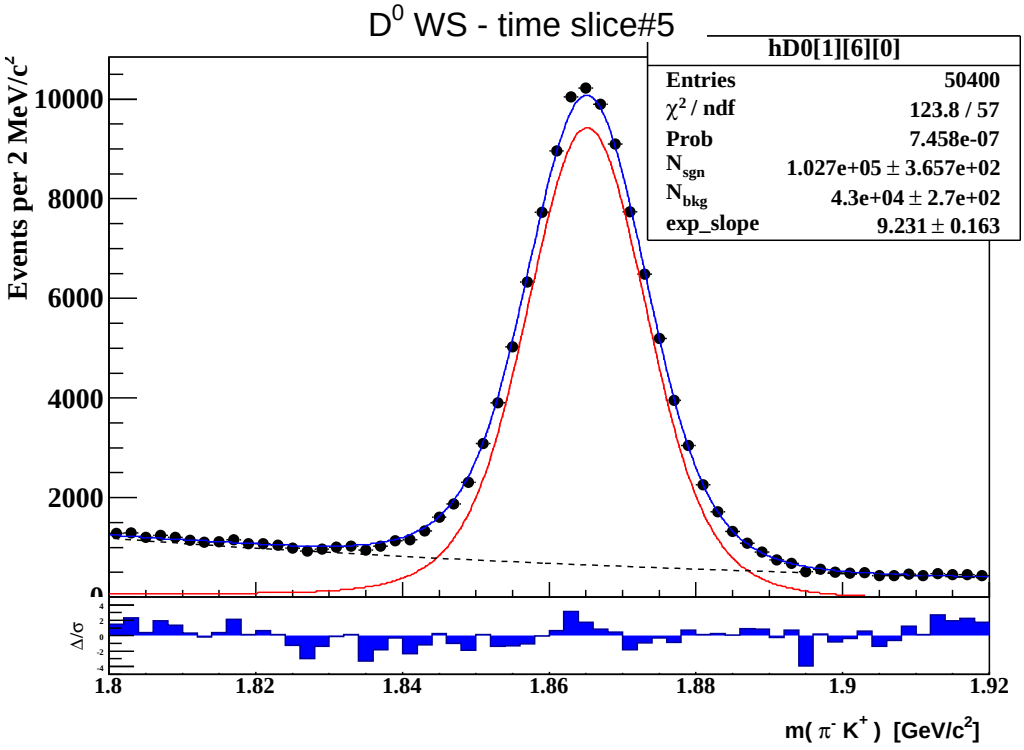

Appendix B: Mass-Difference Integrated $M_{K\pi}$ Distributions

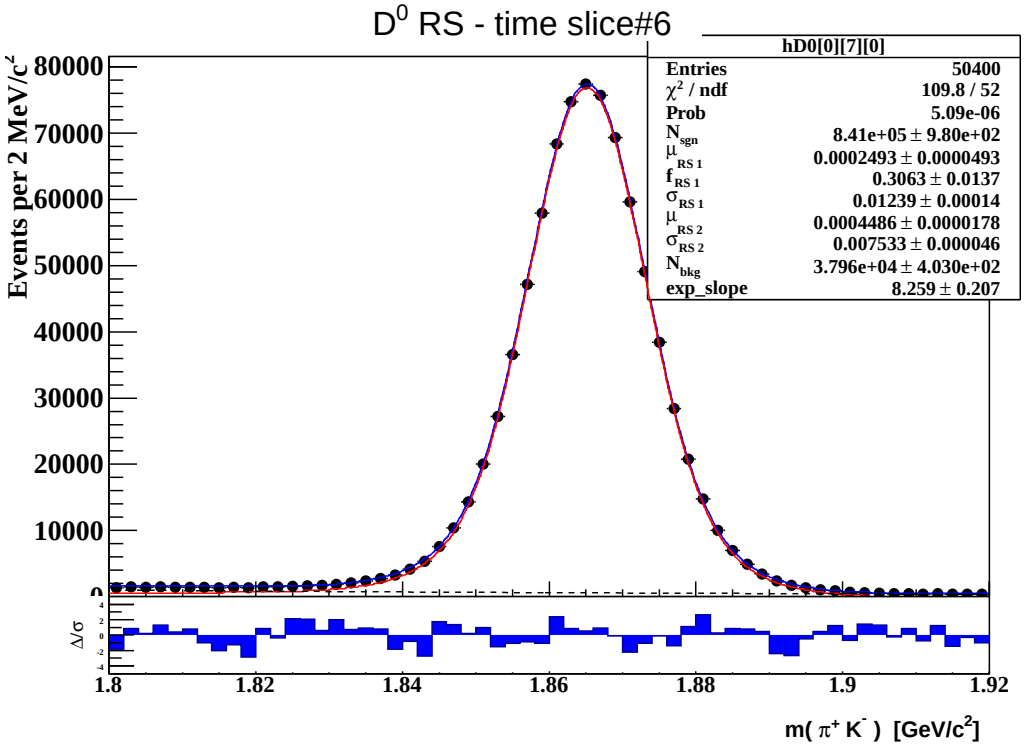

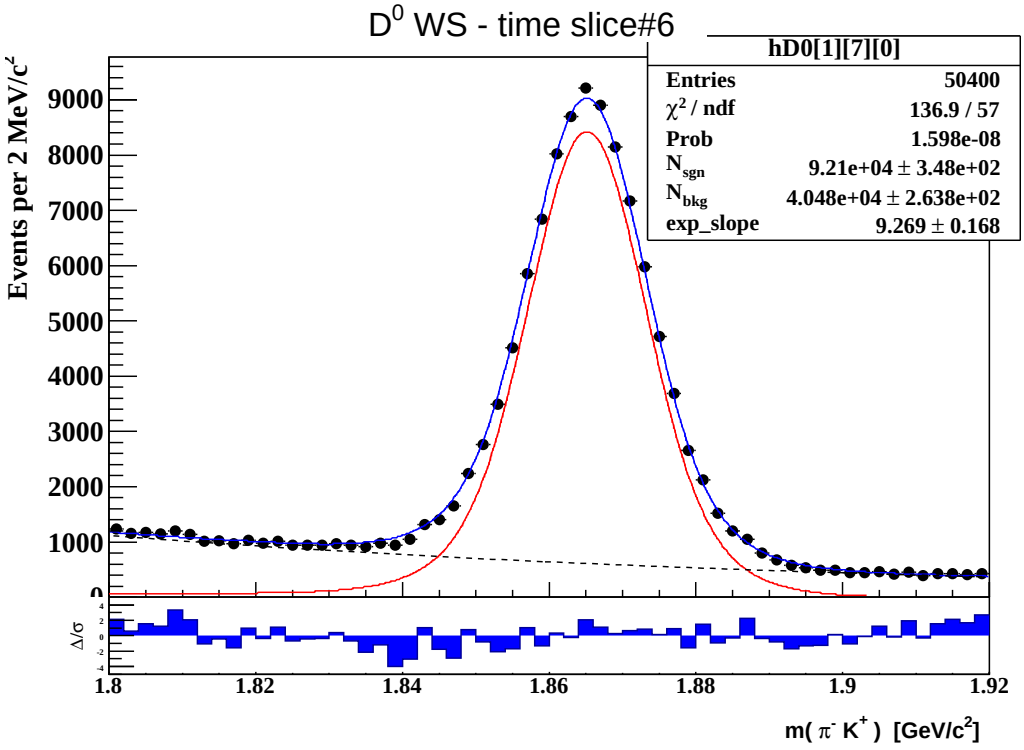

Appendix B: Mass-Difference Integrated $M_{K\pi}$ Distributions

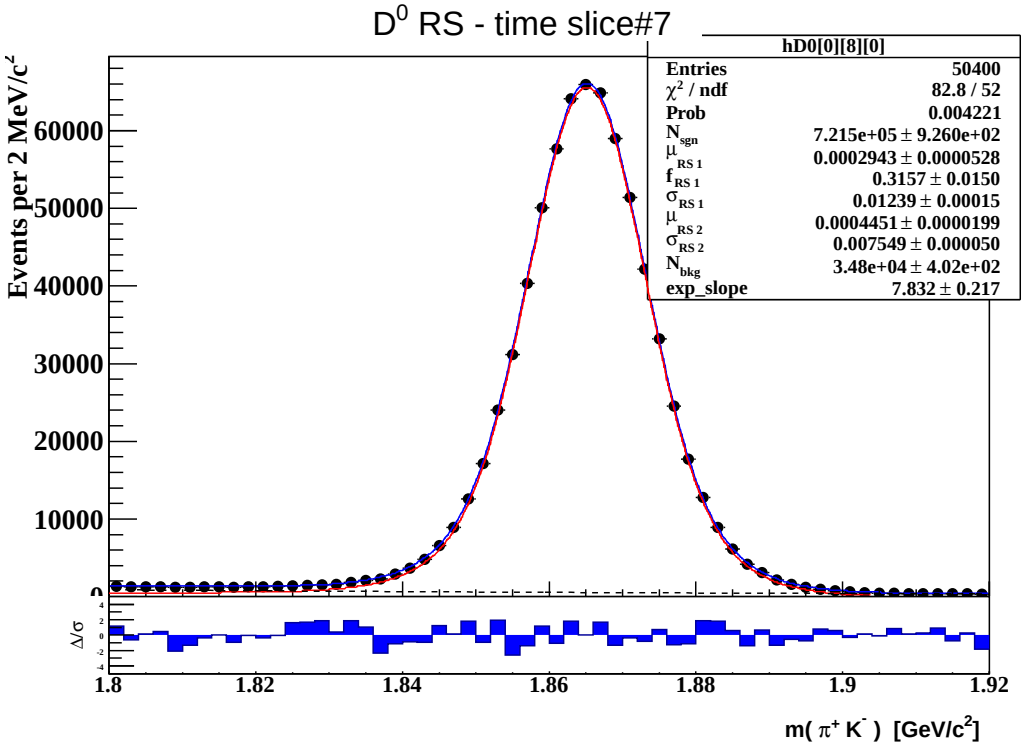

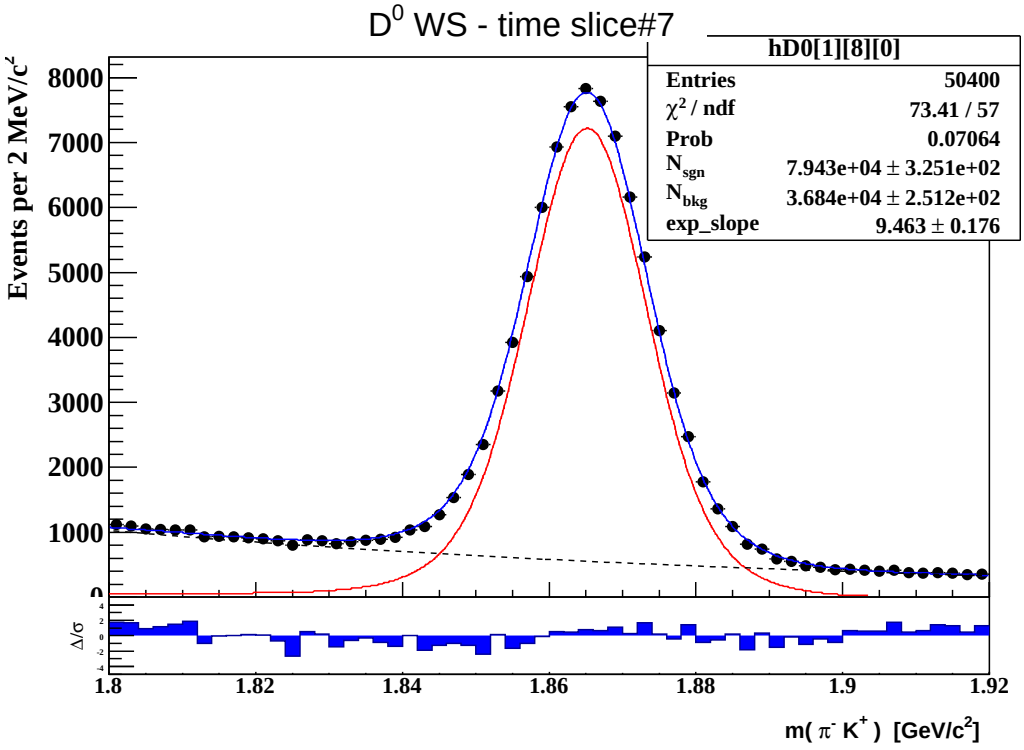

Appendix B: Mass-Difference Integrated $M_{K\pi}$ Distributions

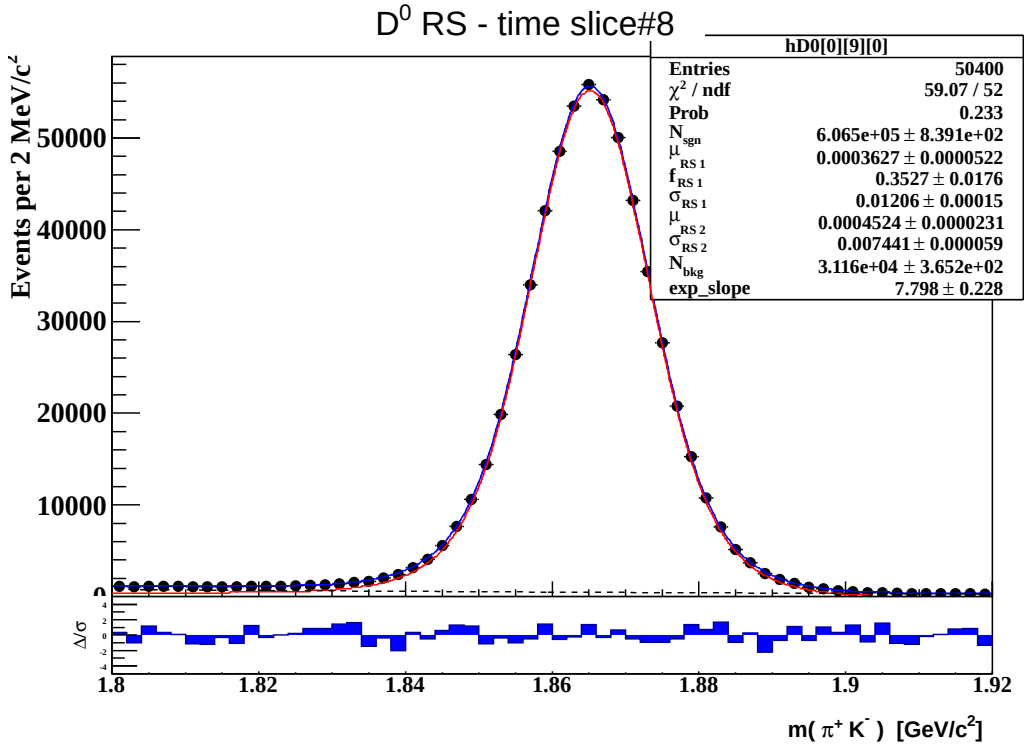

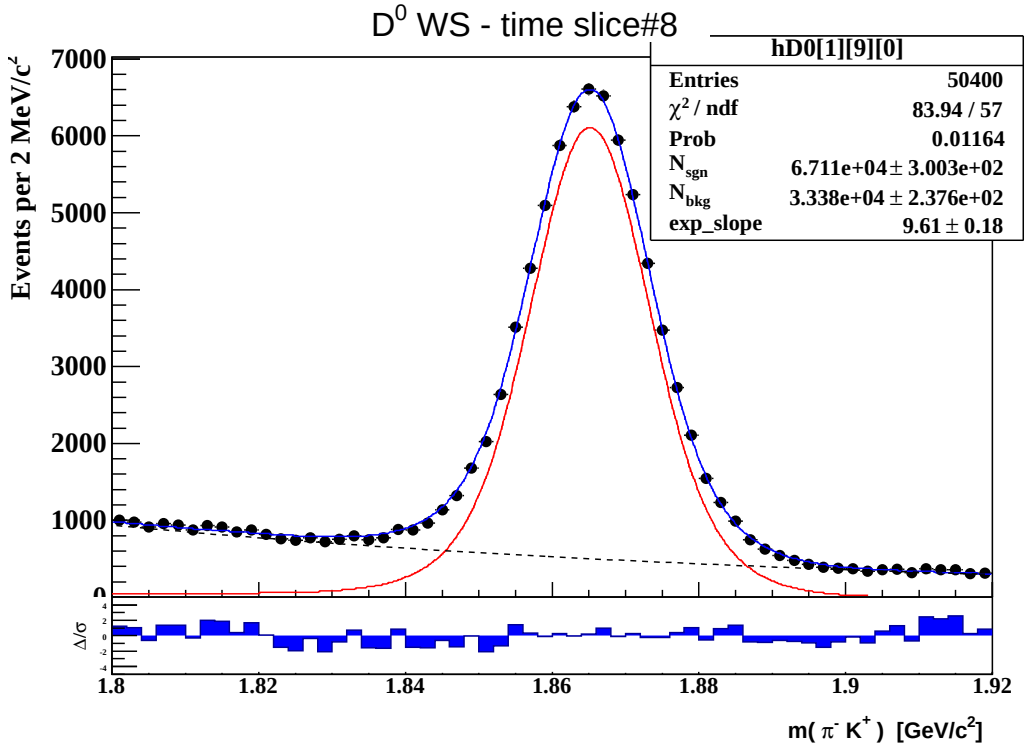

Appendix B: Mass-Difference Integrated $M_{K\pi}$ Distributions

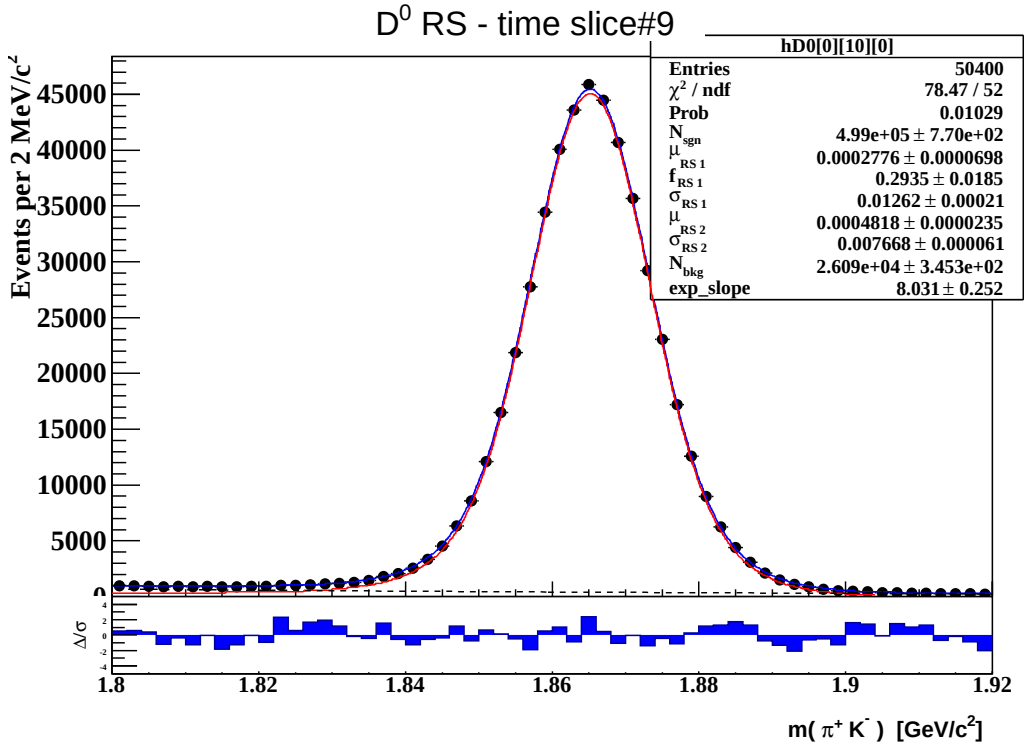

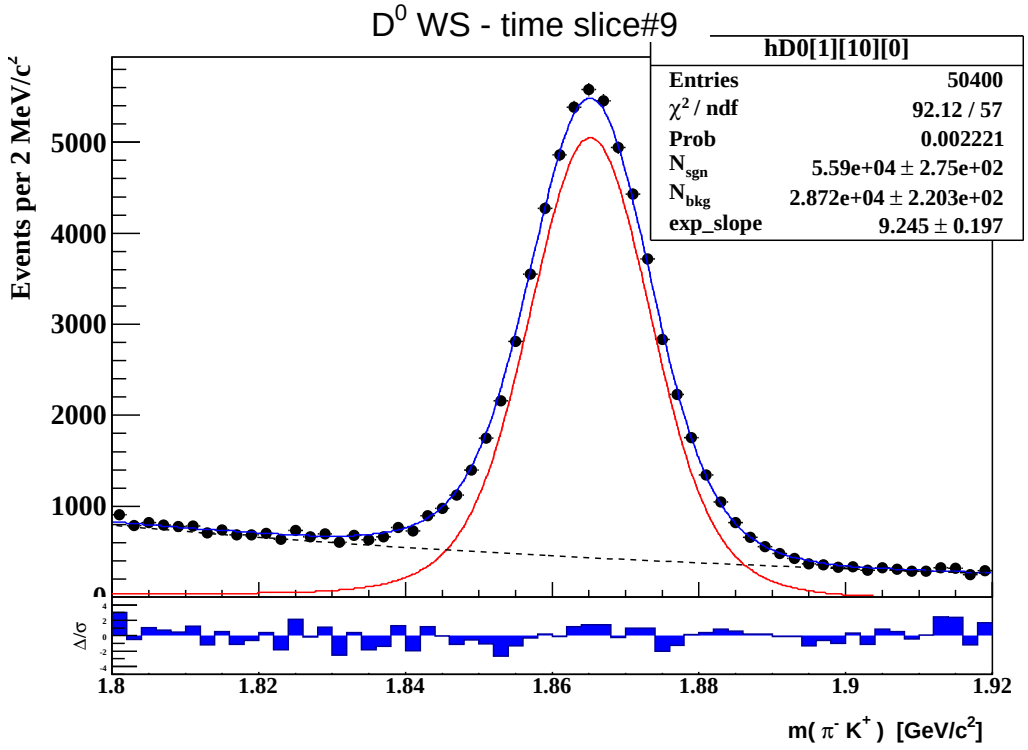

Appendix B: Mass-Difference Integrated $M_{K\pi}$ Distributions

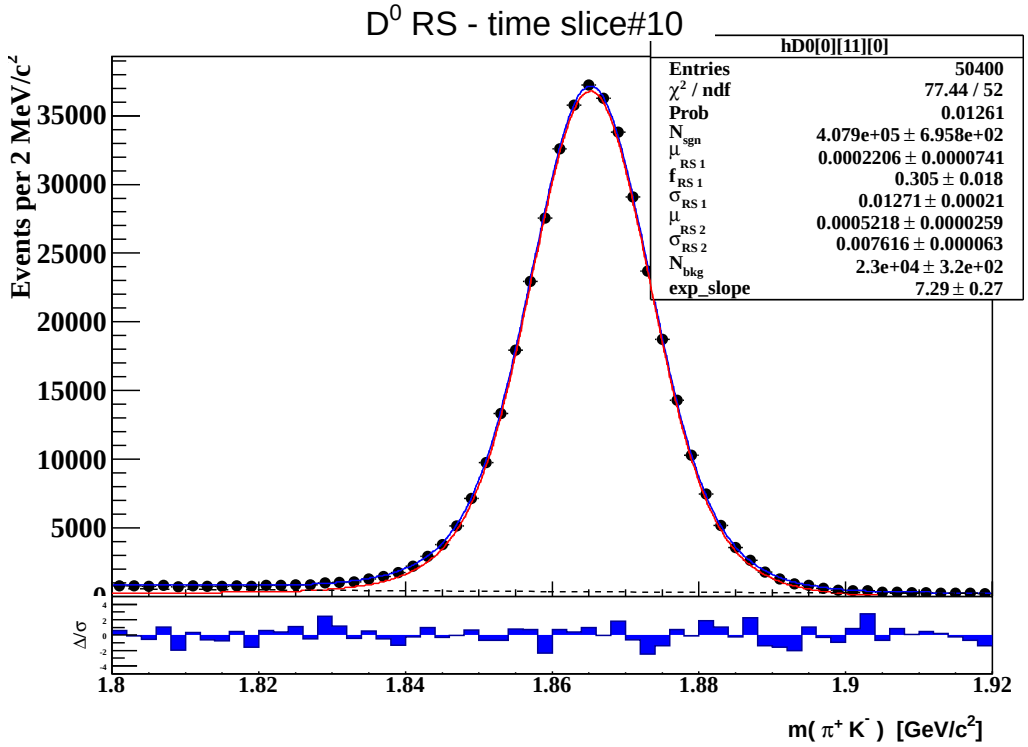

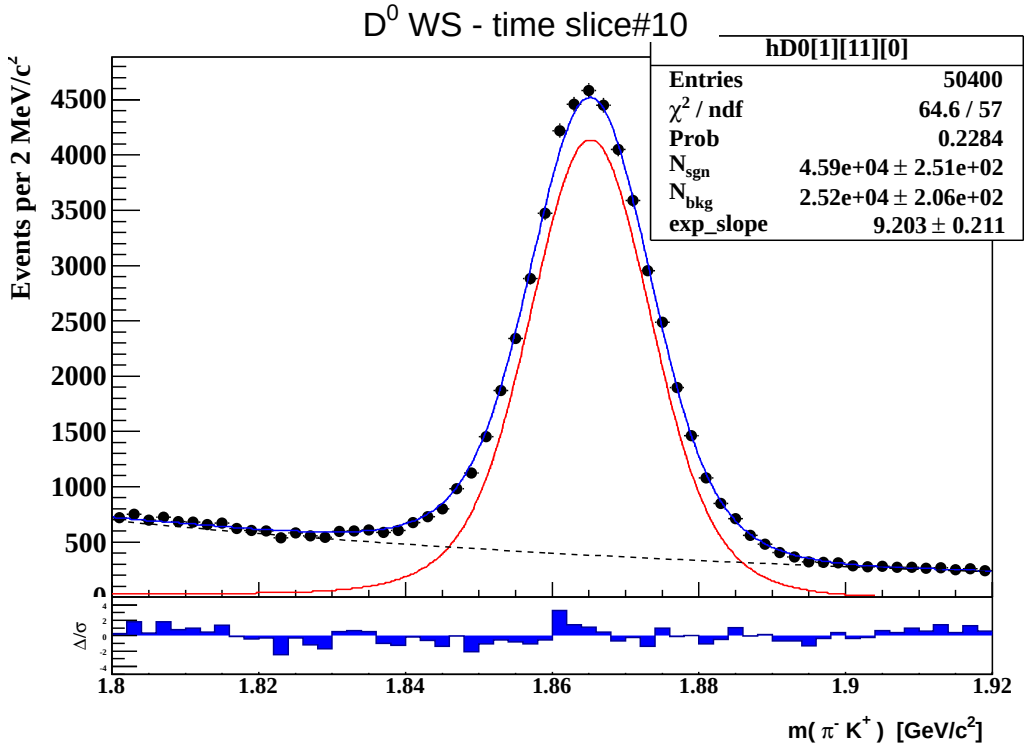

Appendix B: Mass-Difference Integrated $M_{K\pi}$ Distributions

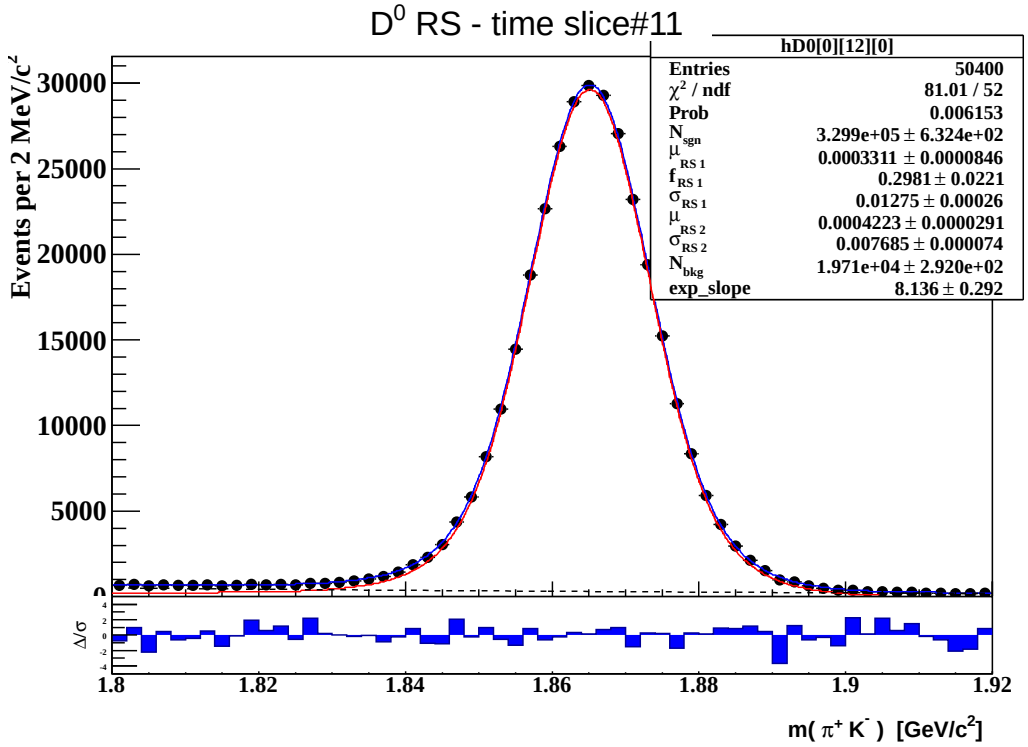

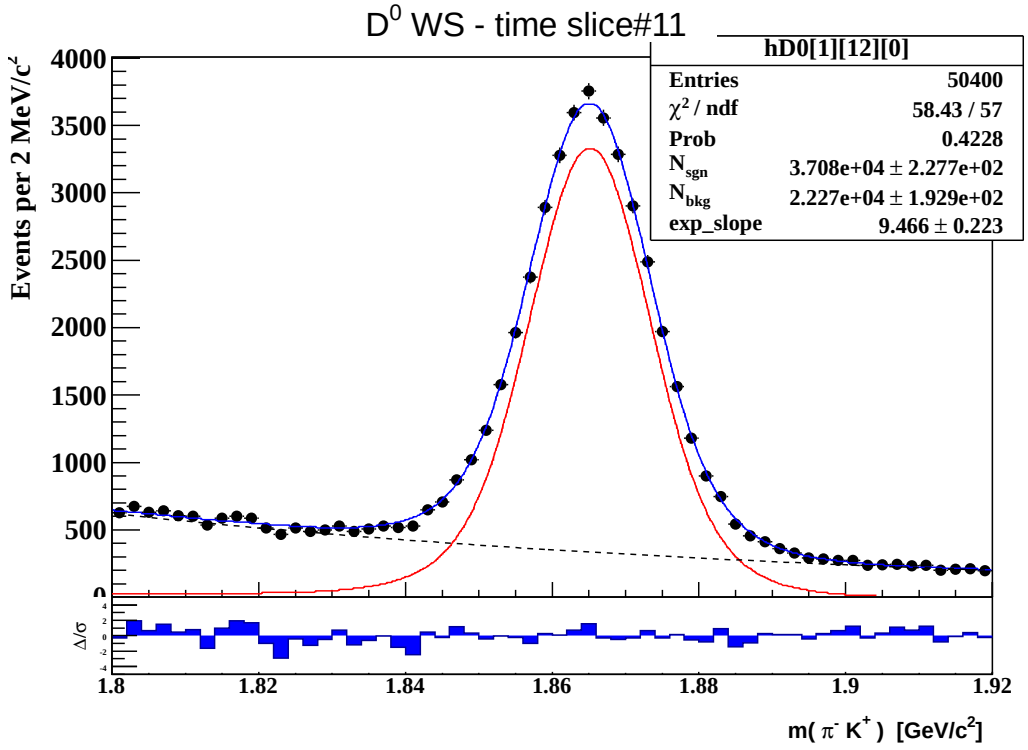

Appendix B: Mass-Difference Integrated $M_{K\pi}$ Distributions

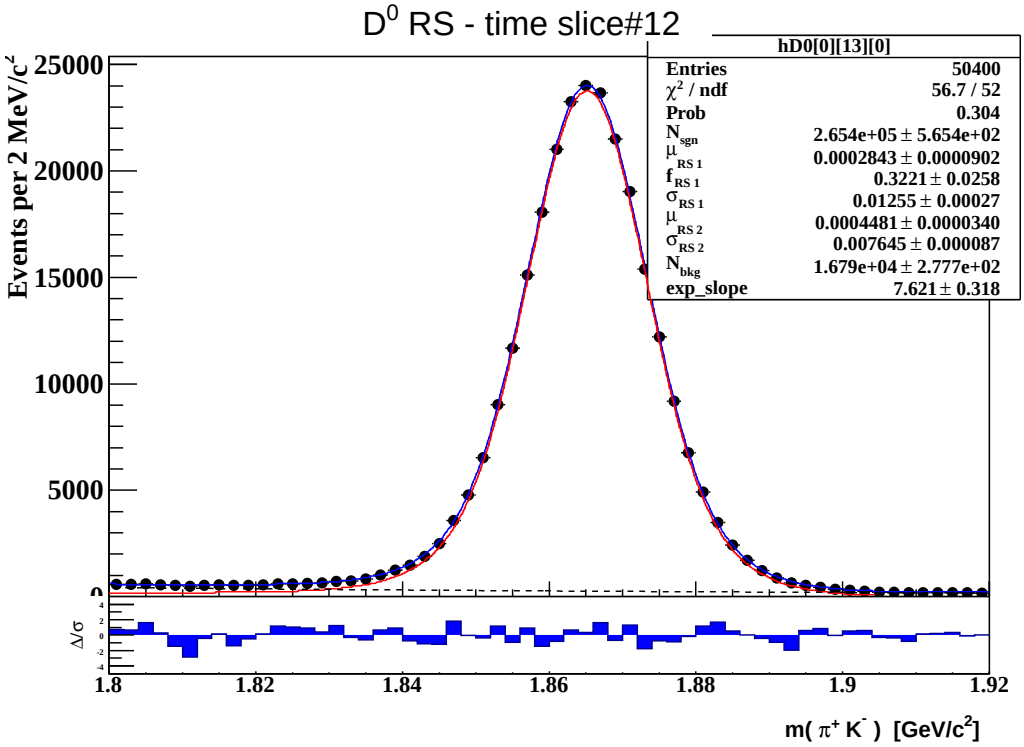

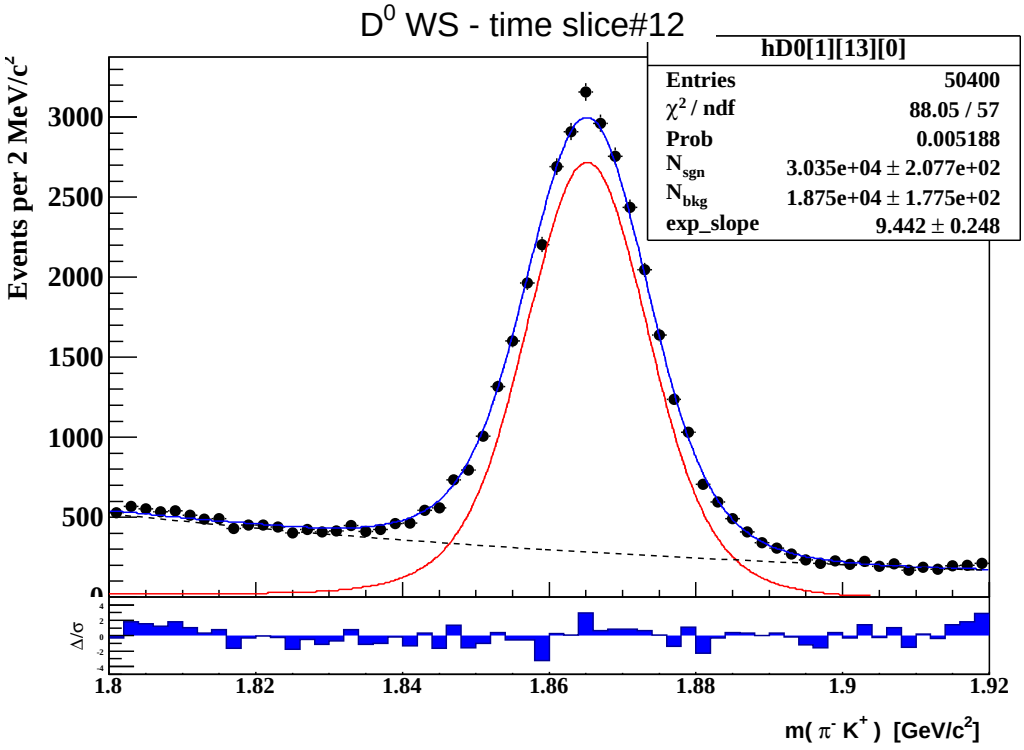

Appendix B: Mass-Difference Integrated $M_{K\pi}$ Distributions

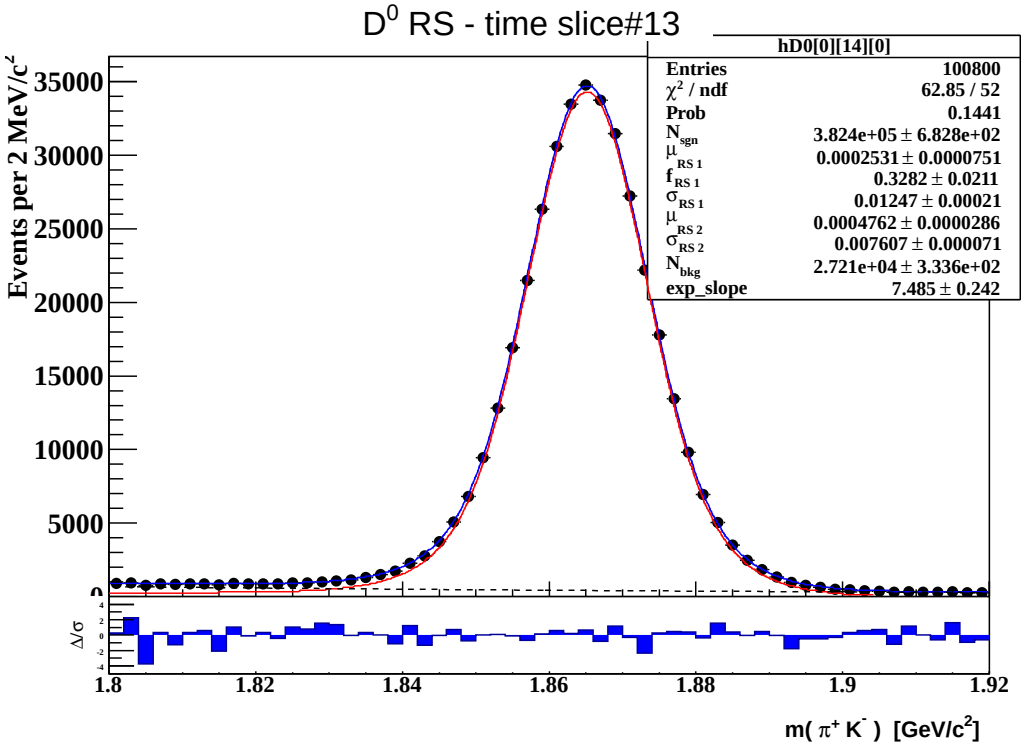

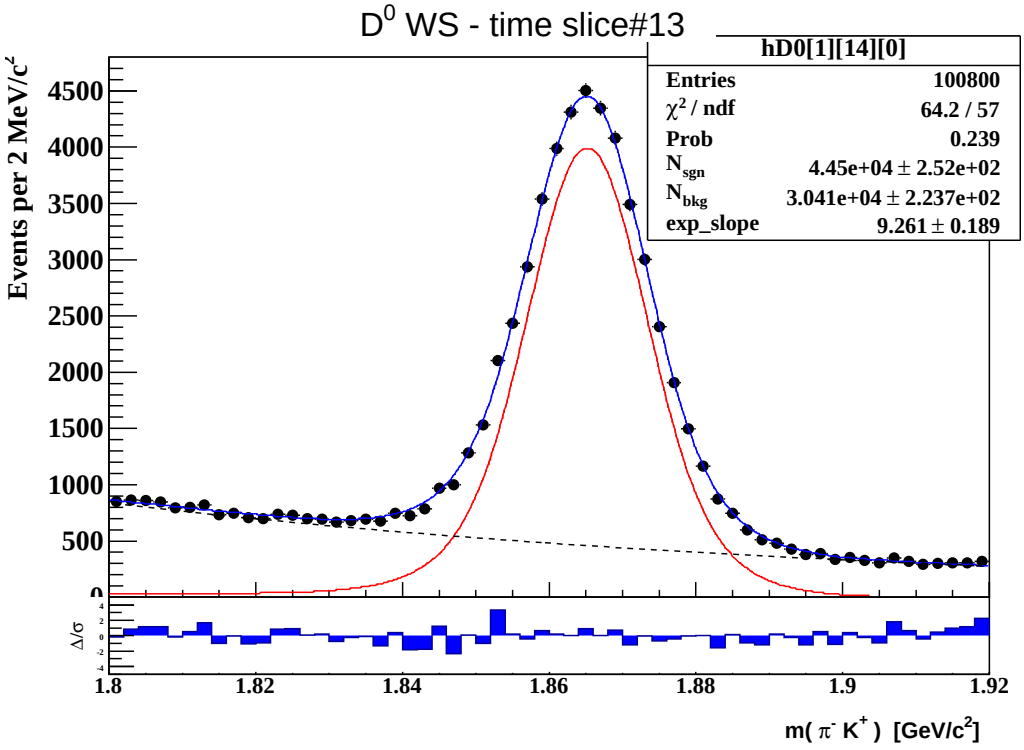

Appendix B: Mass-Difference Integrated $M_{K\pi}$ Distributions

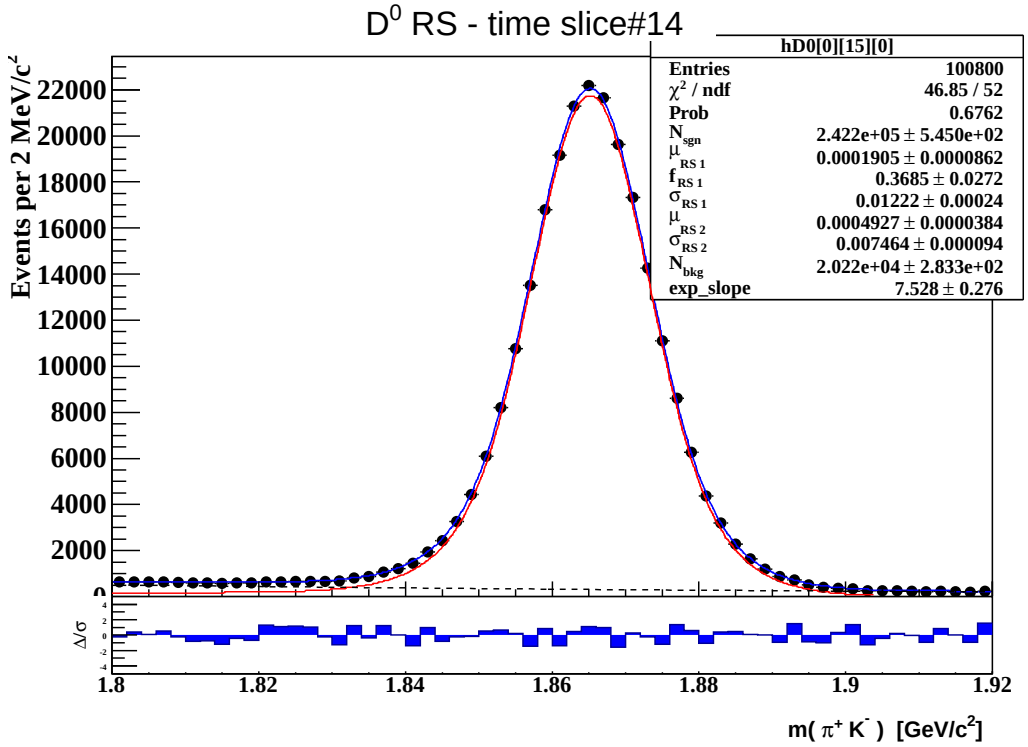

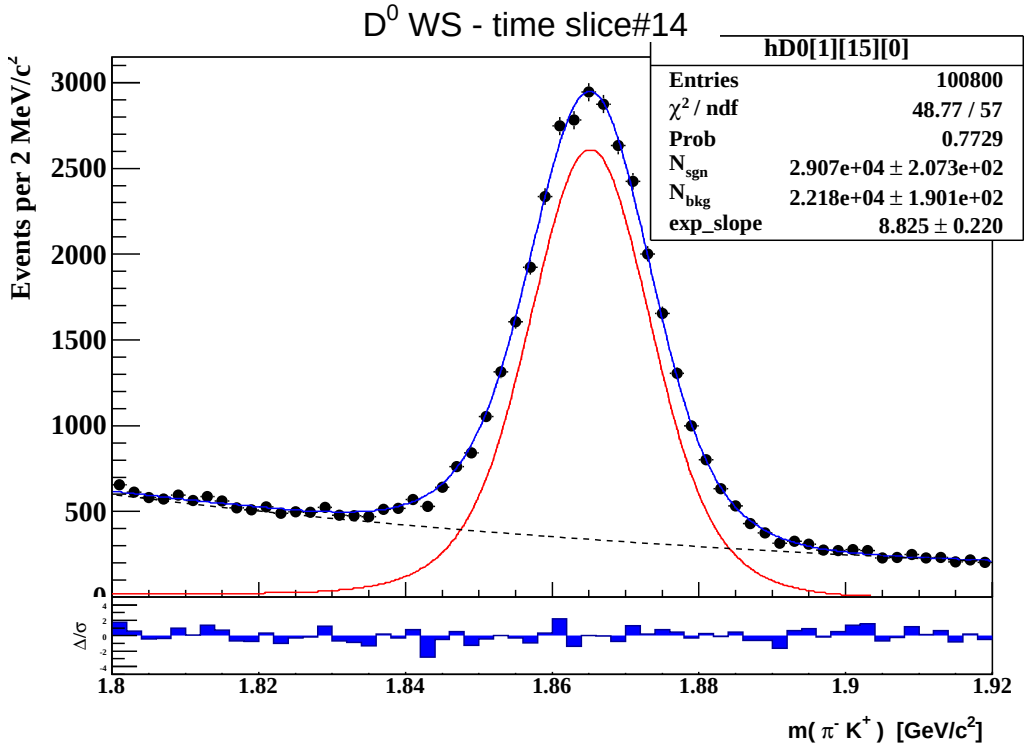

Appendix B: Mass-Difference Integrated $M_{K\pi}$ Distributions

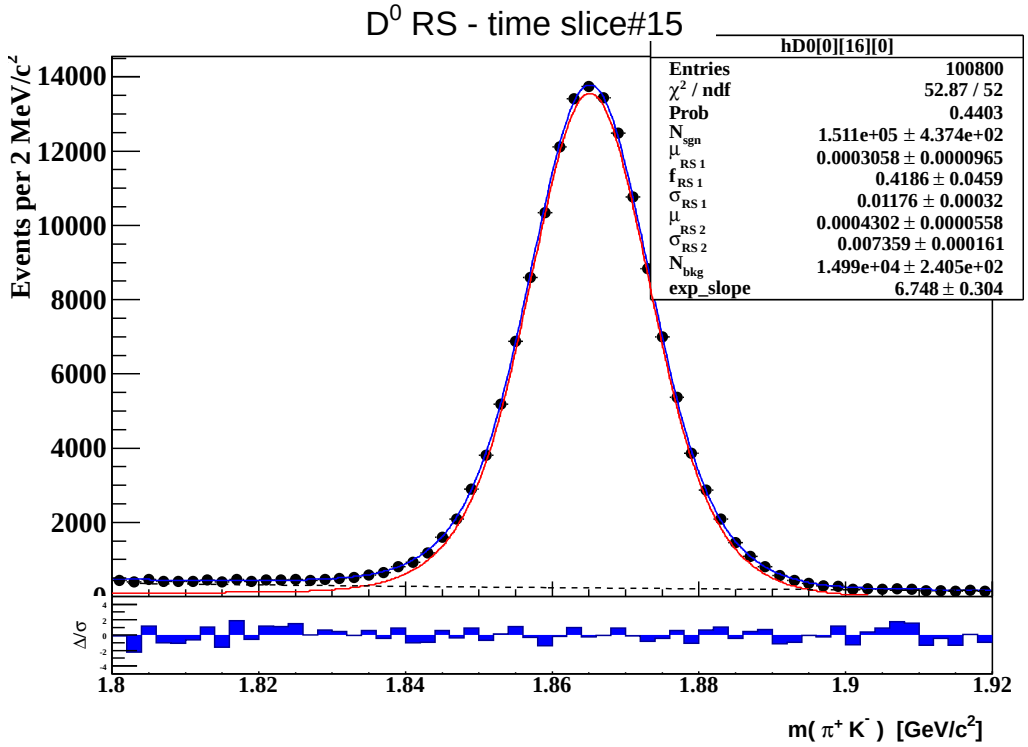

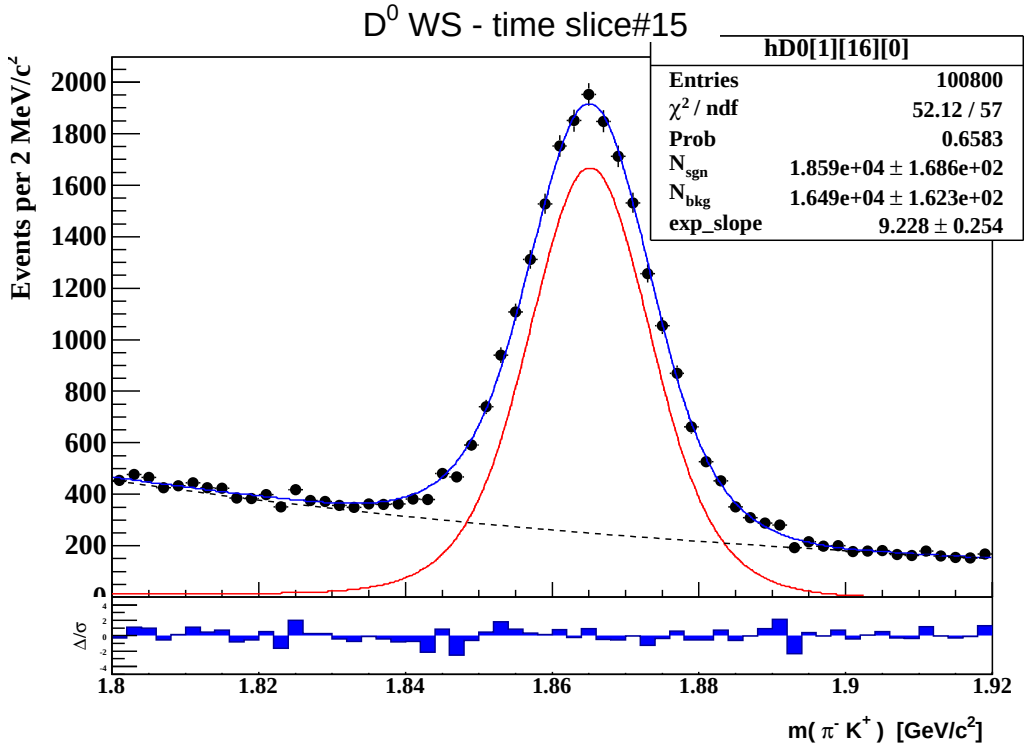

Appendix B: Mass-Difference Integrated $M_{K\pi}$ Distributions

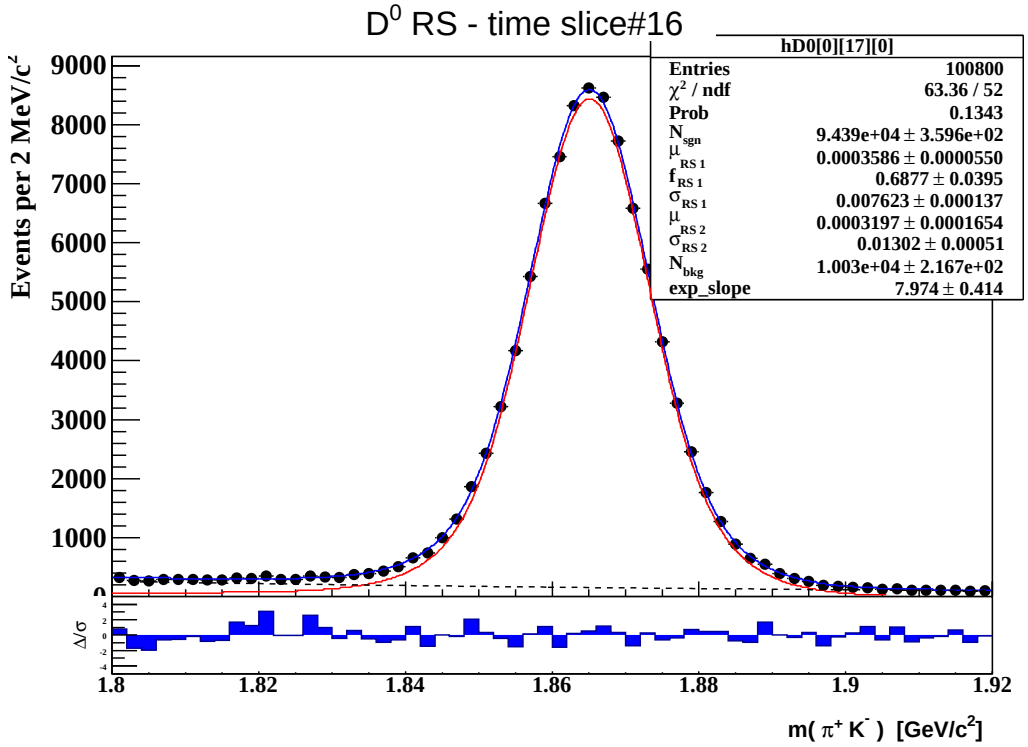

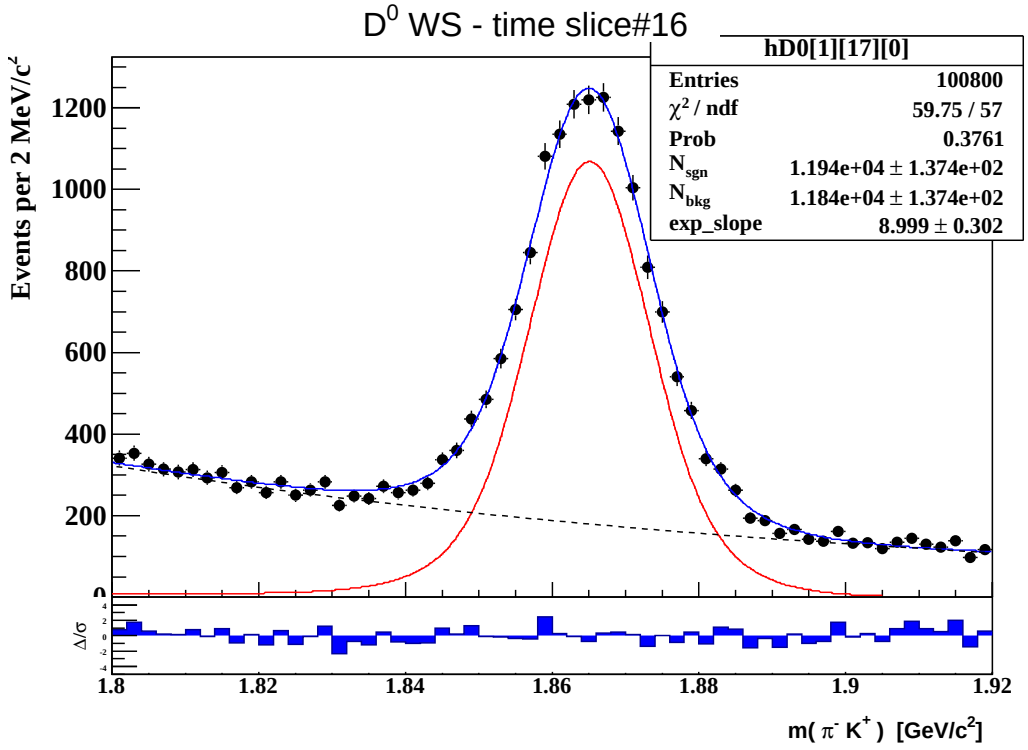

Appendix B: Mass-Difference Integrated $M_{K\pi}$ Distributions

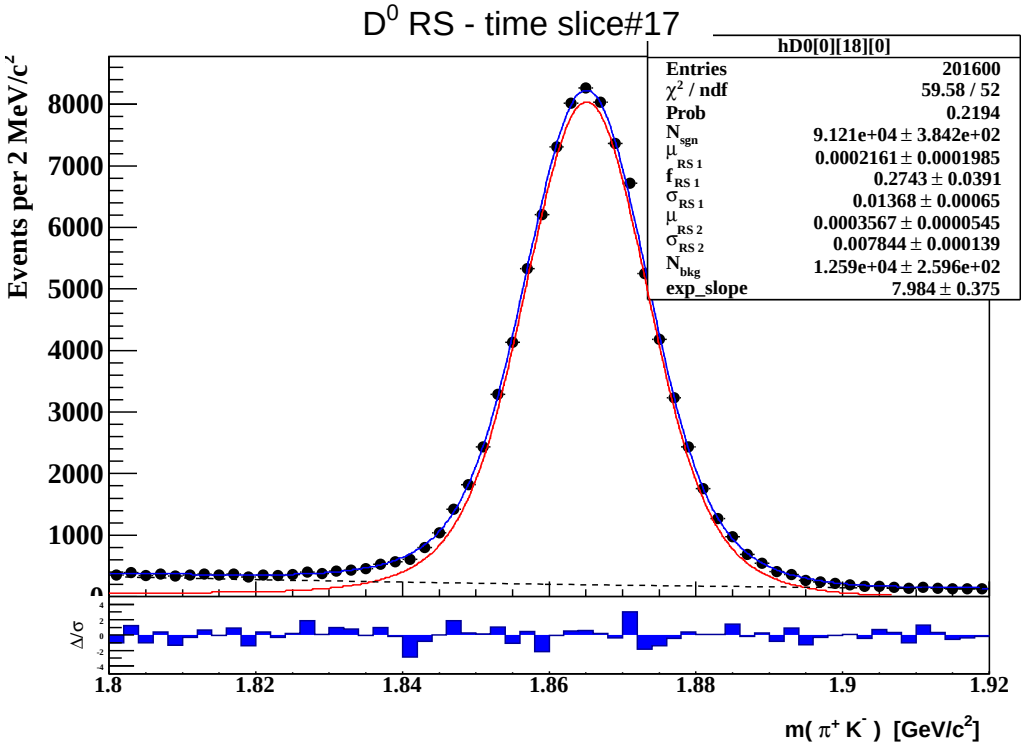

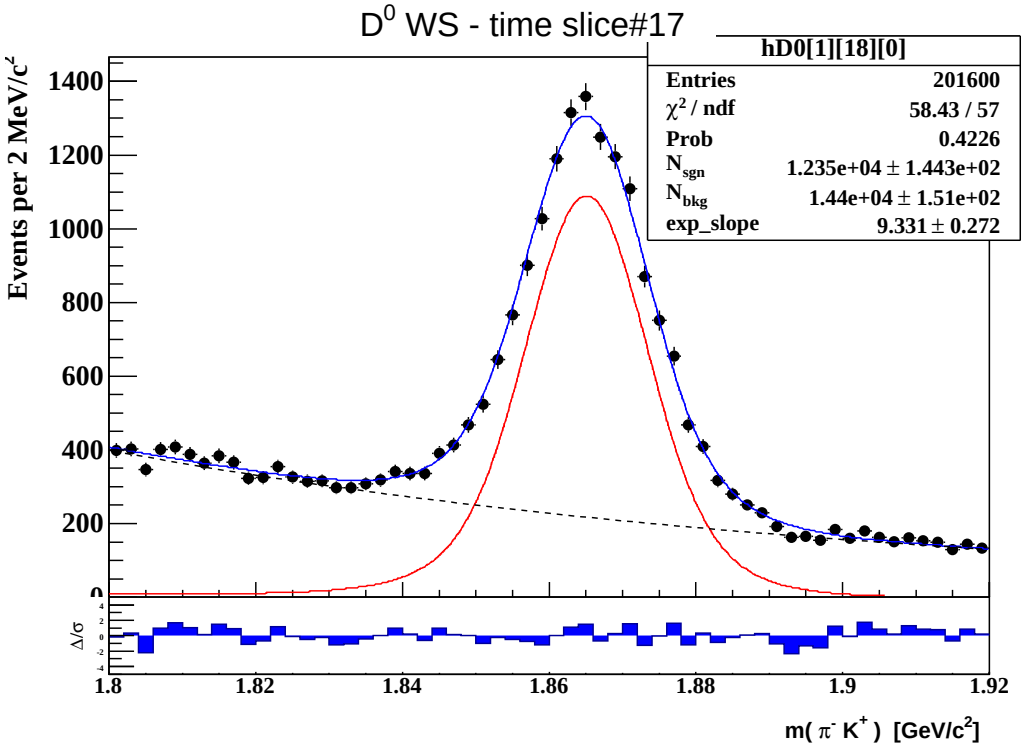

Appendix B: Mass-Difference Integrated $M_{K\pi}$ Distributions

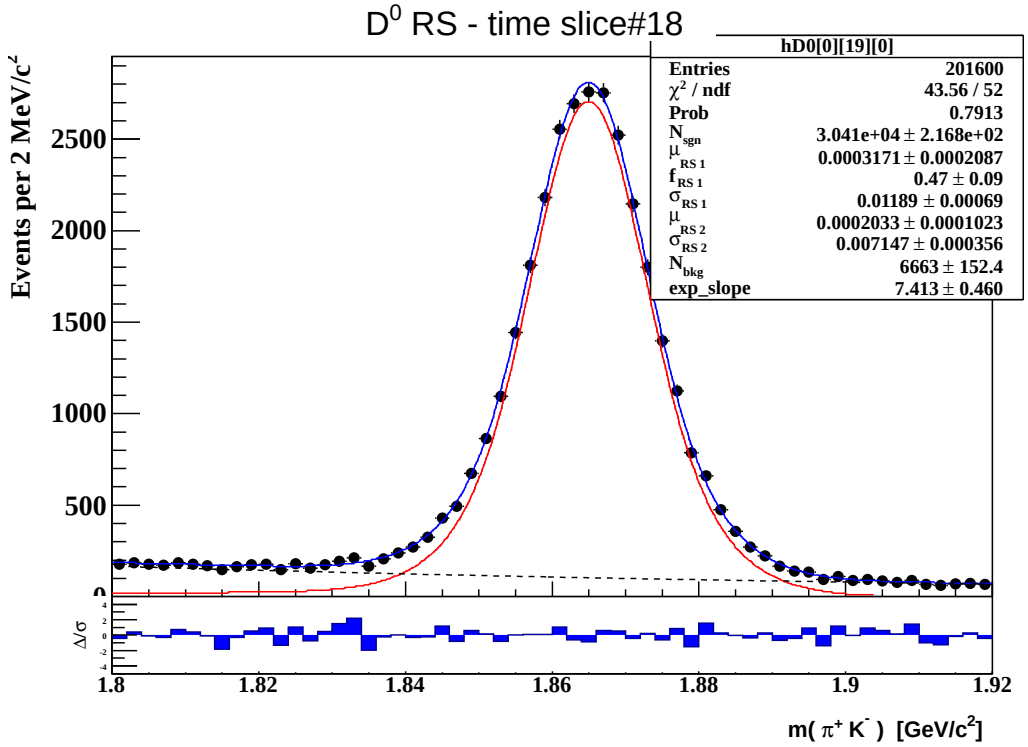

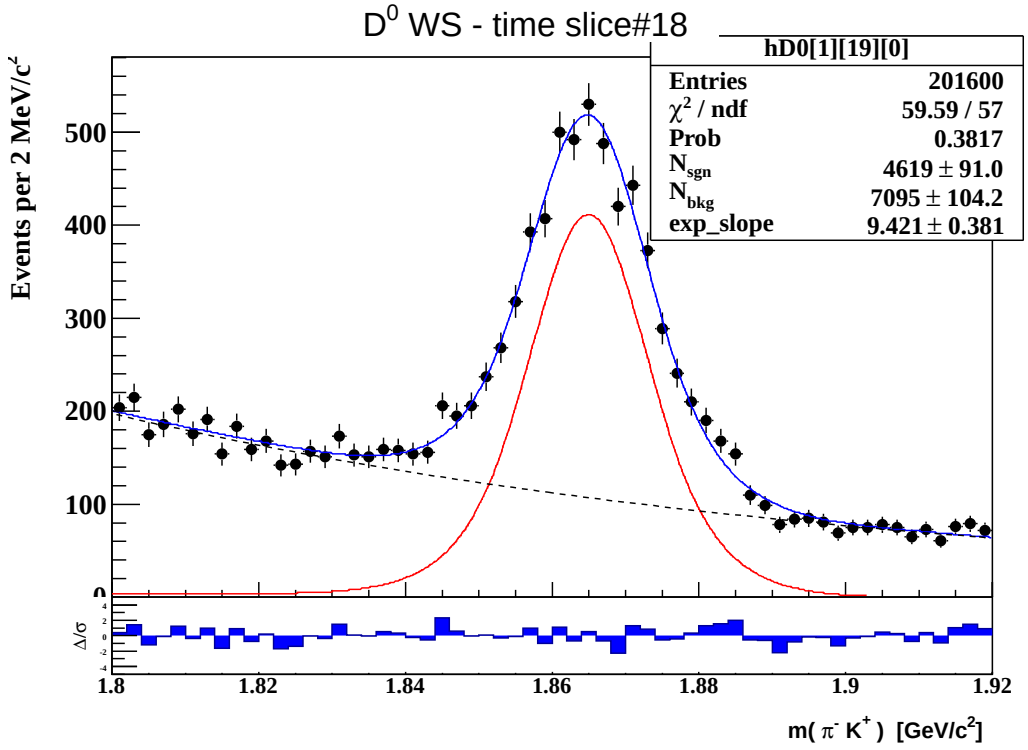

Appendix B: Mass-Difference Integrated $M_{K\pi}$ Distributions

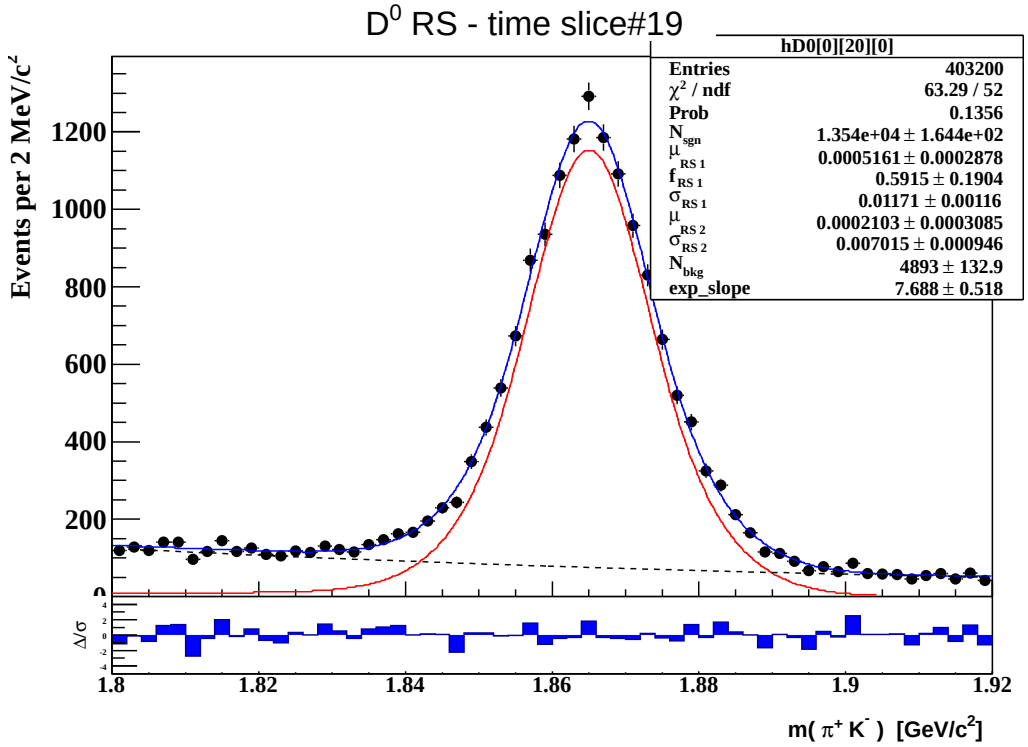

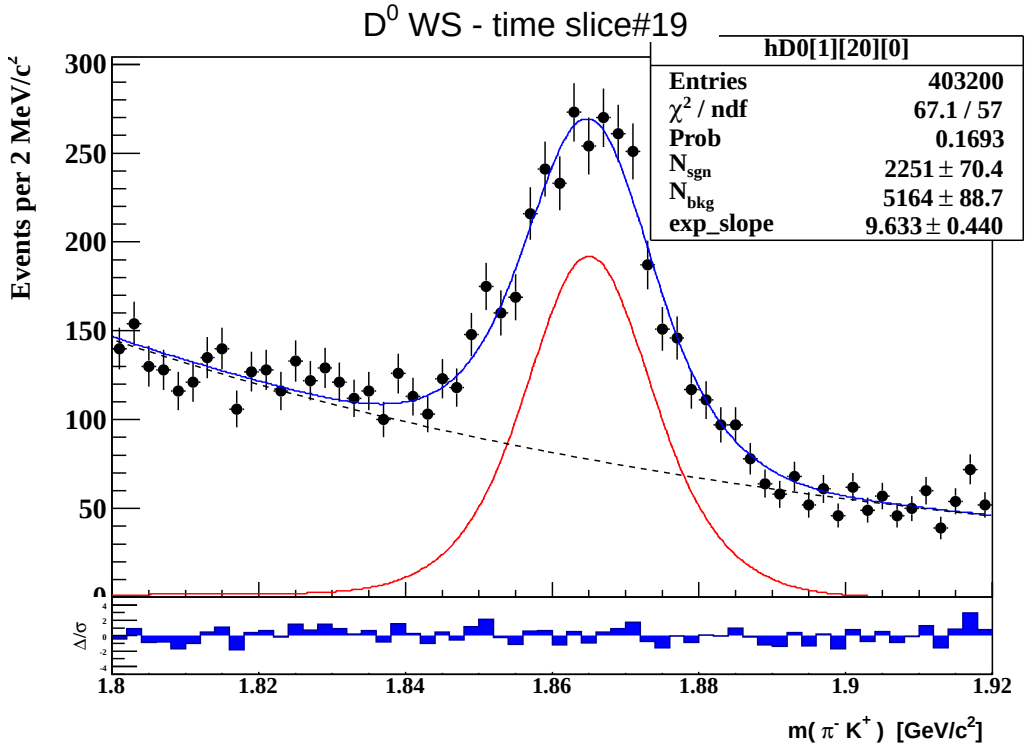

C Mass Difference Fits

The following pages show the fits for the mass difference plots for events $|d_0| \leq 60$ microns, with RS on the left and WS on the right. For each plot, the x-axis is the mass difference $(K\pi\pi^* - K\pi - \pi)$ in GeV. The y-axis is the number of D^0s per 0.5 MeV wide bin. The title shows the decay time slice, from 0 to 19. The black points (with error bars) are the D^0 yields and uncertainties from the fits to the $K\pi$ mass plots. The blue line is the fit. The red line is the signal-only part of the fit.

The fit uses the ROOT "chi-square" option. The signal shape is fixed from the time-integrated fit (shown in the main text), and is the same for RS/WS for all time bins.

Appendix C: Δm Yield Fits $d_0 < 60\mu$m

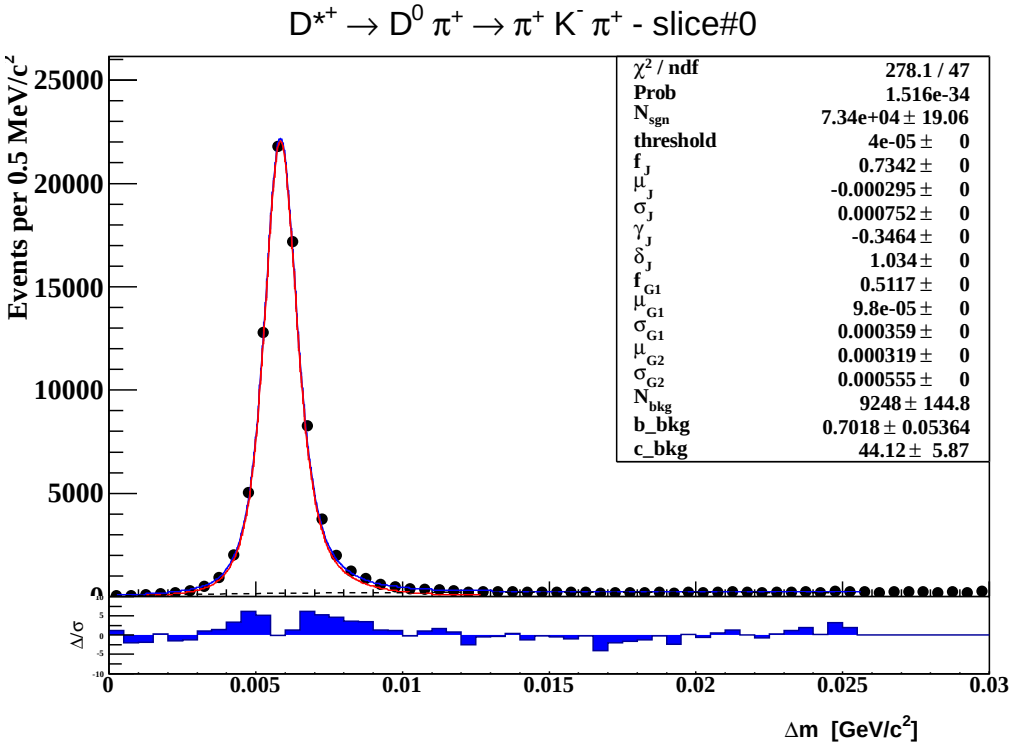

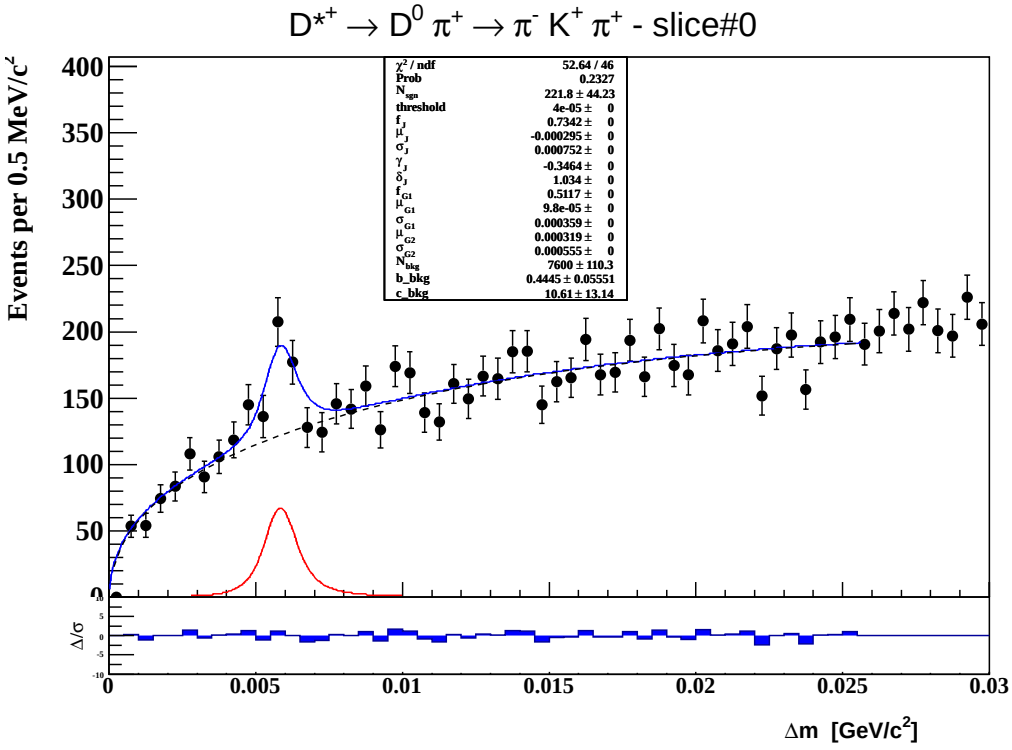

Appendix C: Δm Yield Fits $d_0 < 60\mu$m

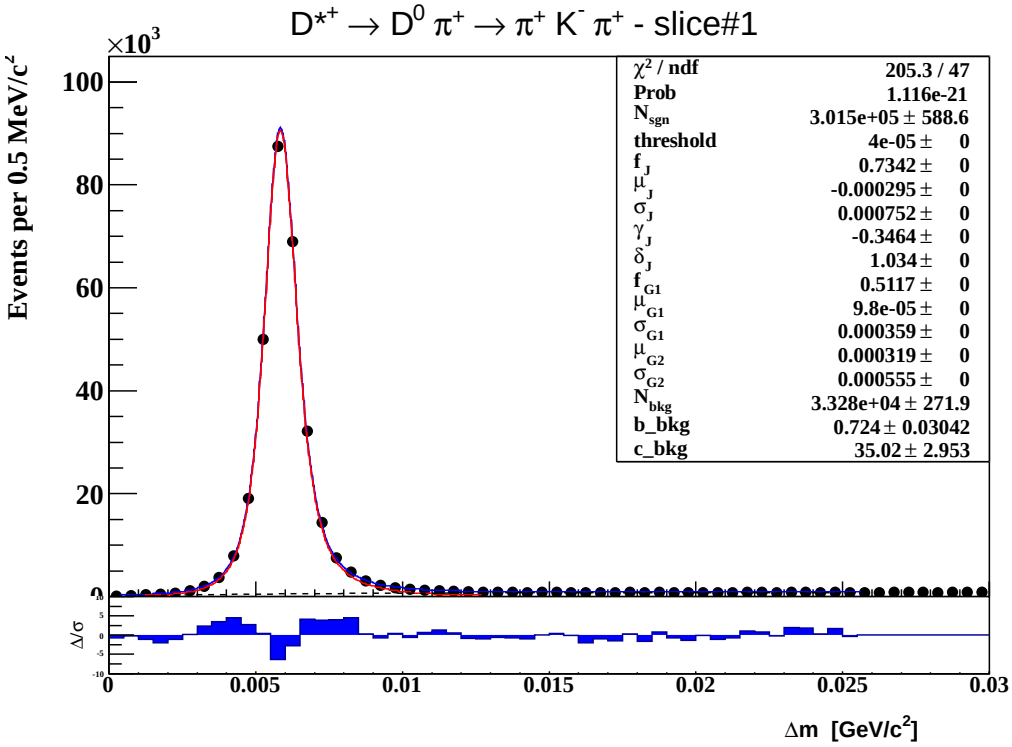

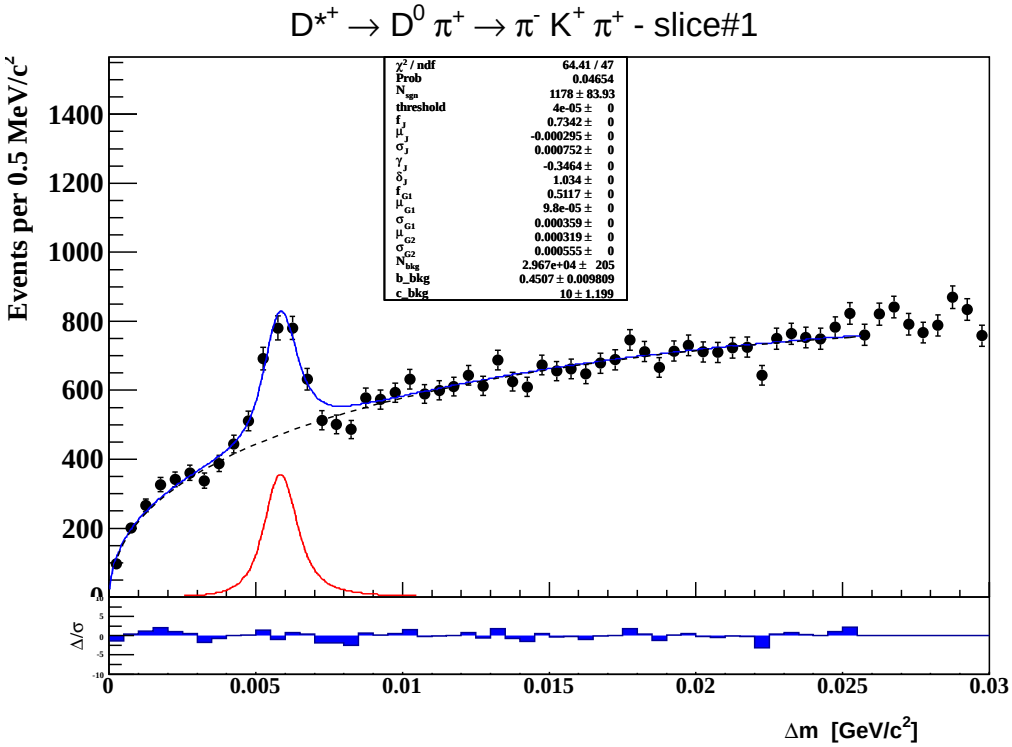

Appendix C: Δm Yield Fits $d_0 < 60\mu$m

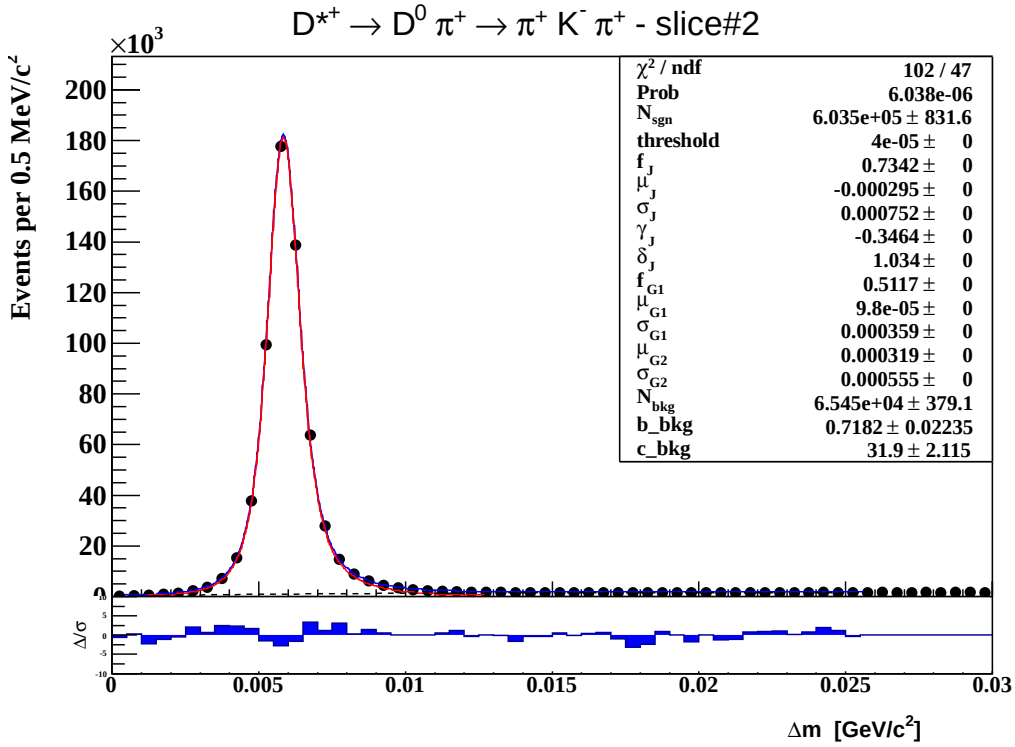

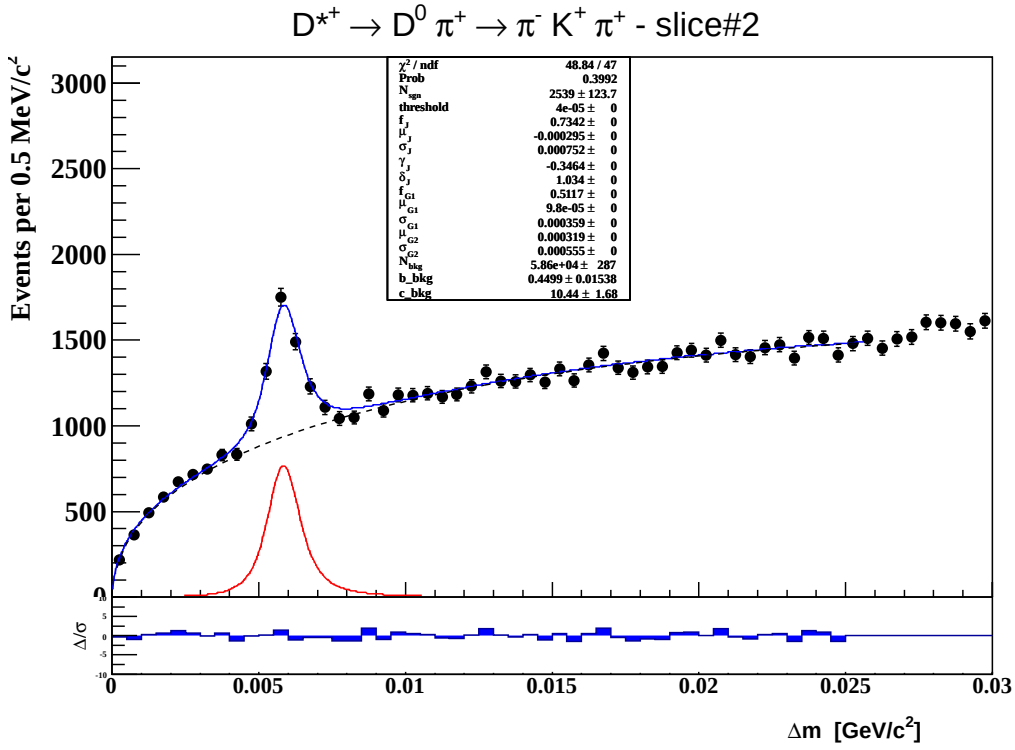

Appendix C: Δm Yield Fits $d_0 < 60\mu$m

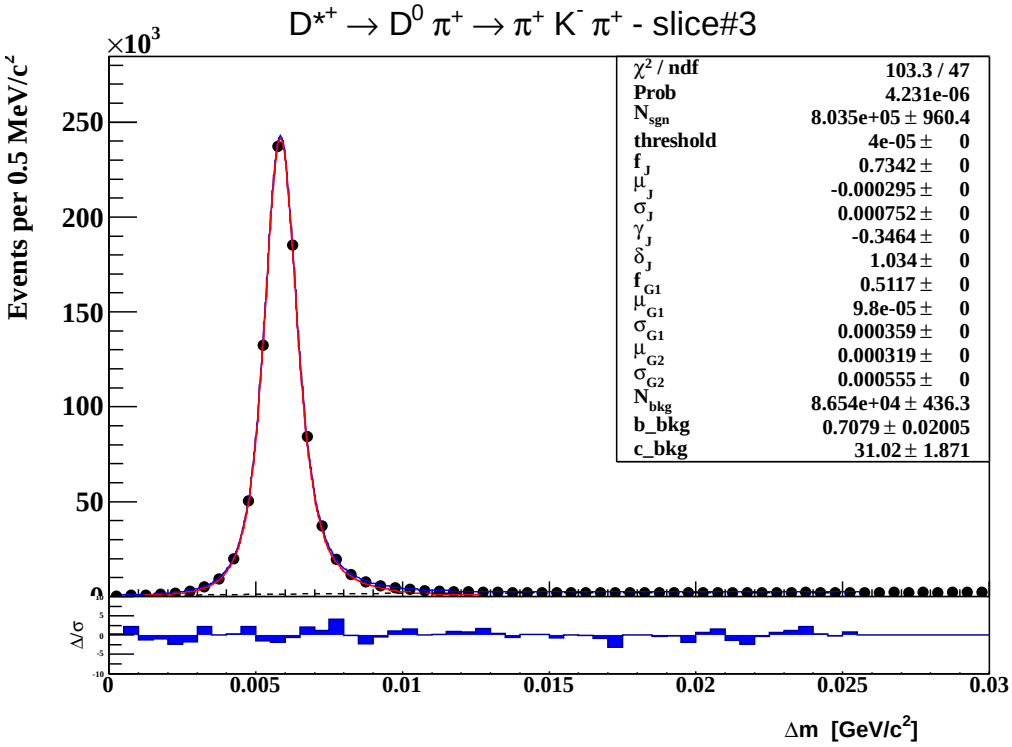

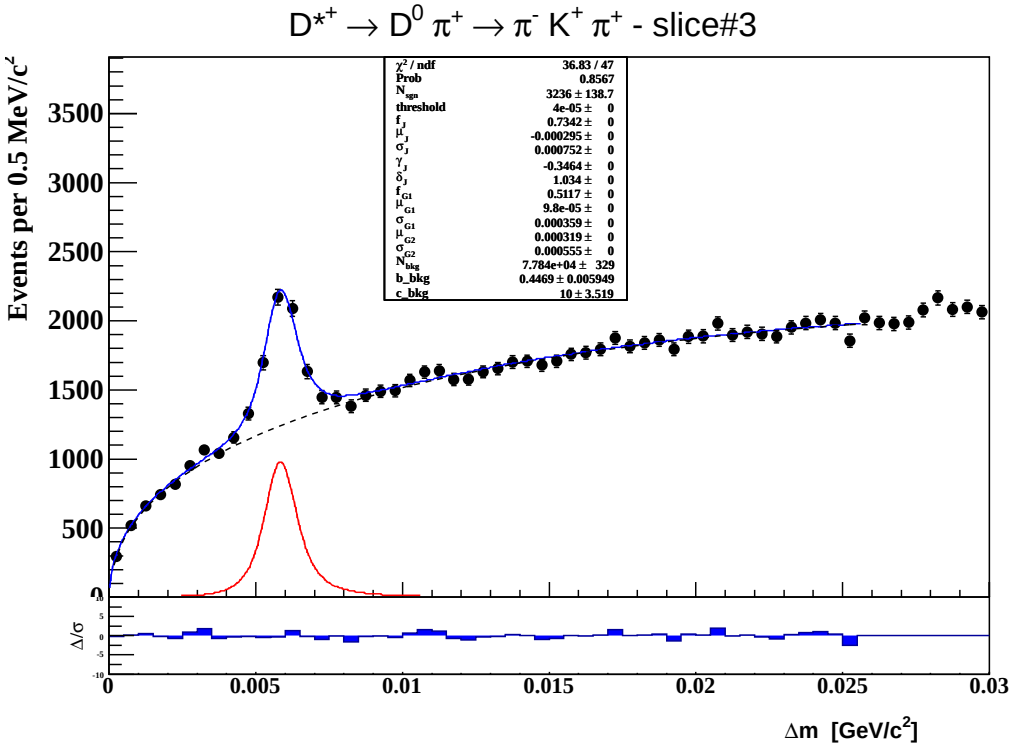

Appendix C: Δm Yield Fits $d_0 < 60\mu$m

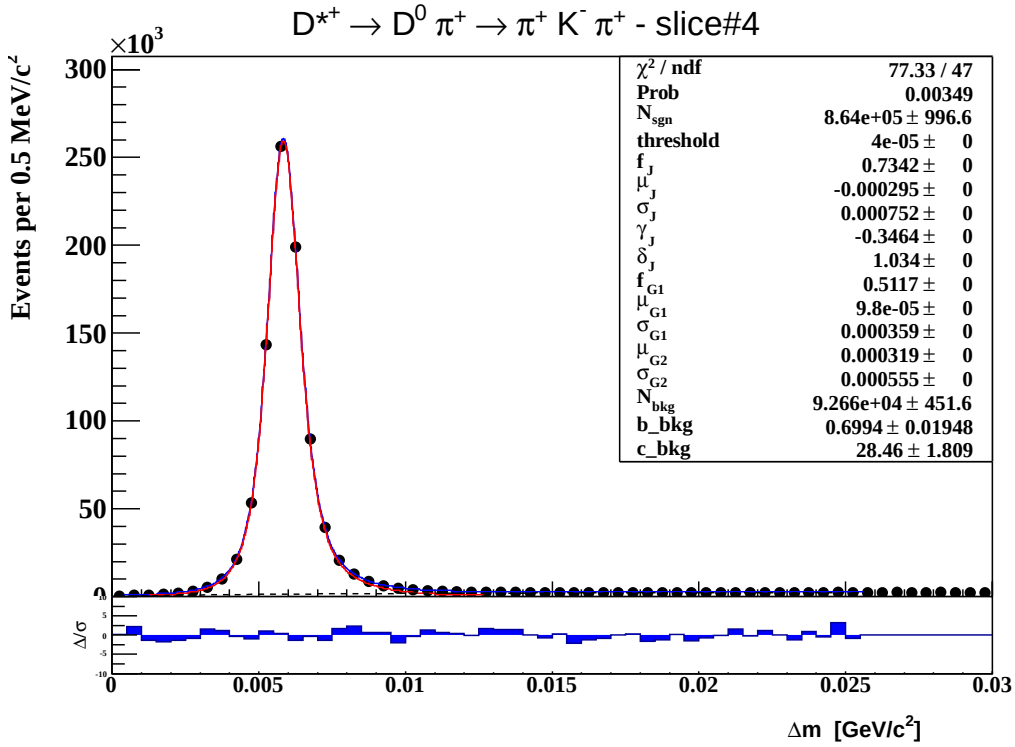

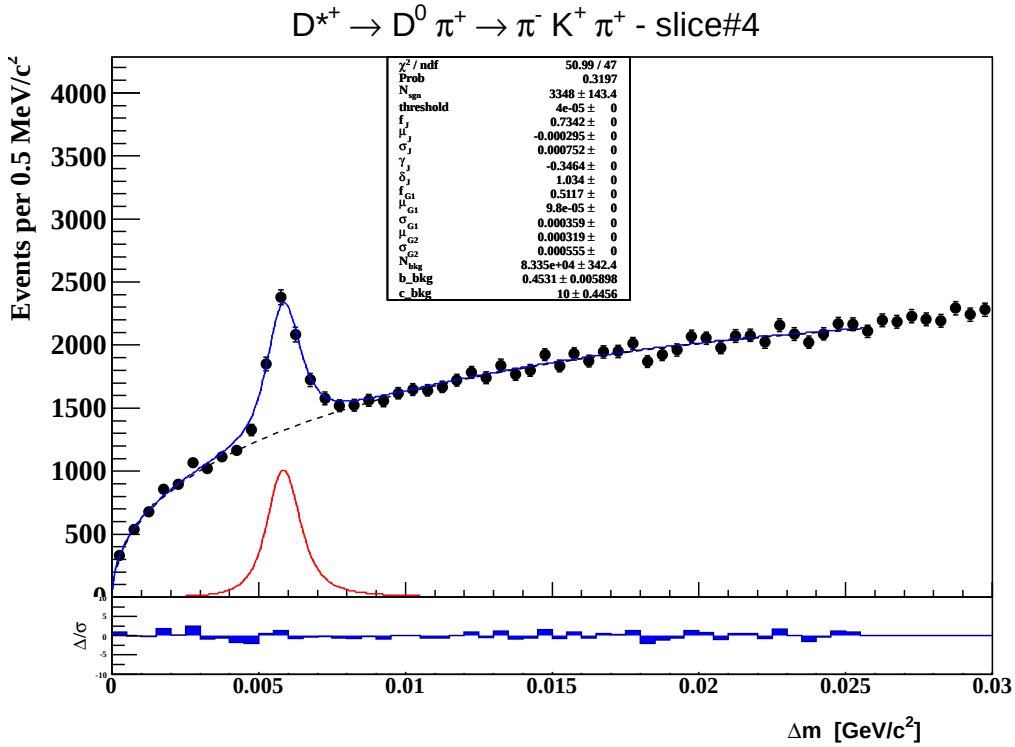

Appendix C: Δm Yield Fits $d_0 < 60\mu$m

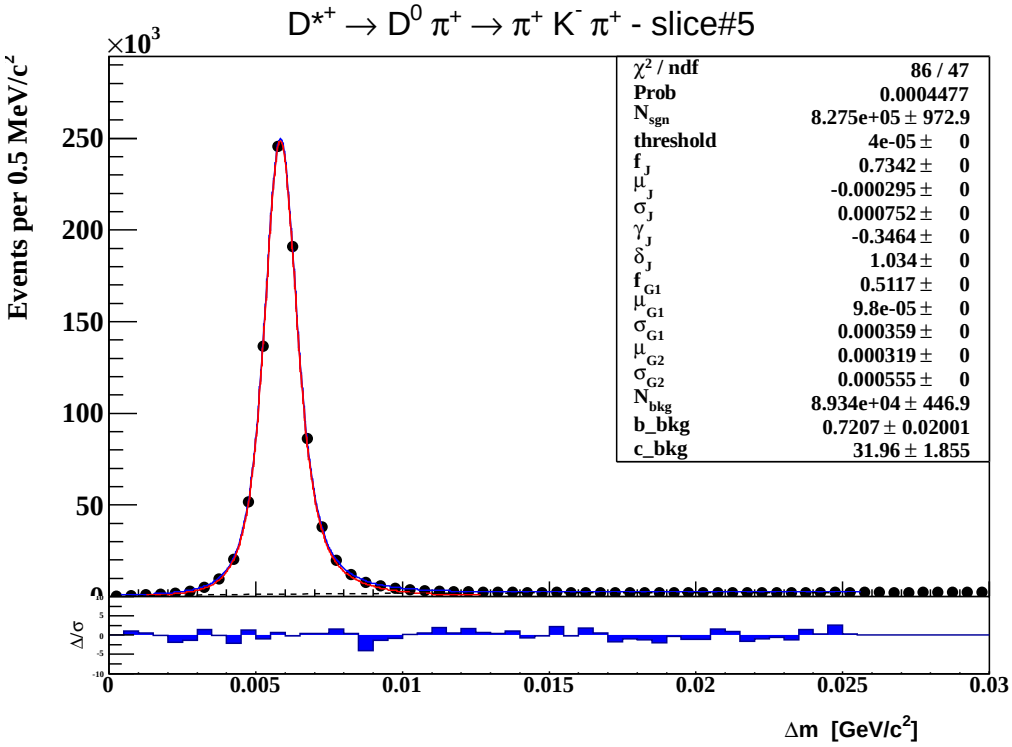

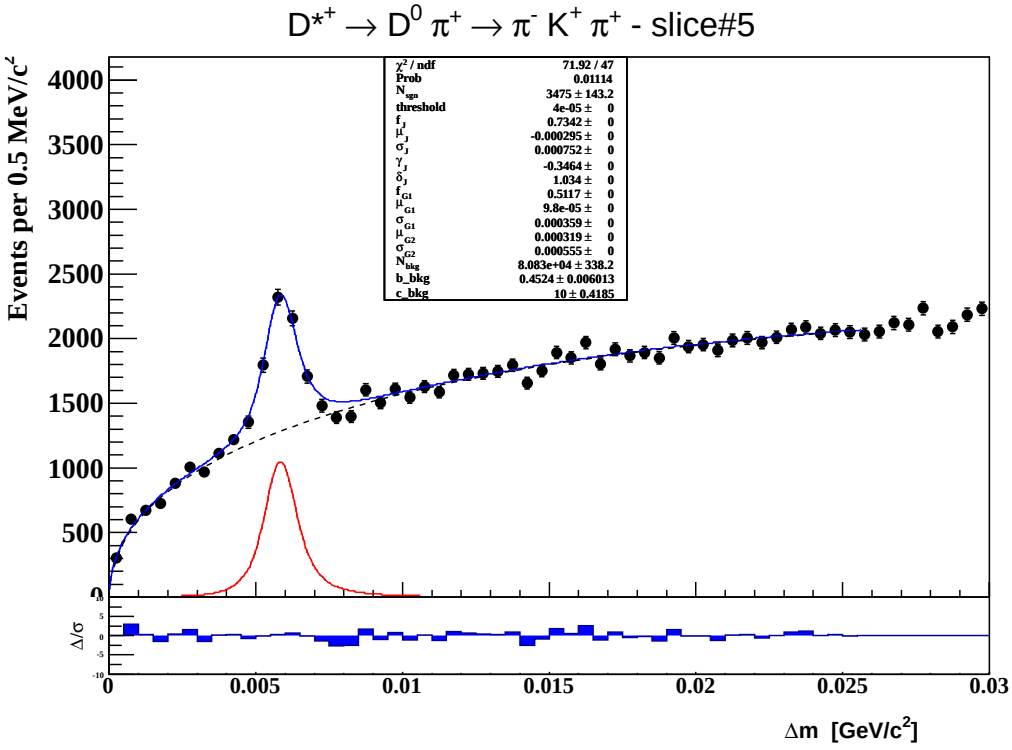

Appendix C: Δm Yield Fits $d_0 < 60\mu$m

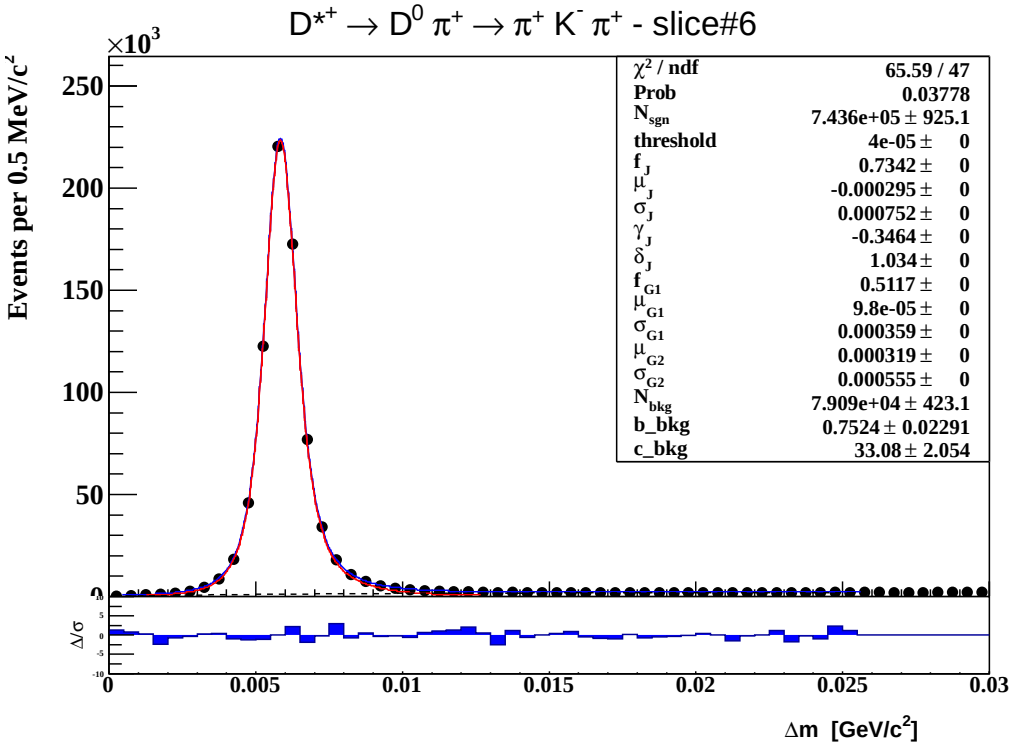

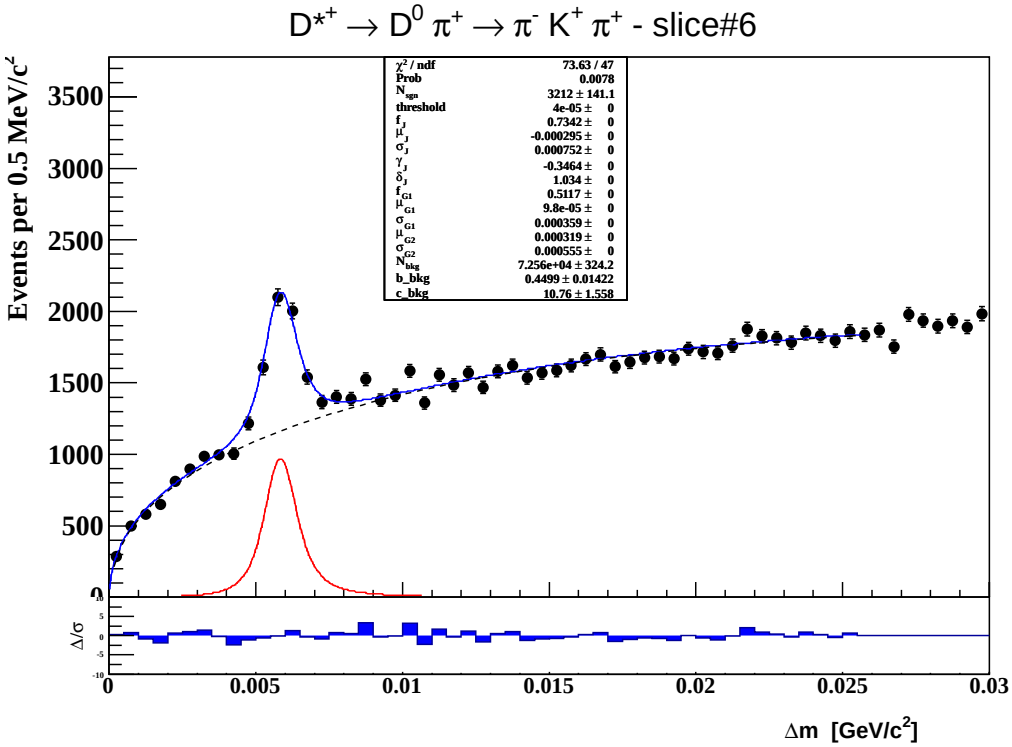

Appendix C: Δm Yield Fits $d_0 < 60\mu$m

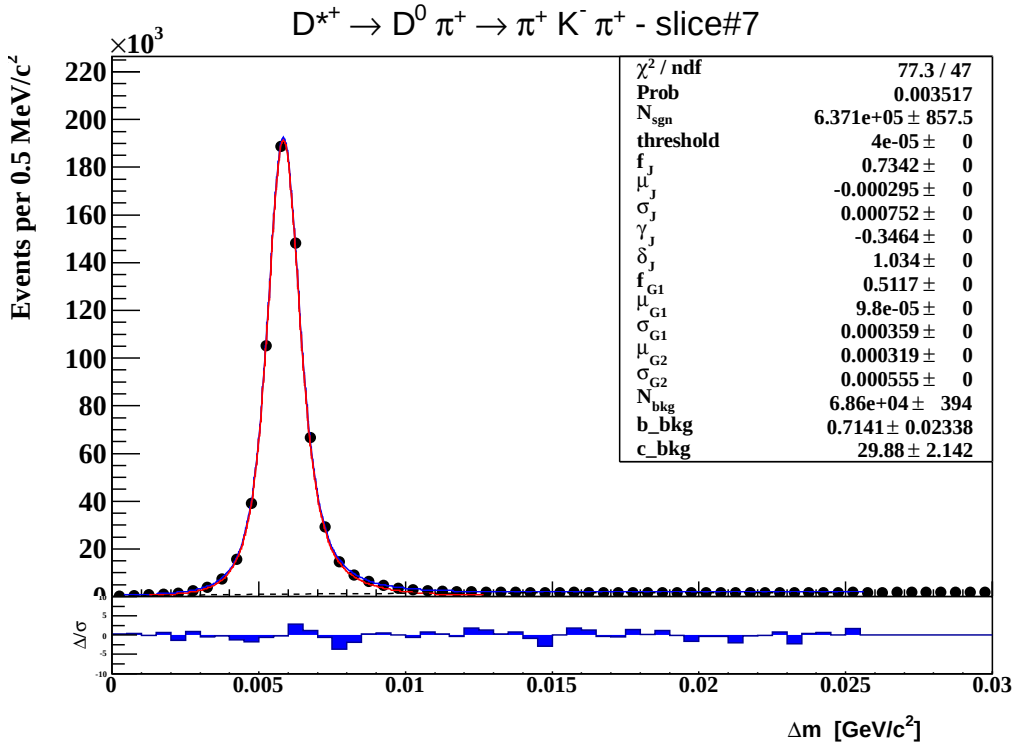

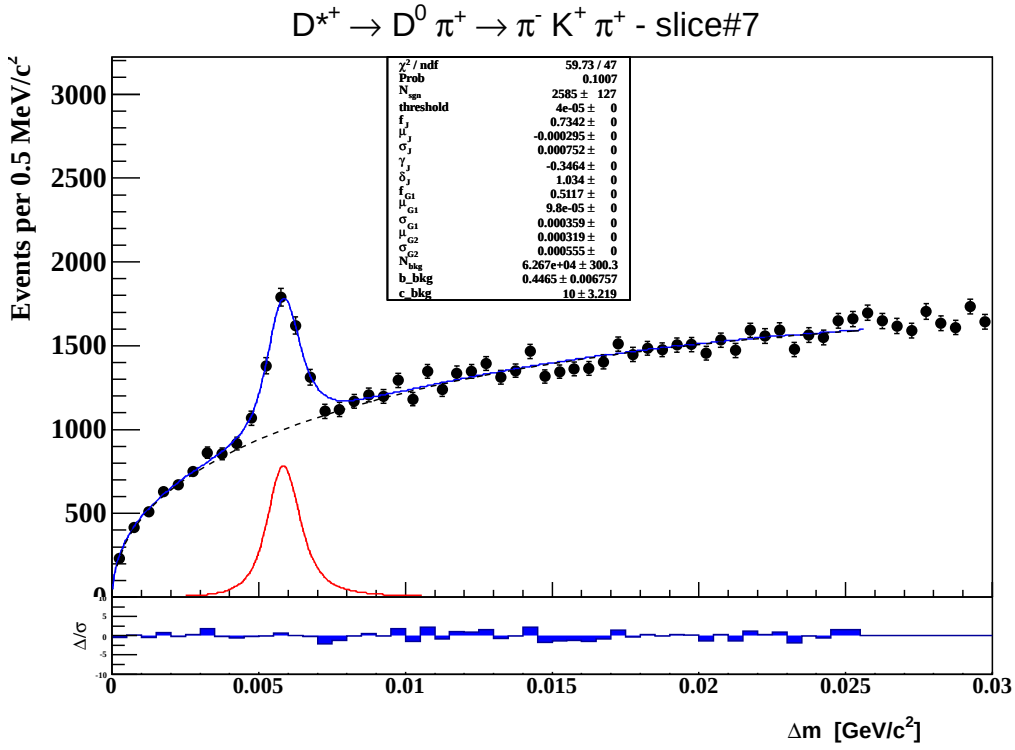

Appendix C: Δm Yield Fits $d_0 < 60\mu$m

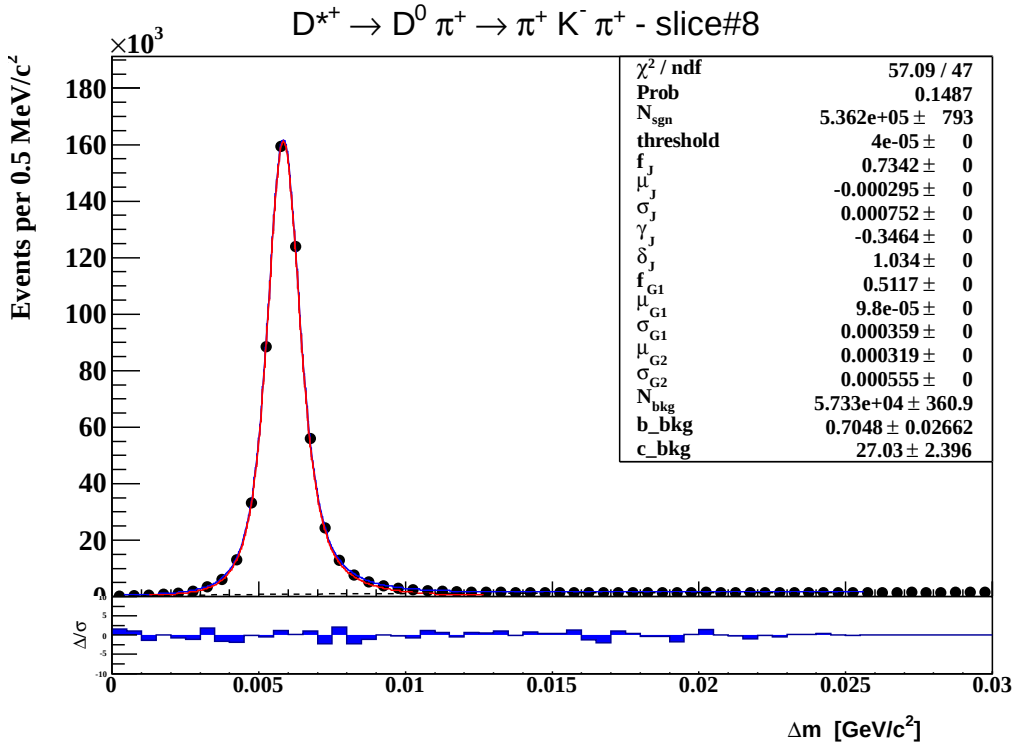

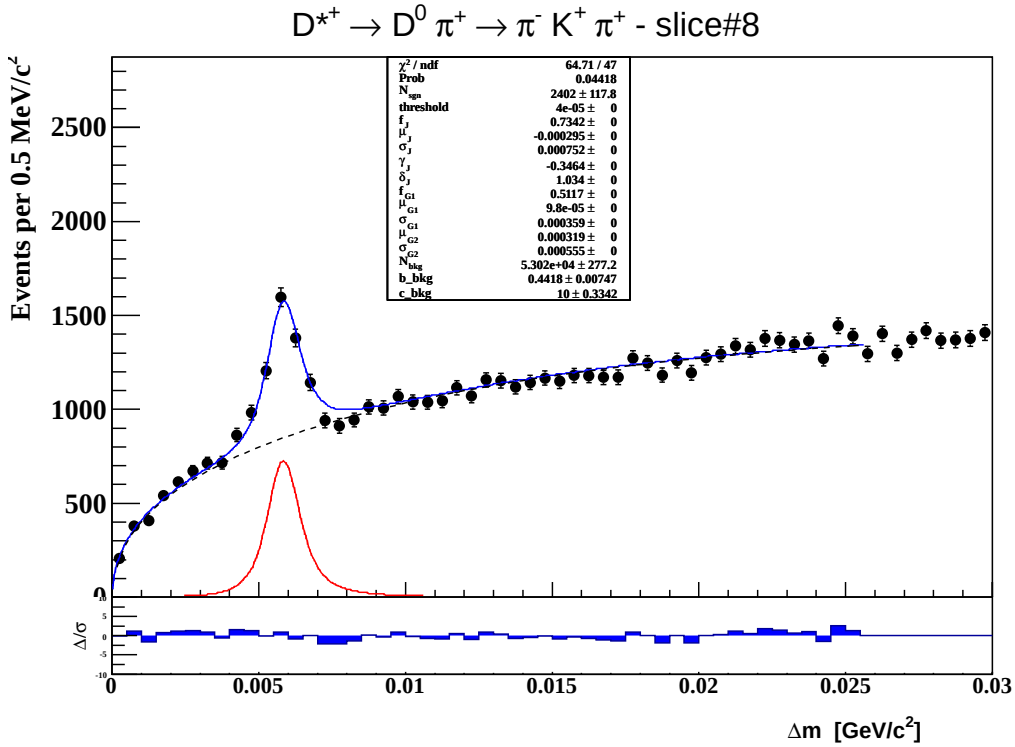

Appendix C: Δm Yield Fits $d_0 < 60\mu$m

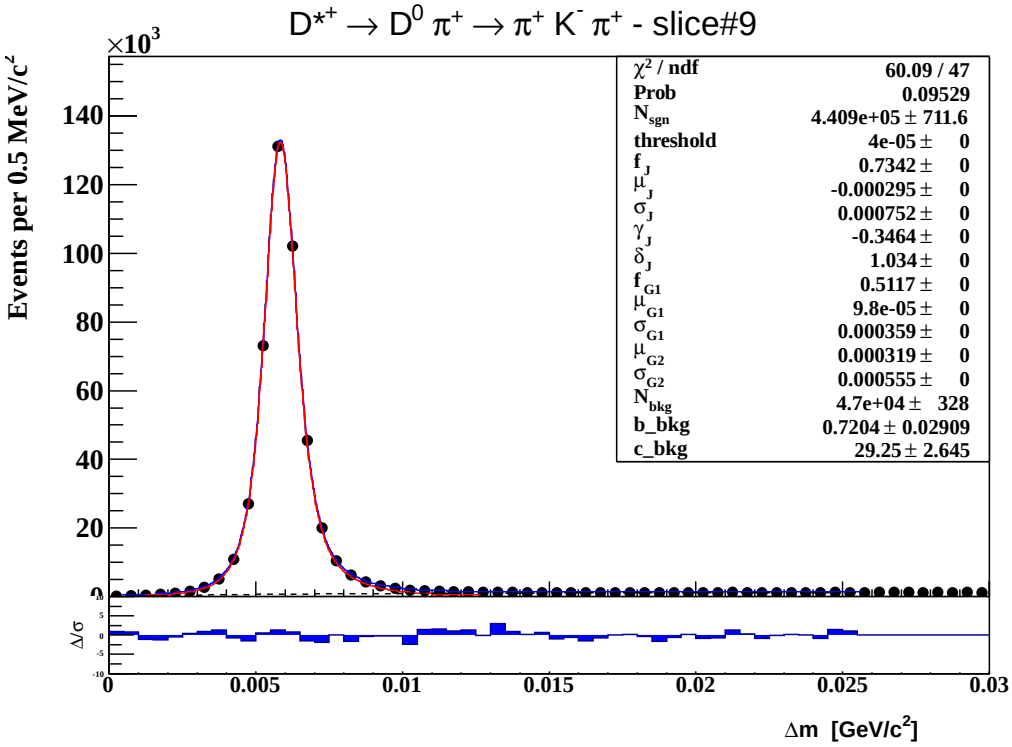

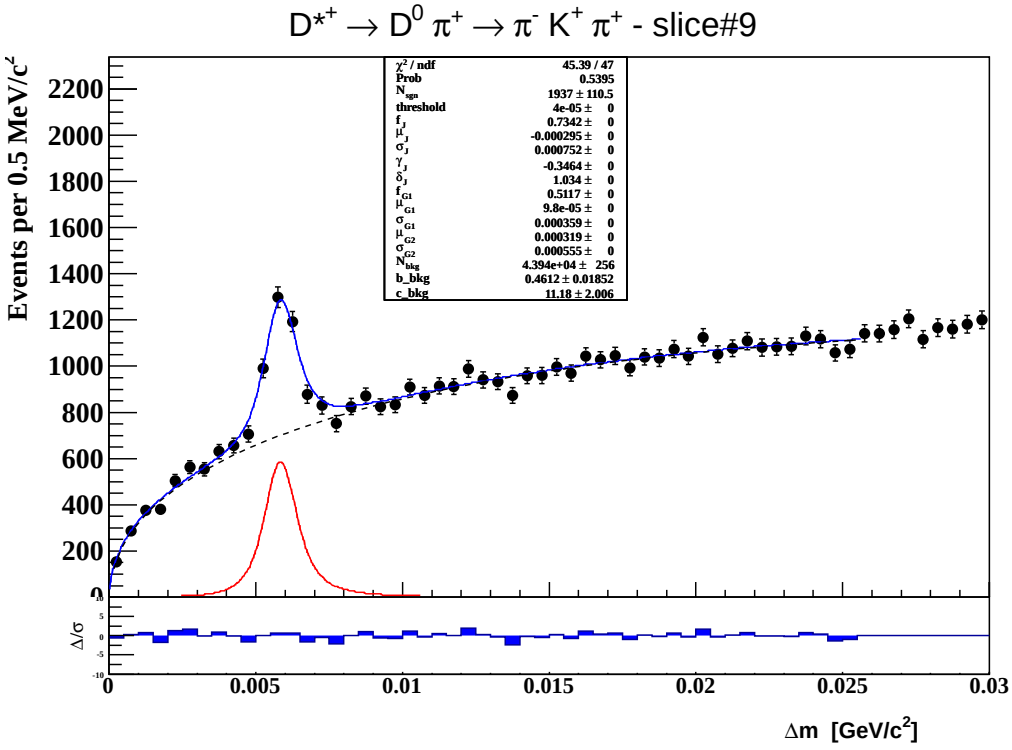

Appendix C: Δm Yield Fits $d_0 < 60\mu$m

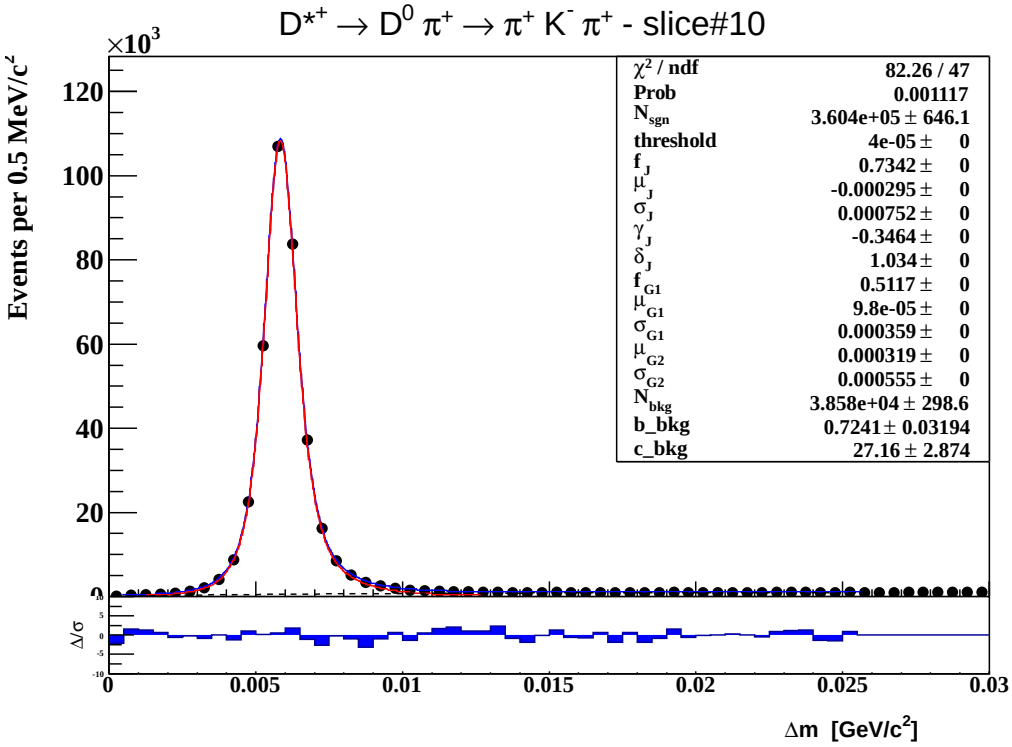

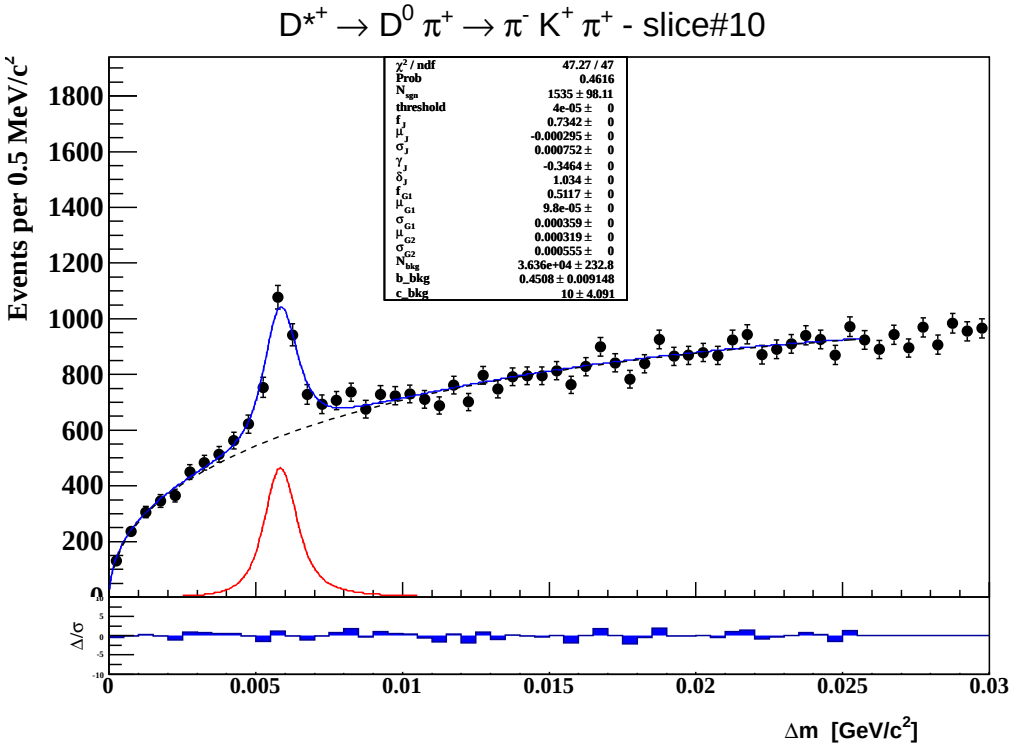

Appendix C: Δm Yield Fits $d_0 < 60\mu$m

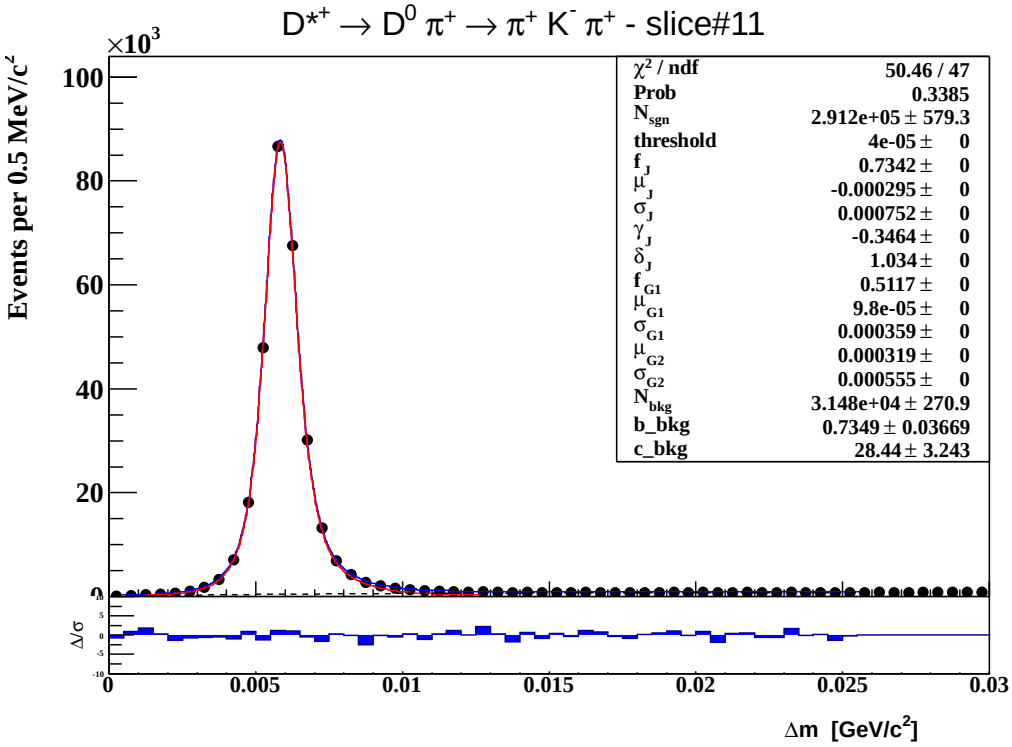

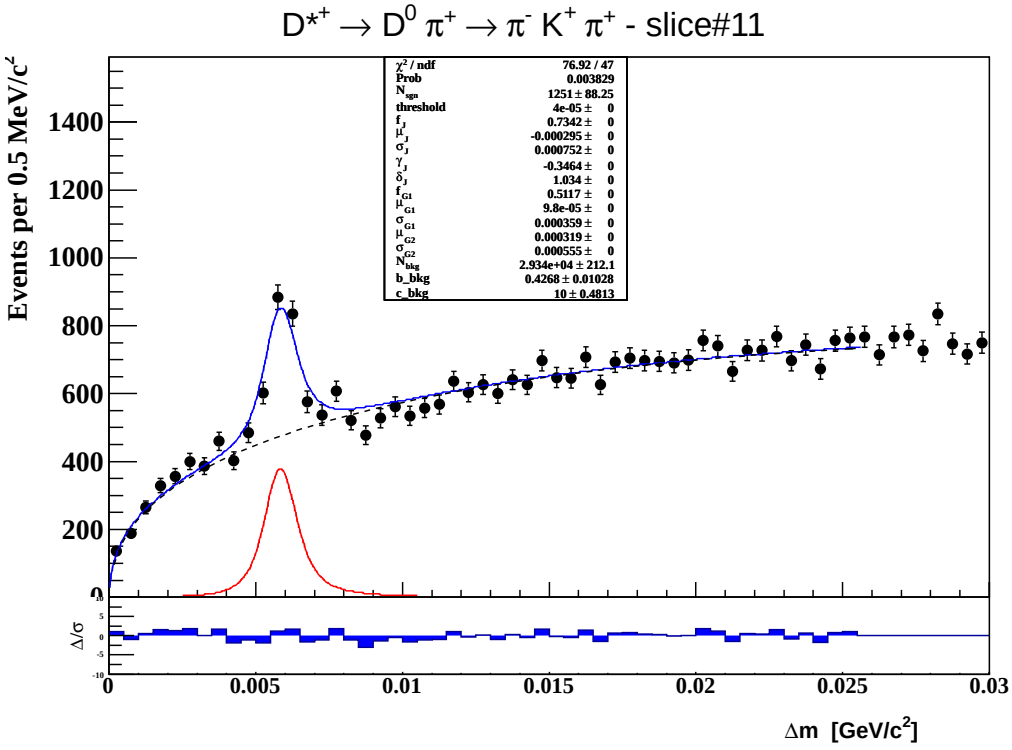

Appendix C: Δm Yield Fits $d_0 < 60\mu$m

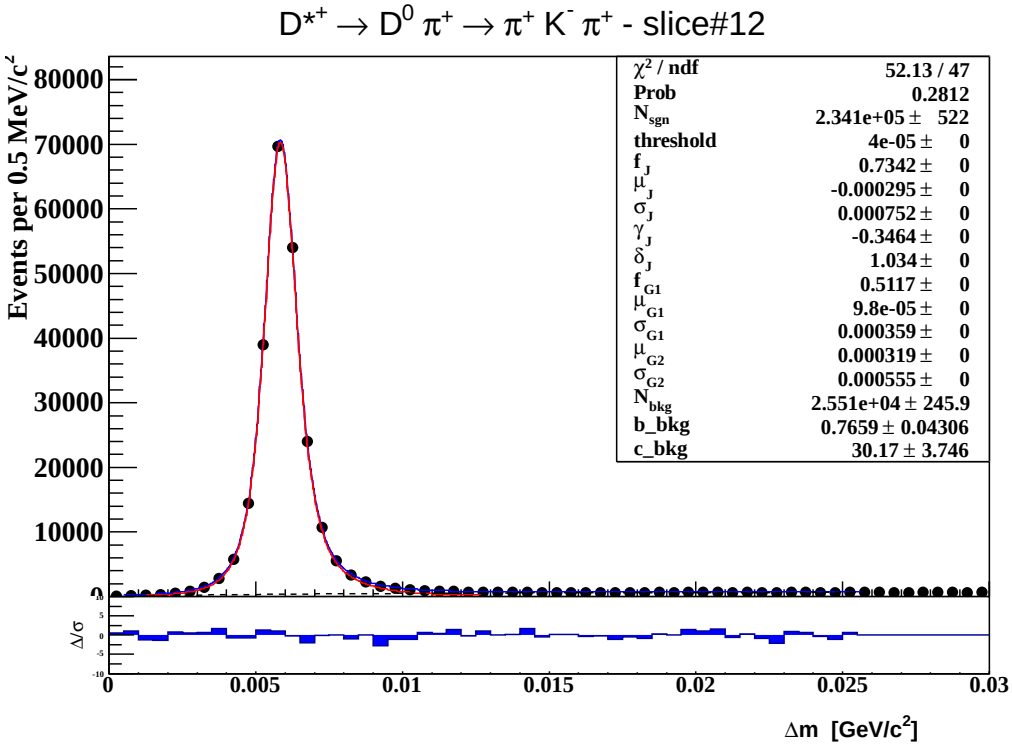

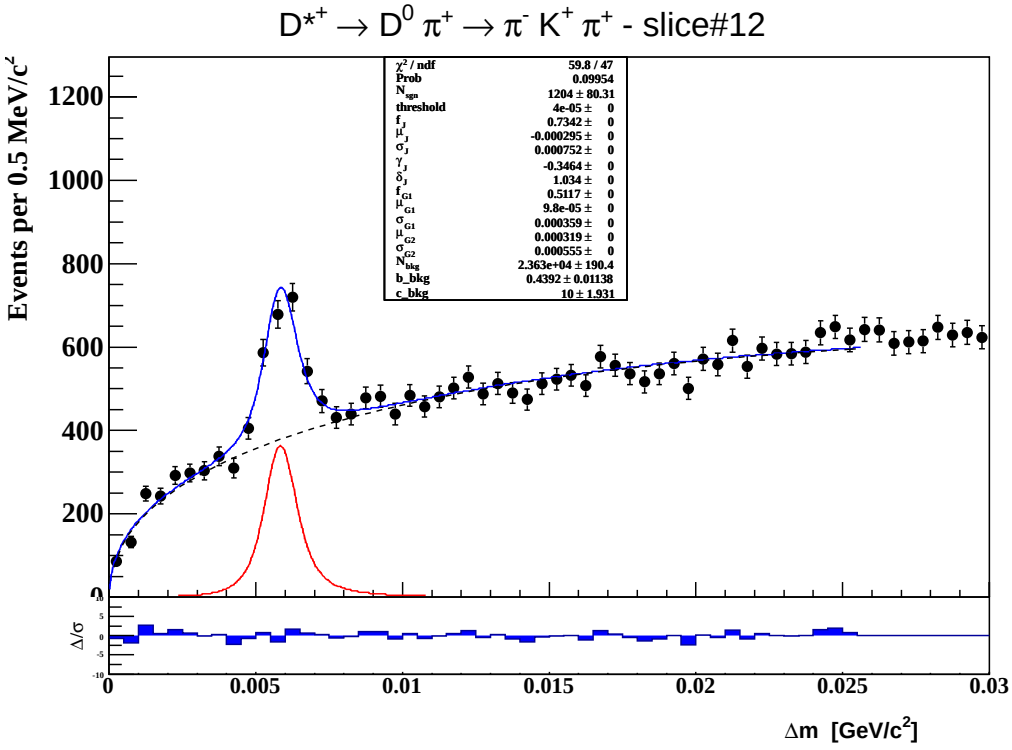

Appendix C: Δm Yield Fits $d_0 < 60\mu$m

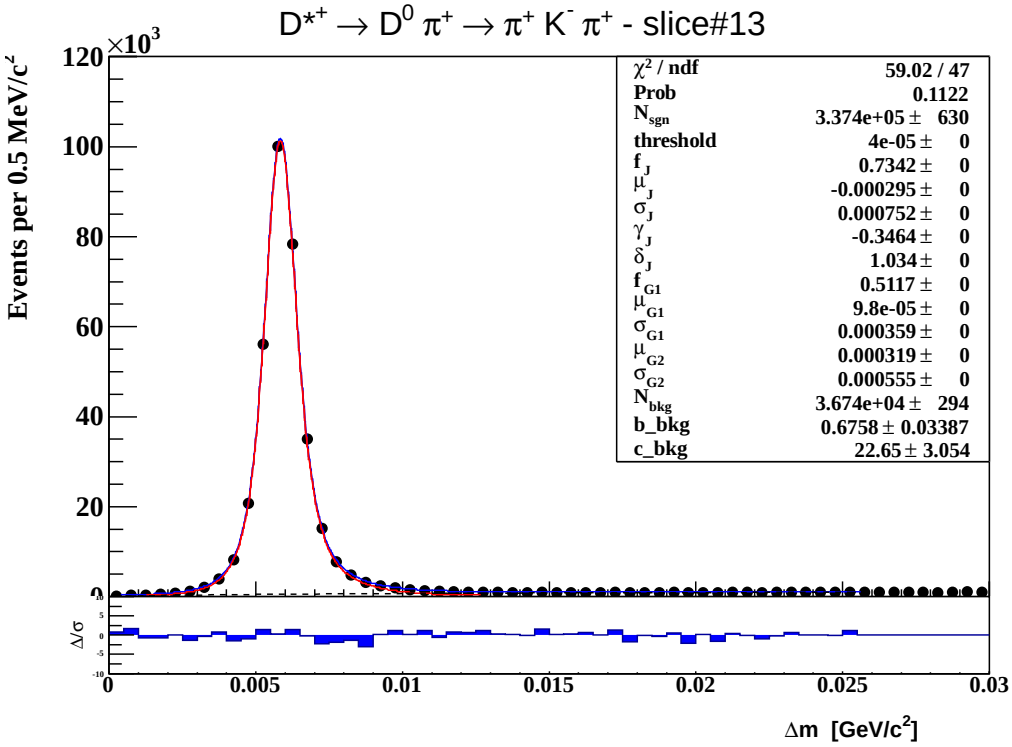

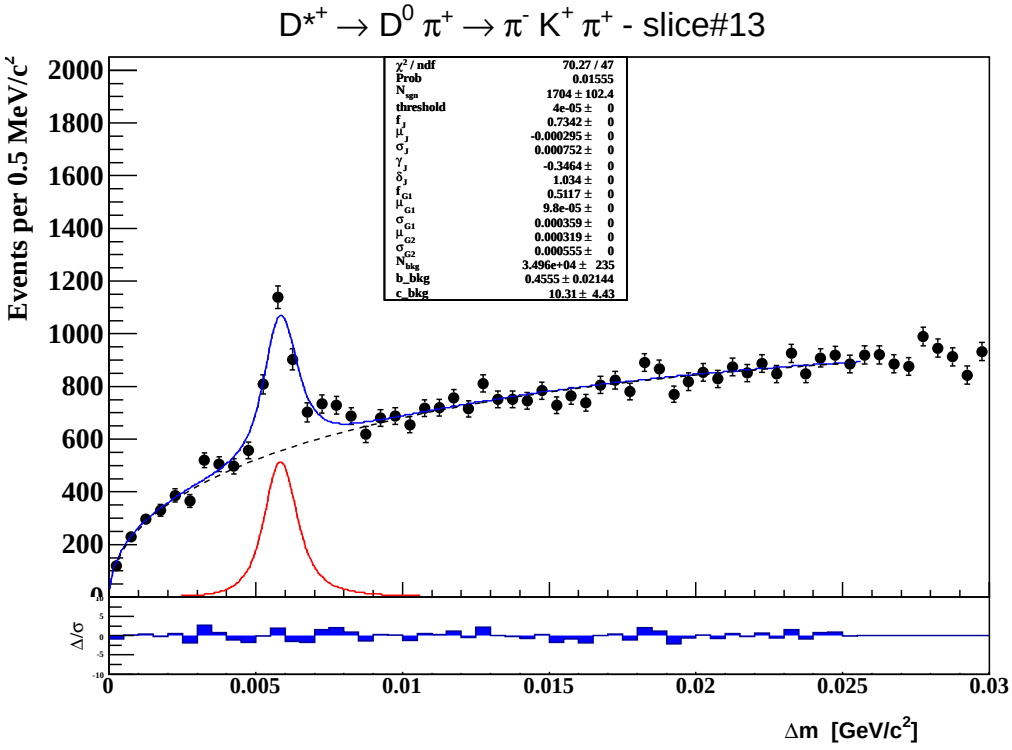

Appendix C: Δm Yield Fits $d_0 < 60\mu$m

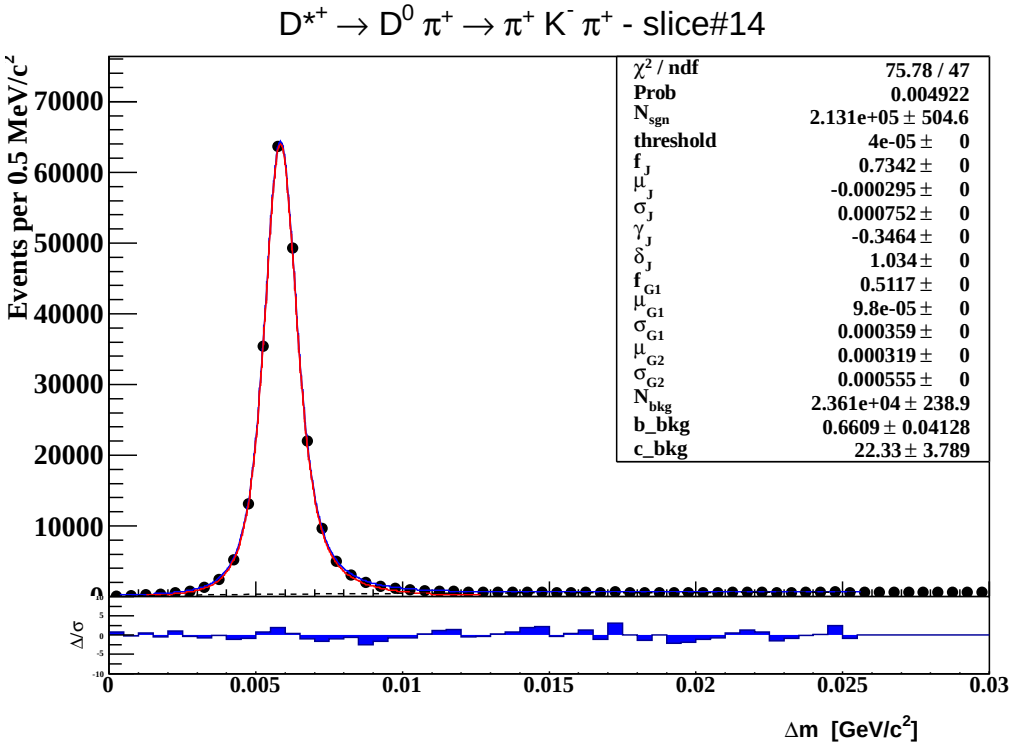

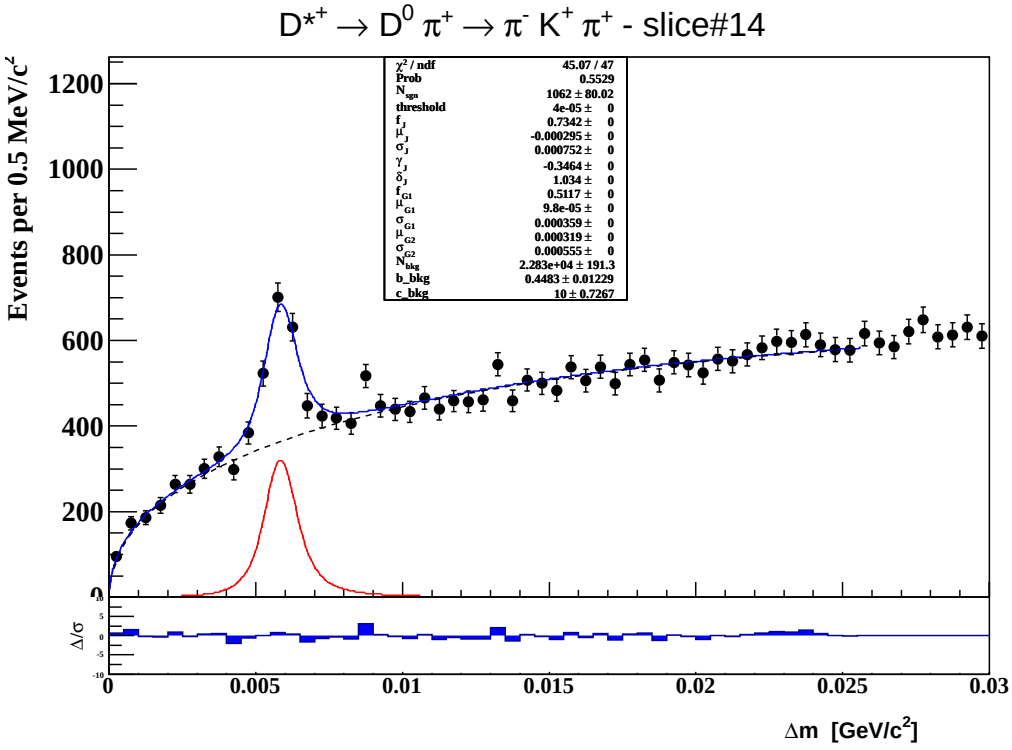

Appendix C: Δm Yield Fits $d_0 < 60\mu$m

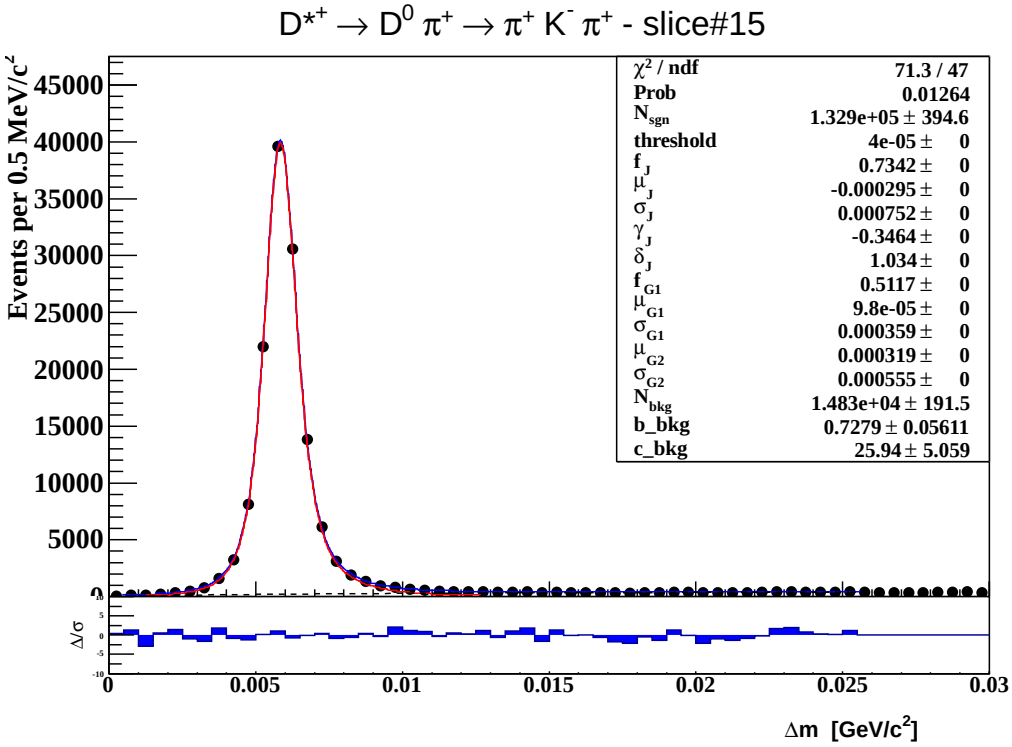

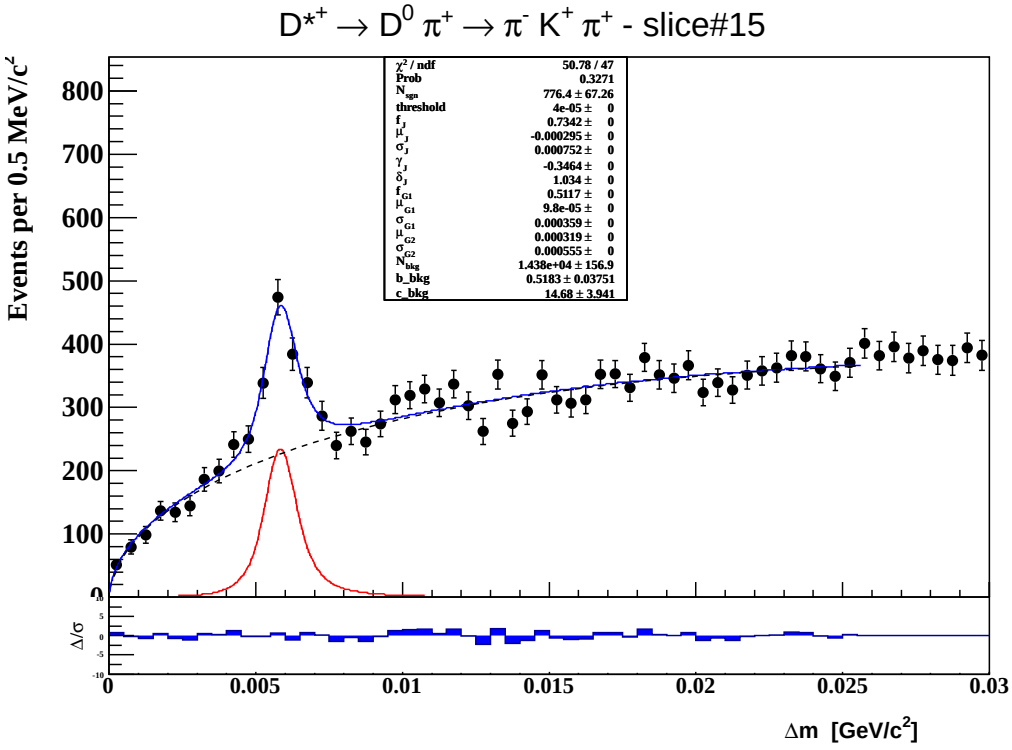

Appendix C: Δm Yield Fits $d_0 < 60\mu$m

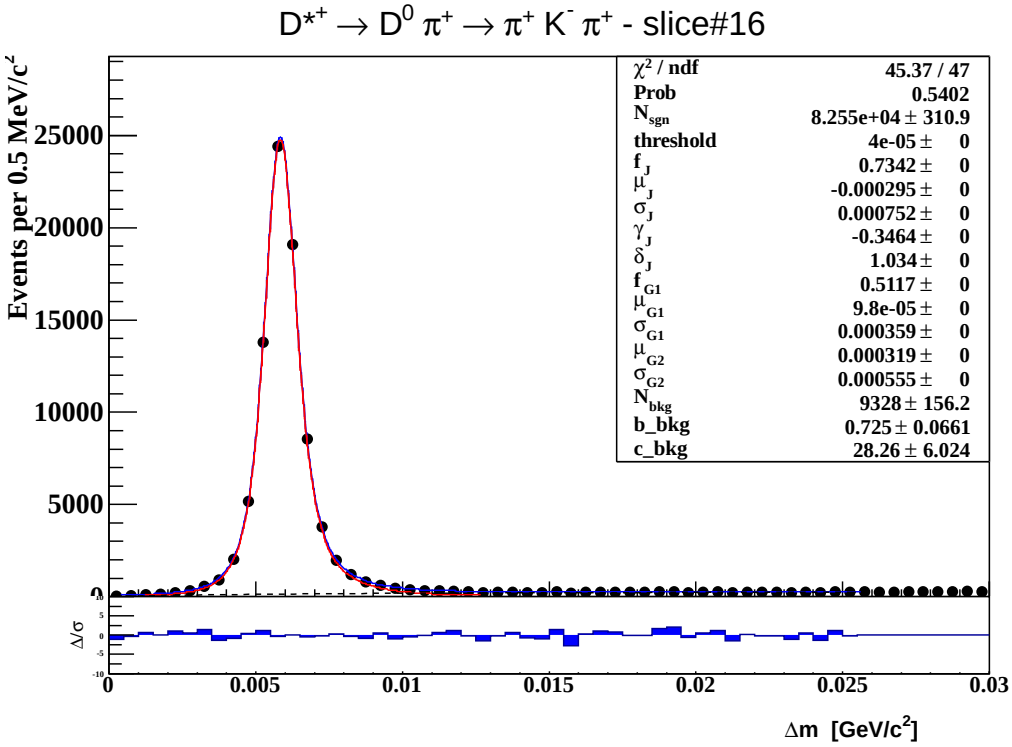

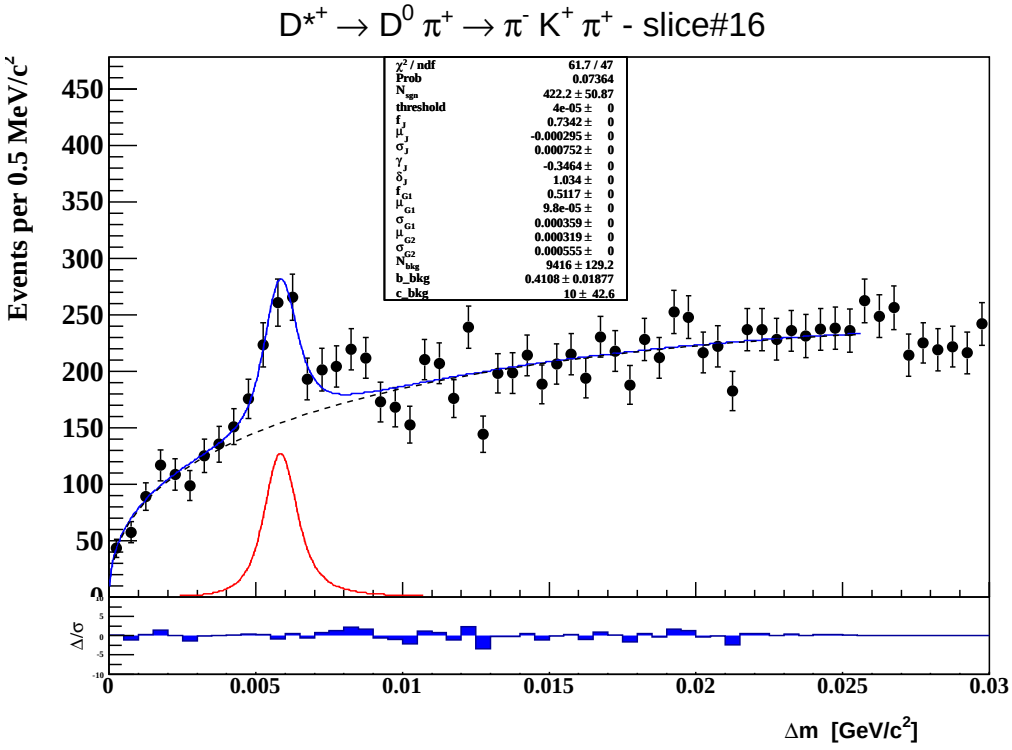

Appendix C: Δm Yield Fits $d_0 < 60\mu$m

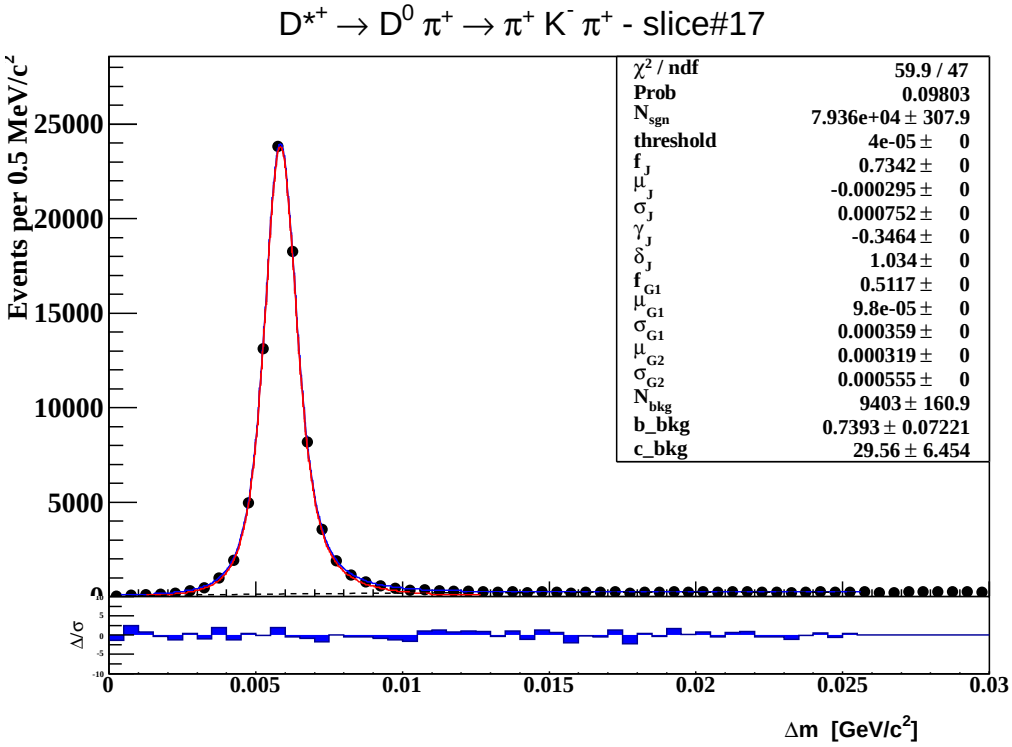

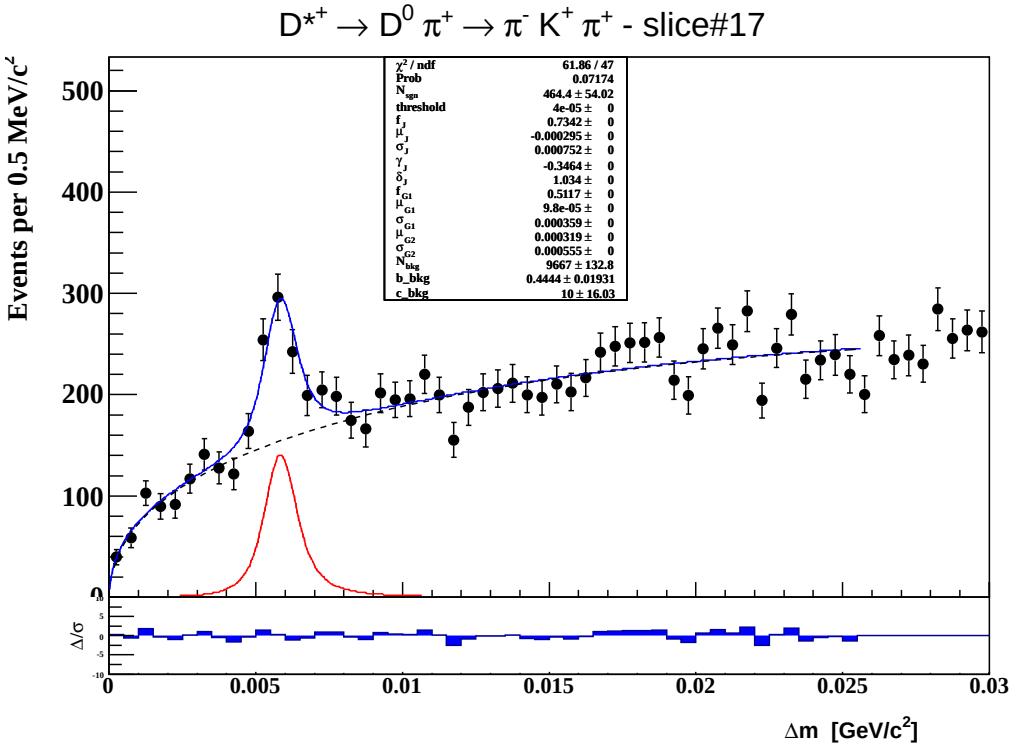

Appendix C: Δm Yield Fits $d_0 < 60\mu$m

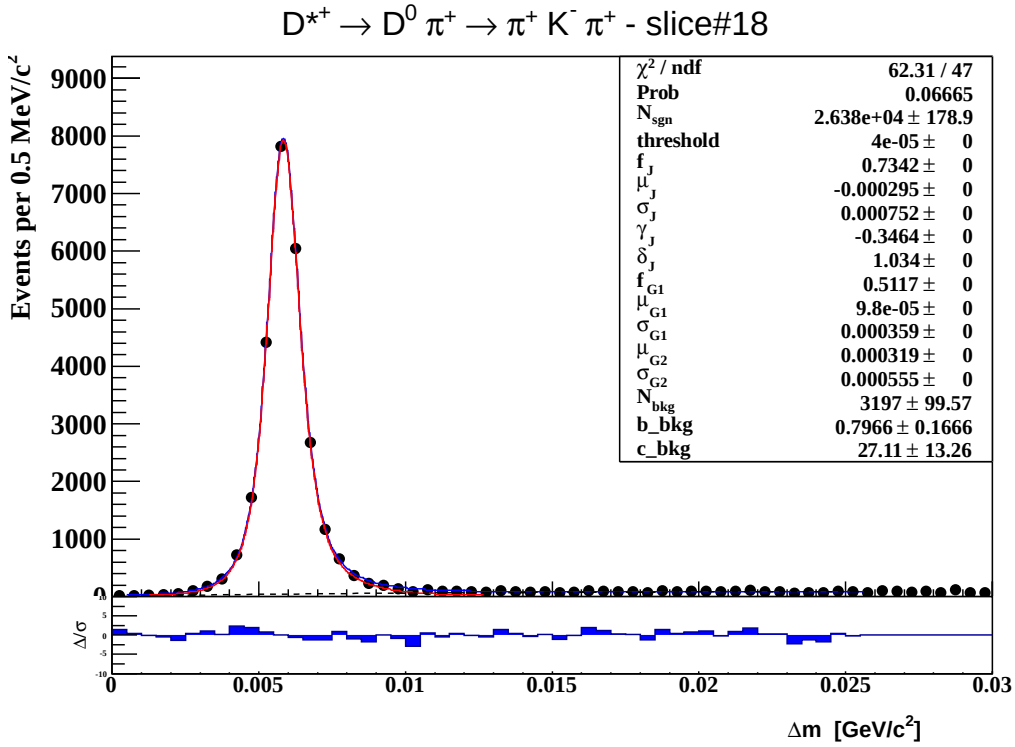

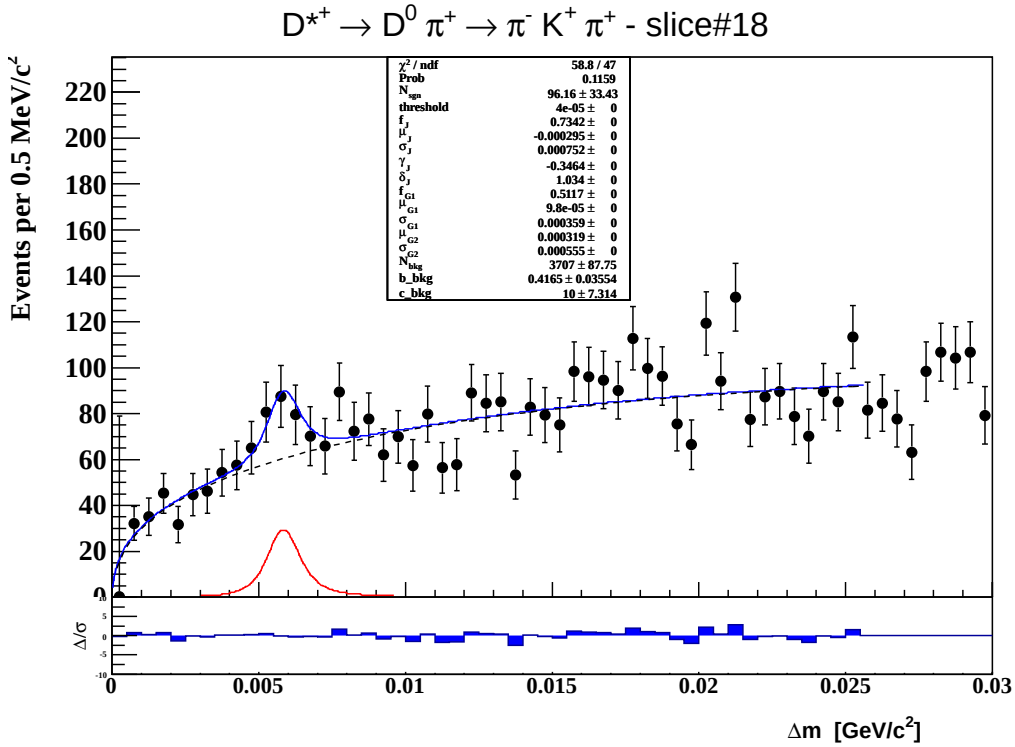

Appendix C: Δm Yield Fits $d_0 < 60\mu$m

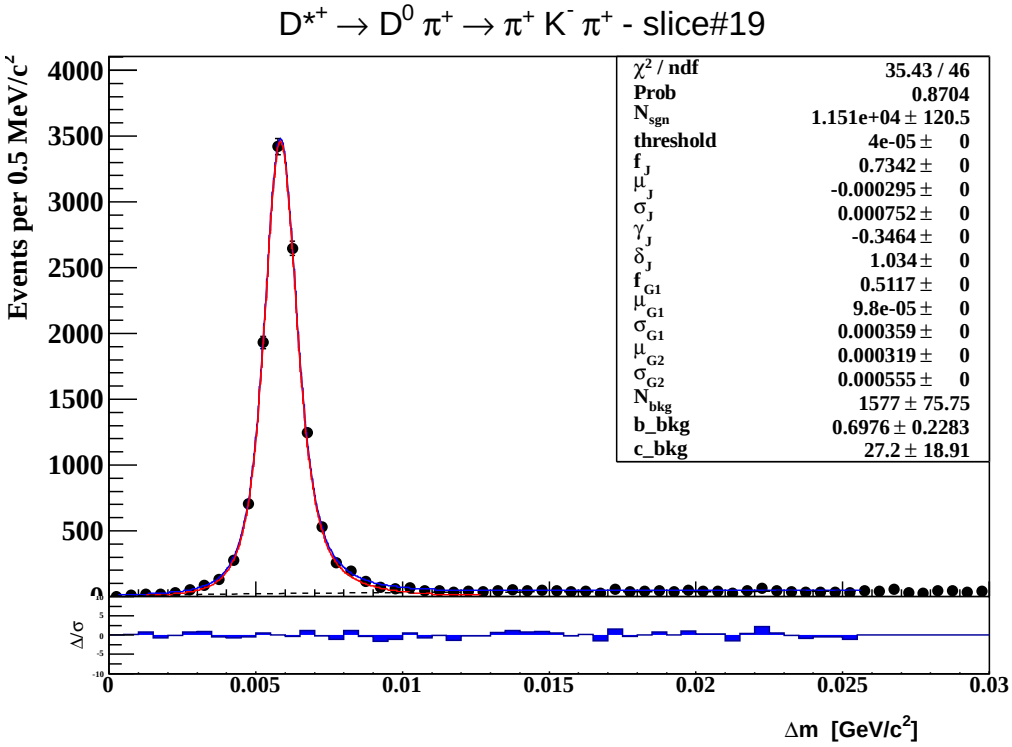

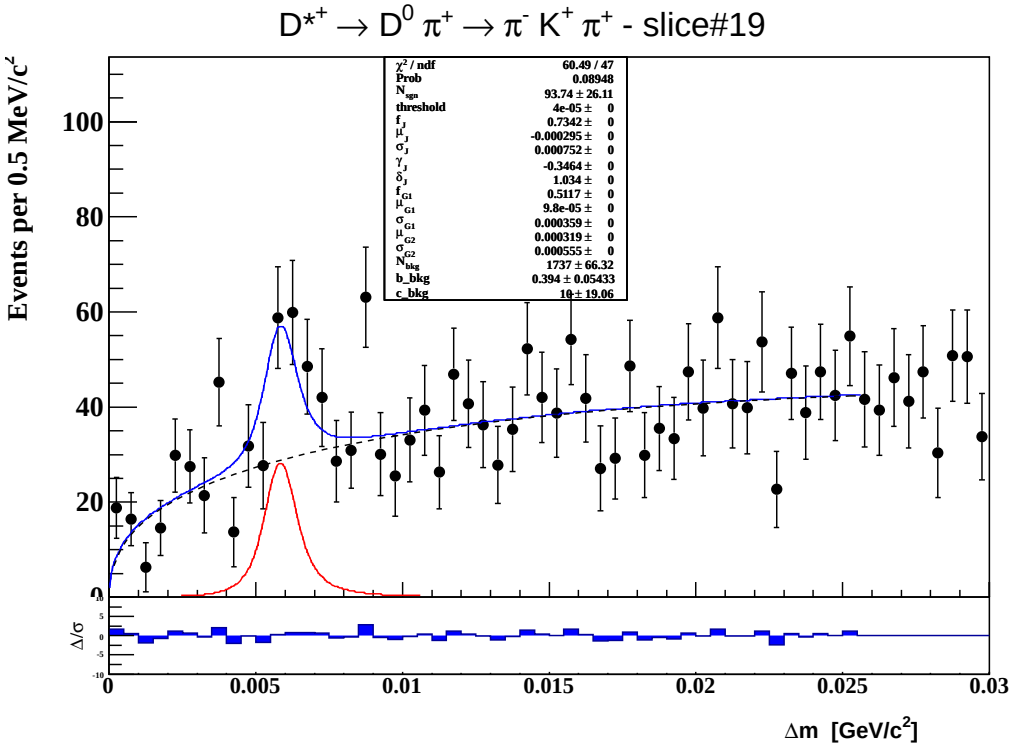

D Non-Prompt D^* Correction Details

This appendix shows the data fits for the time-binned $d0$ distributions. We use RS D^* events, with $(K\pi)$ sideband-subtraction. The distribution for each time bin is fit with a double Gaussian for the prompt (signal) peak, and a double Gaussian for the non-prompt distribution. Each plot covers the (unsigned) d_0 values from 0 to 500 microns.

The red curve is the combined fit to the data points. The dashed line is the projection of the non-prompt component, while the blue is the projection of the prompt component. Each fit has 50 bins, with 10 fit parameters (6 for the prompt component, 4 for the non-prompt component).

Appendix D: RS d_0 Distributions By Decay Time

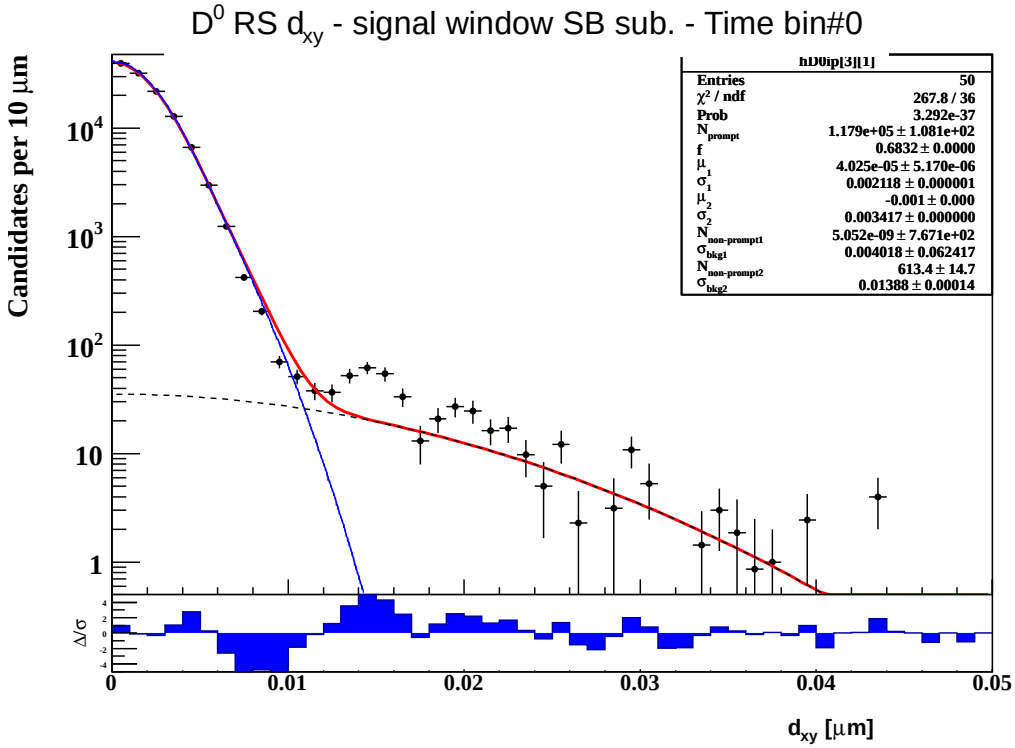

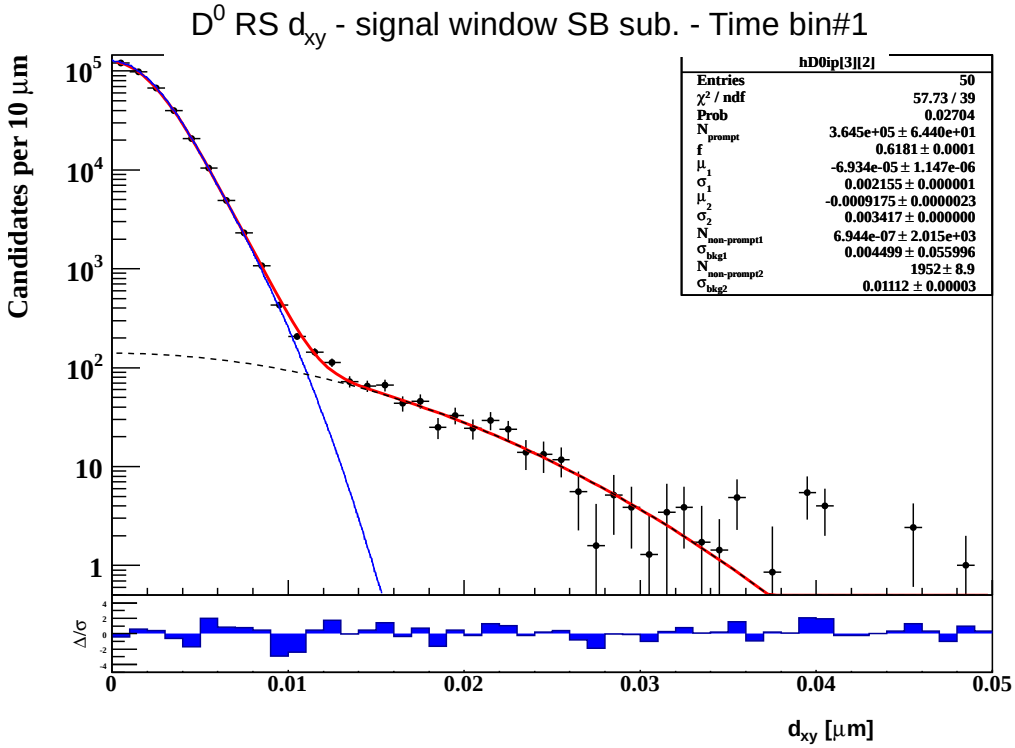

Appendix D: RS d_0 Distributions By Decay Time

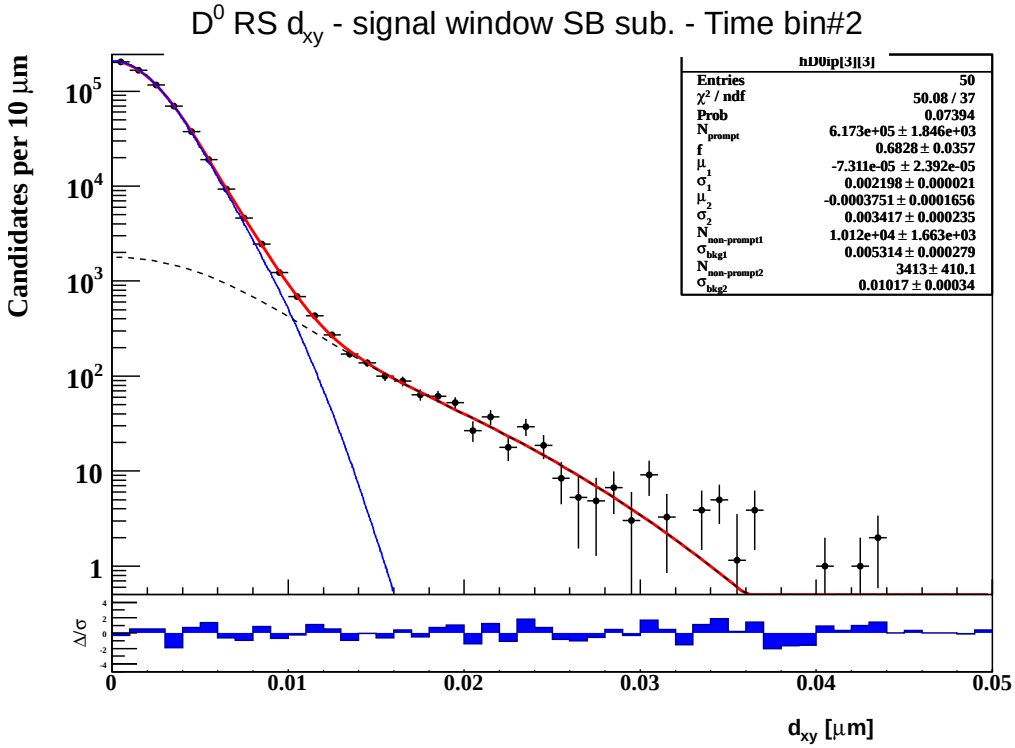

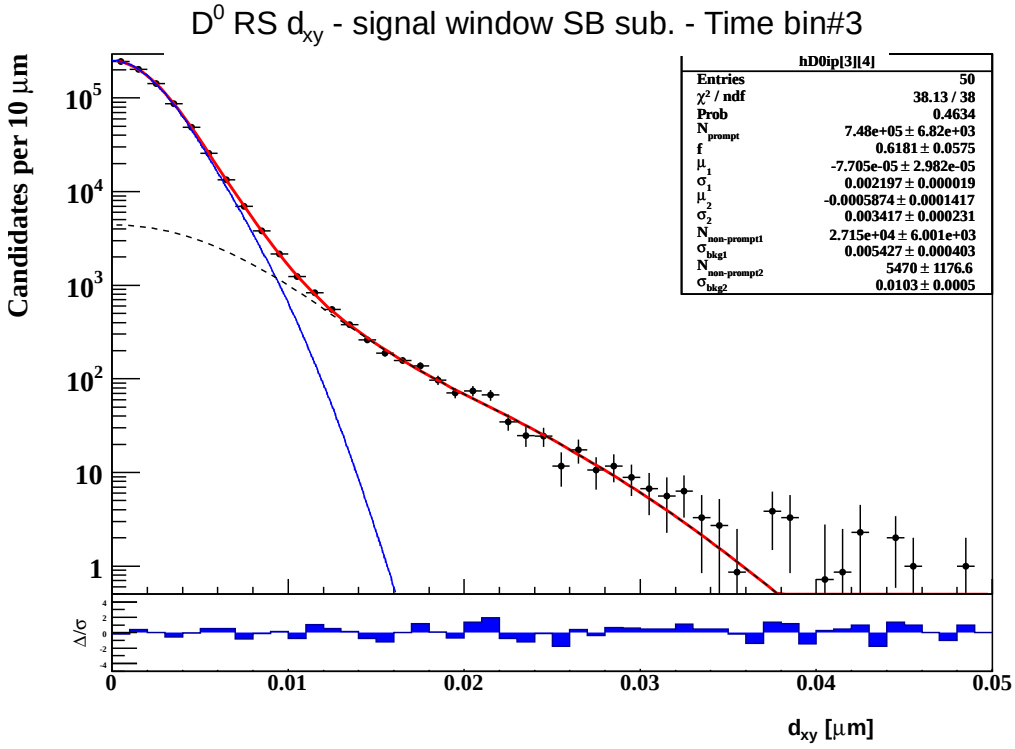

Appendix D: RS d_0 Distributions By Decay Time

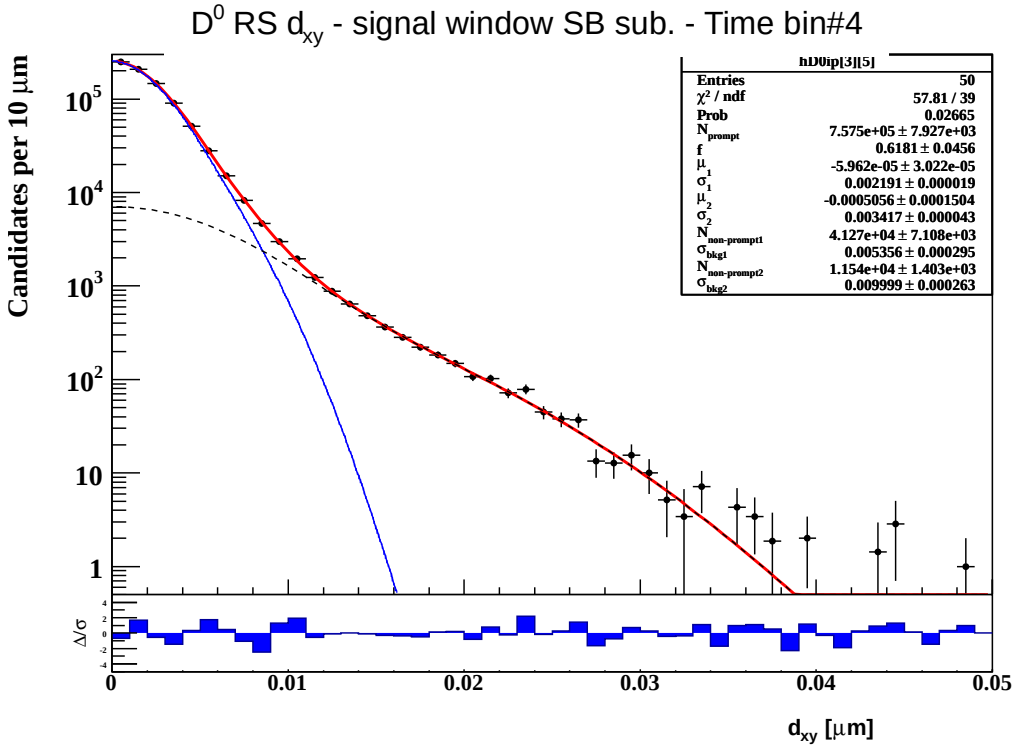

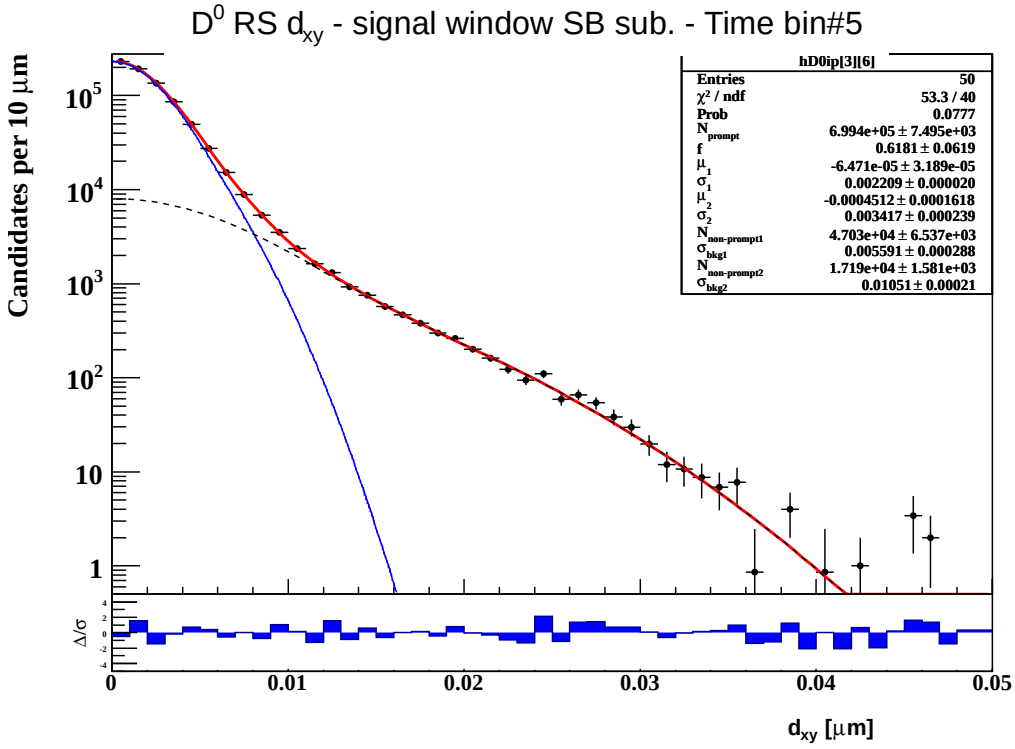

Appendix D: RS d_0 Distributions By Decay Time

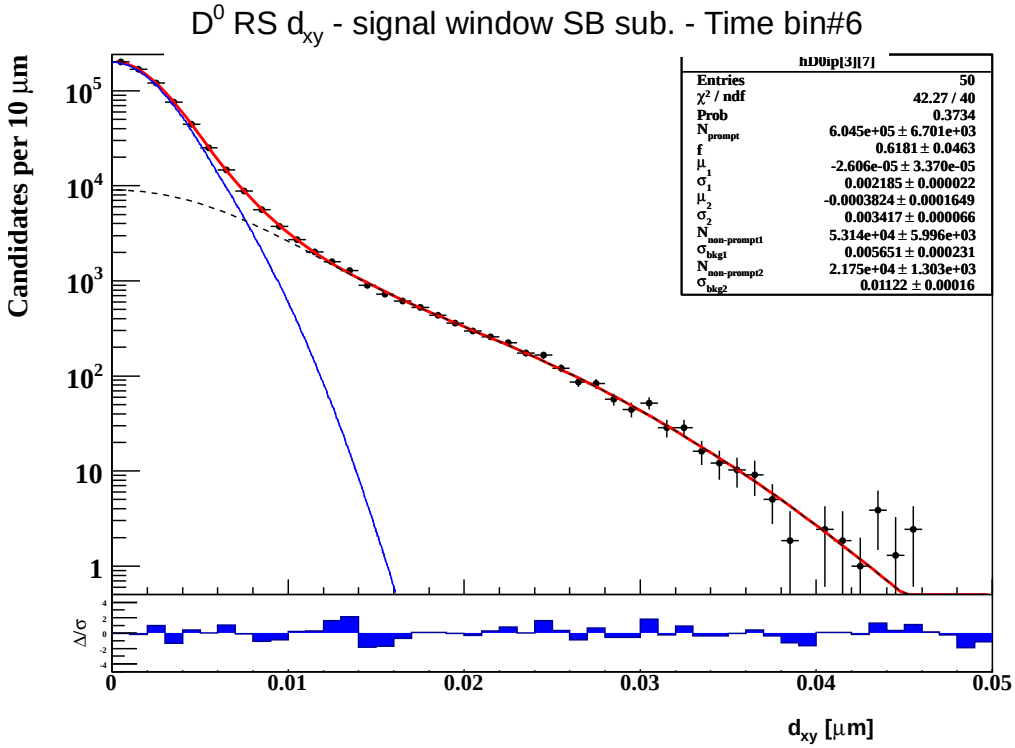

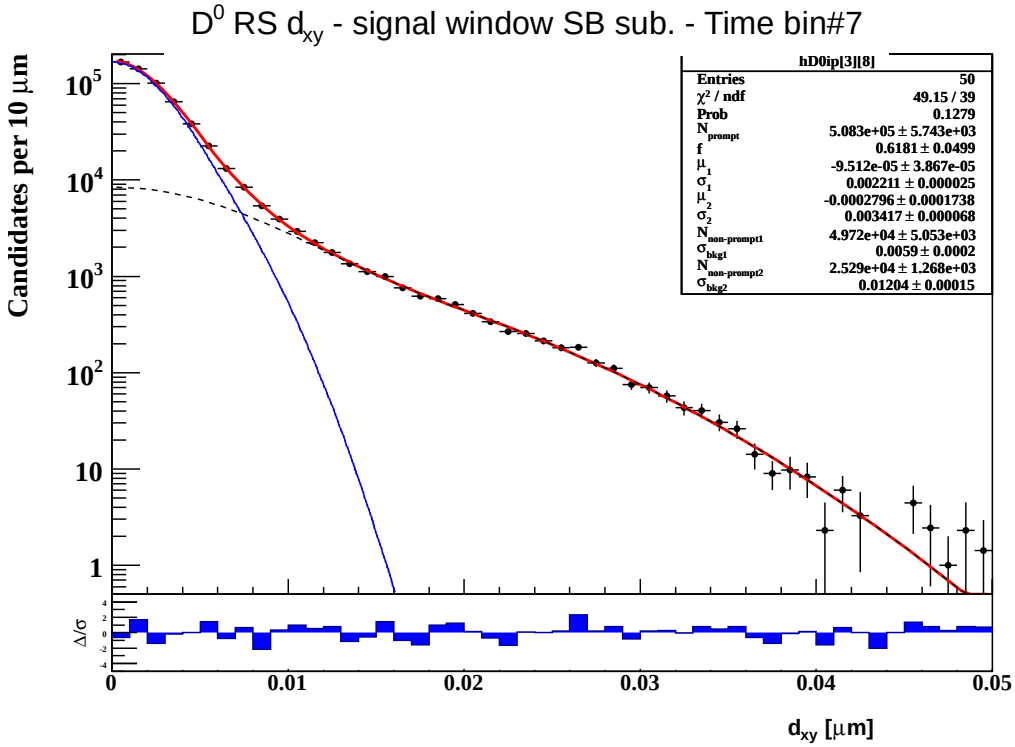

Appendix D: RS d_0 Distributions By Decay Time

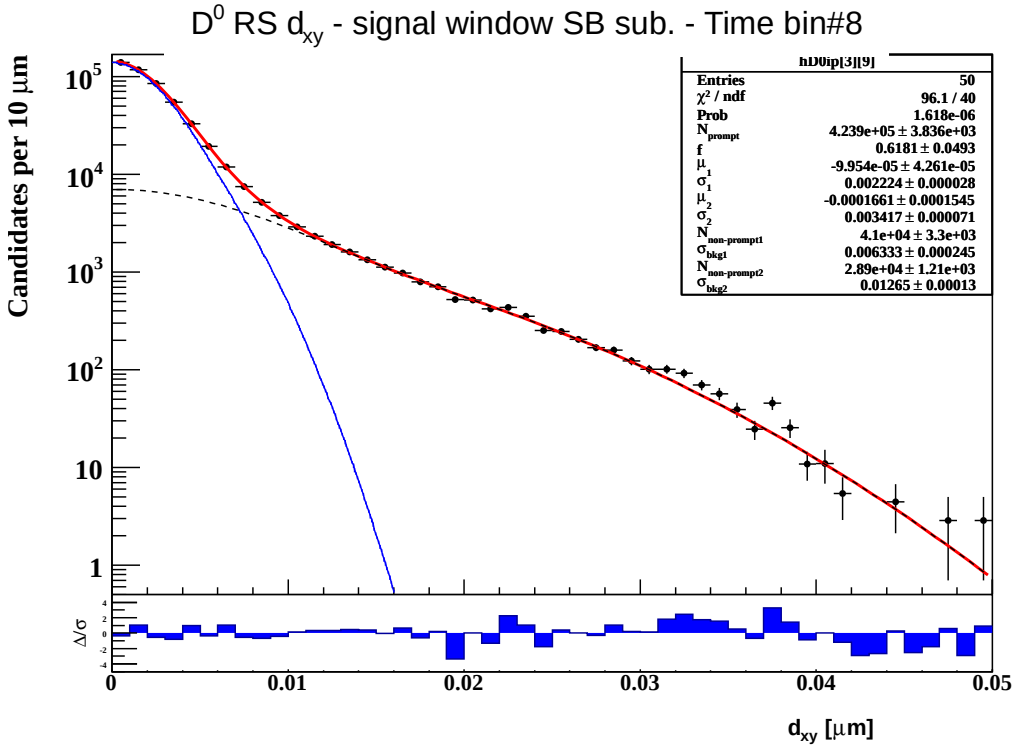

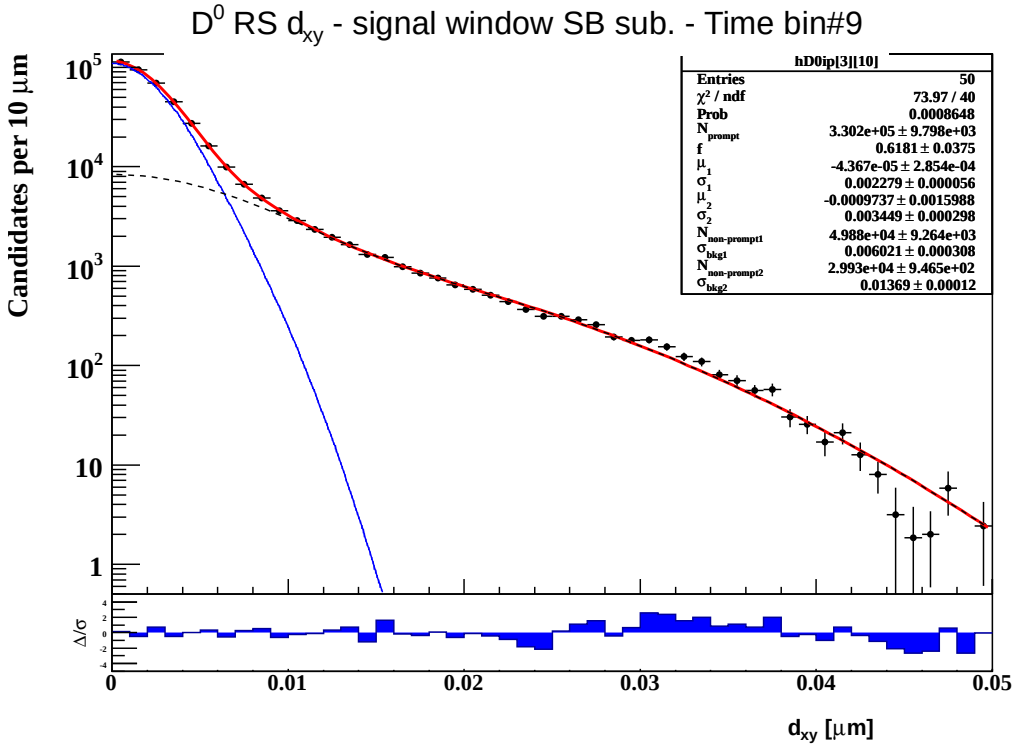

Appendix D: RS d_0 Distributions By Decay Time

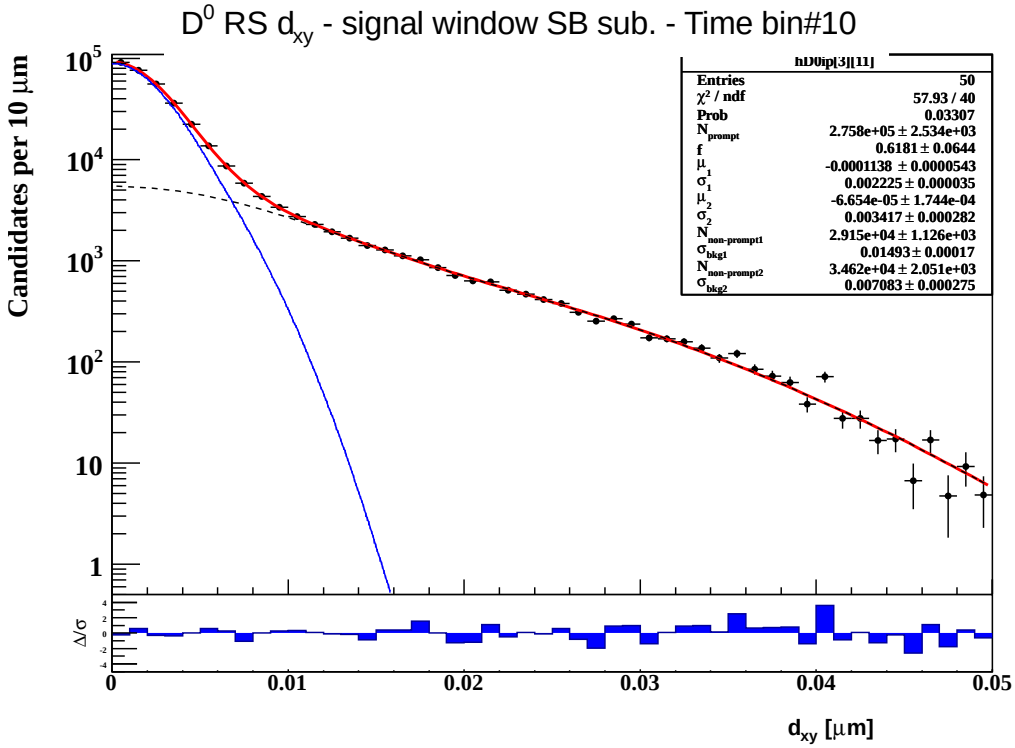

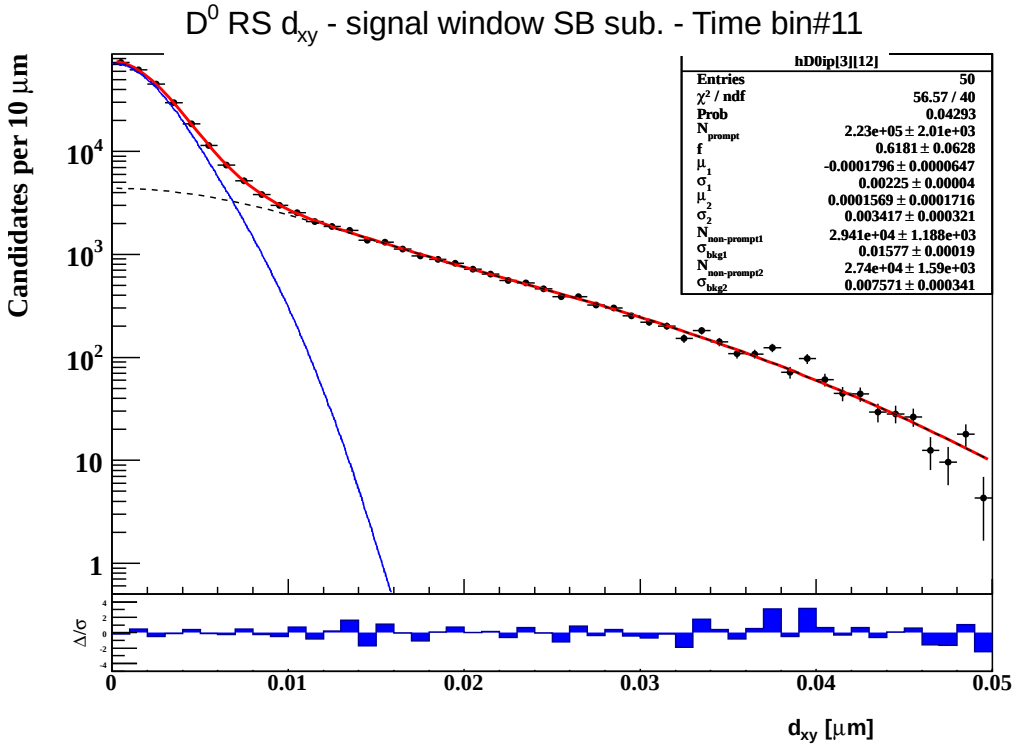

Appendix D: RS d_0 Distributions By Decay Time

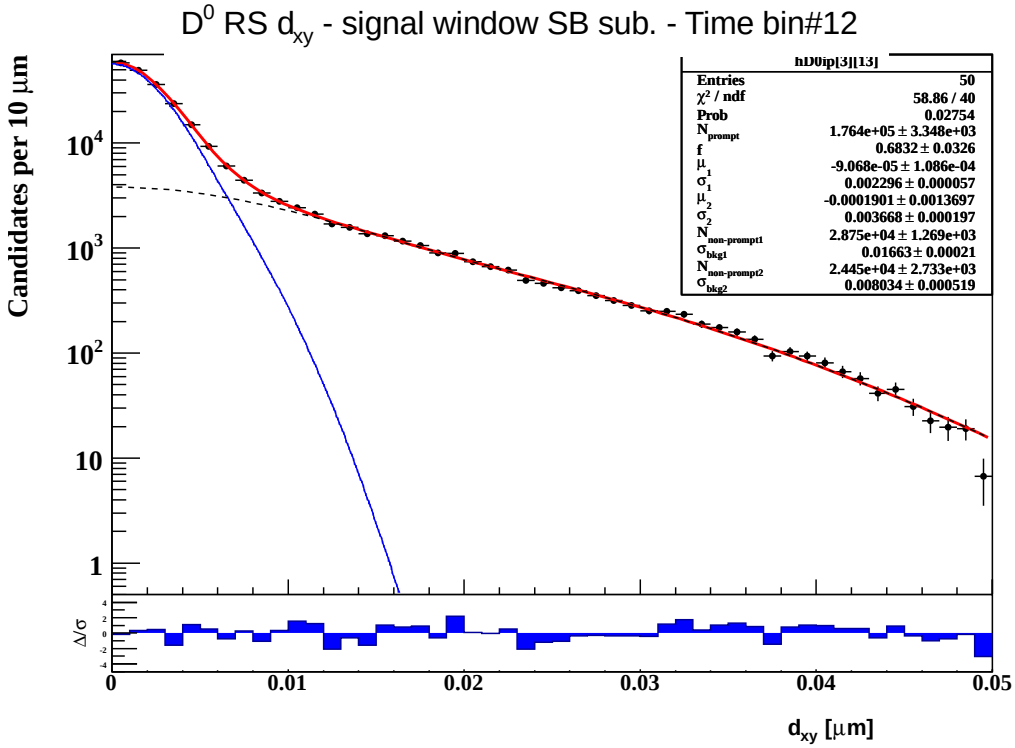

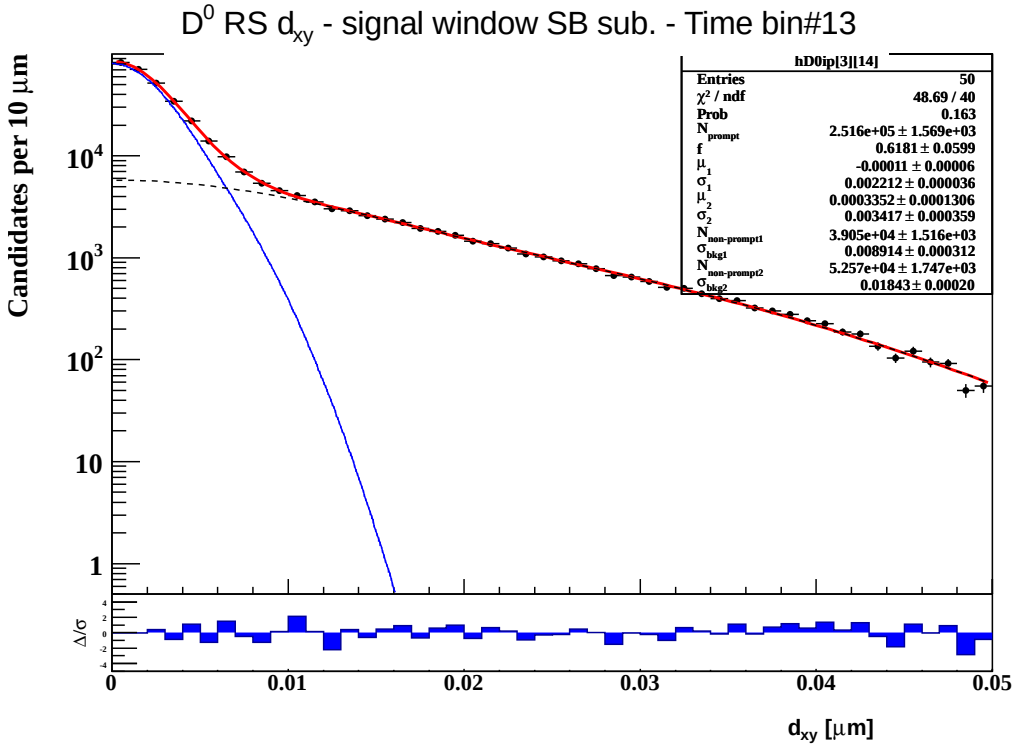

Appendix D: RS d_0 Distributions By Decay Time

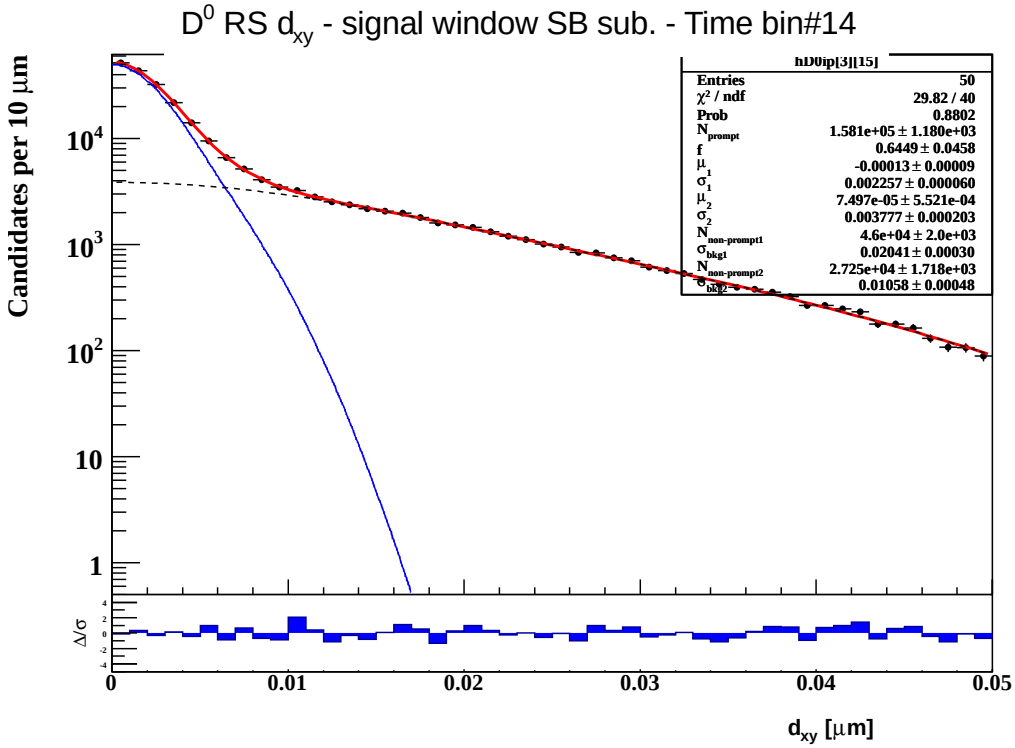

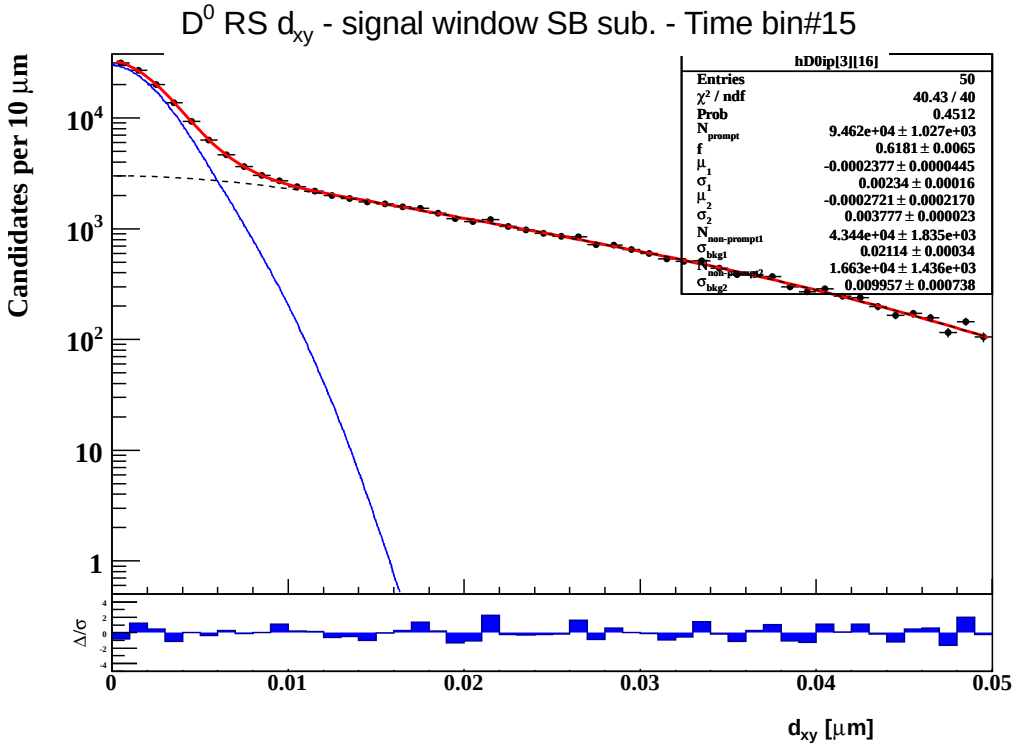

Appendix D: RS d_0 Distributions By Decay Time

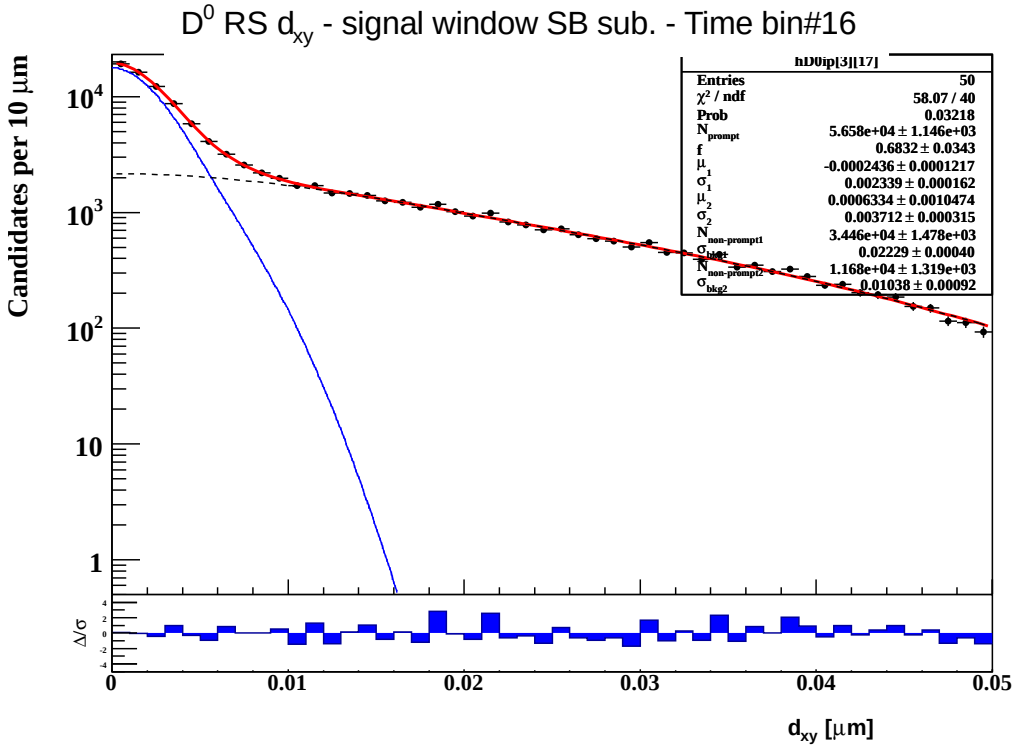

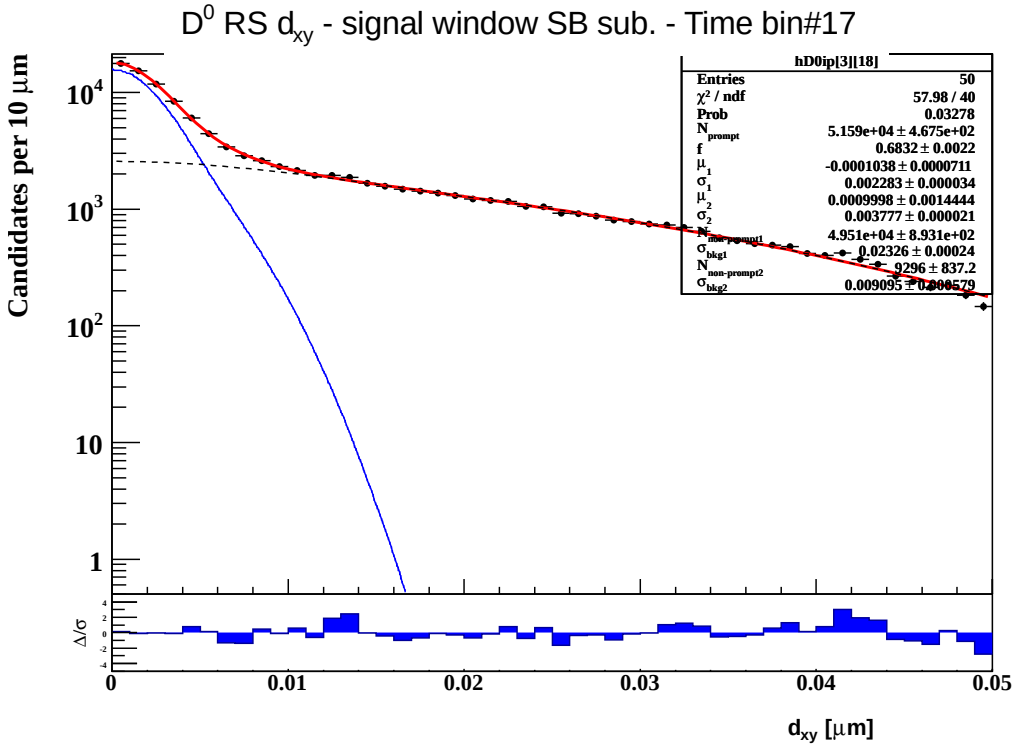

Appendix D: RS d_0 Distributions By Decay Time

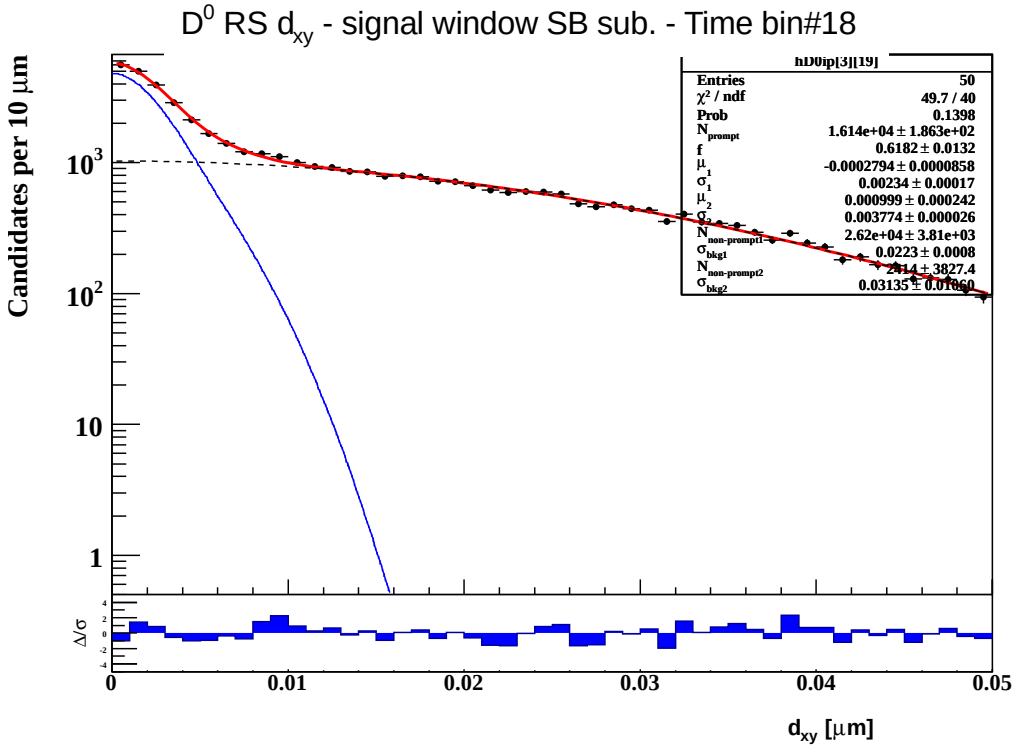

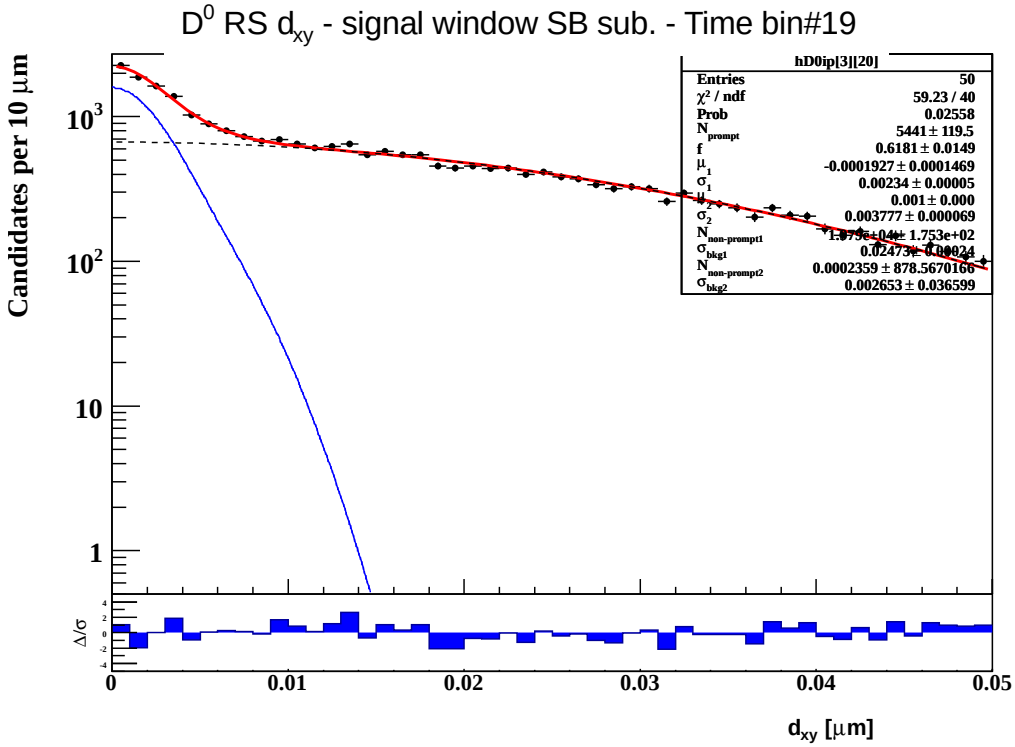

E MC Histograms for Non-Prompt D^* Correction

We use a Monte Carlo sample where a B meson decays inclusively to decay modes containing a D^0 meson. This sample requires BCHARM trigger path and was used in BR, A_{CP} in DCS B decays analysis (CDF note 10264; section 6) and the ΔA_{CP} in $D^0 \to h^+h^-$ analysis (CDF note 10213; section 6.1.3). It is available in BstNtuple (v80) format at `fcdfprj1.fnal.gov:/cdf/proj/201.bottom/dicanto/BMC/B_DX`.

We analyze the MC events in a similar way as the data. A trigger confirmed opposite charged track pair candidate is considered if it satisfies $1.78 < m(K\pi) < 1.95$ GeV/c^2 and in the generator level has a D^0 candidate from a B. The $ct(D^0)$ for the candidate is calculated from its generator level time with respect to B. Figures 36 and 38 show t/τ distributions for $|d_0(D^0)| < 60$ μm and $60 < |d_0(D^0)| < 500$ μm cases, respectively. We include a time bin shorter than 0.75 lifetimes (bin 0) and two bins longer than 10 lifetimes (bins 21 and 22). Figures 37 and 39 show the same plots with logarithmic scale.

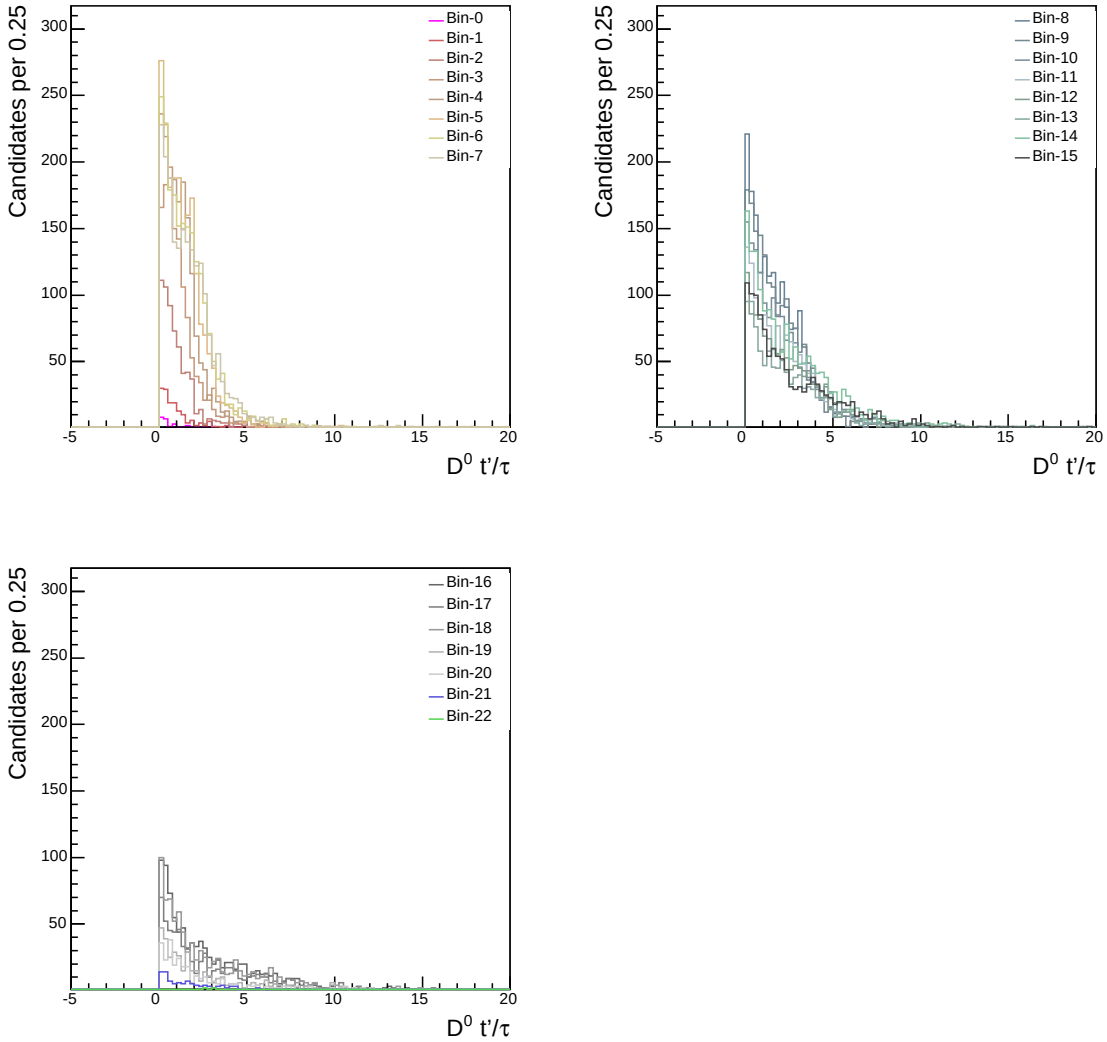

Figure 36: D^0 true t/τ distribution from a $B \to DX$ MC shown for $|d_0(D^0)| < 60$ μm and all time bins in linear scale

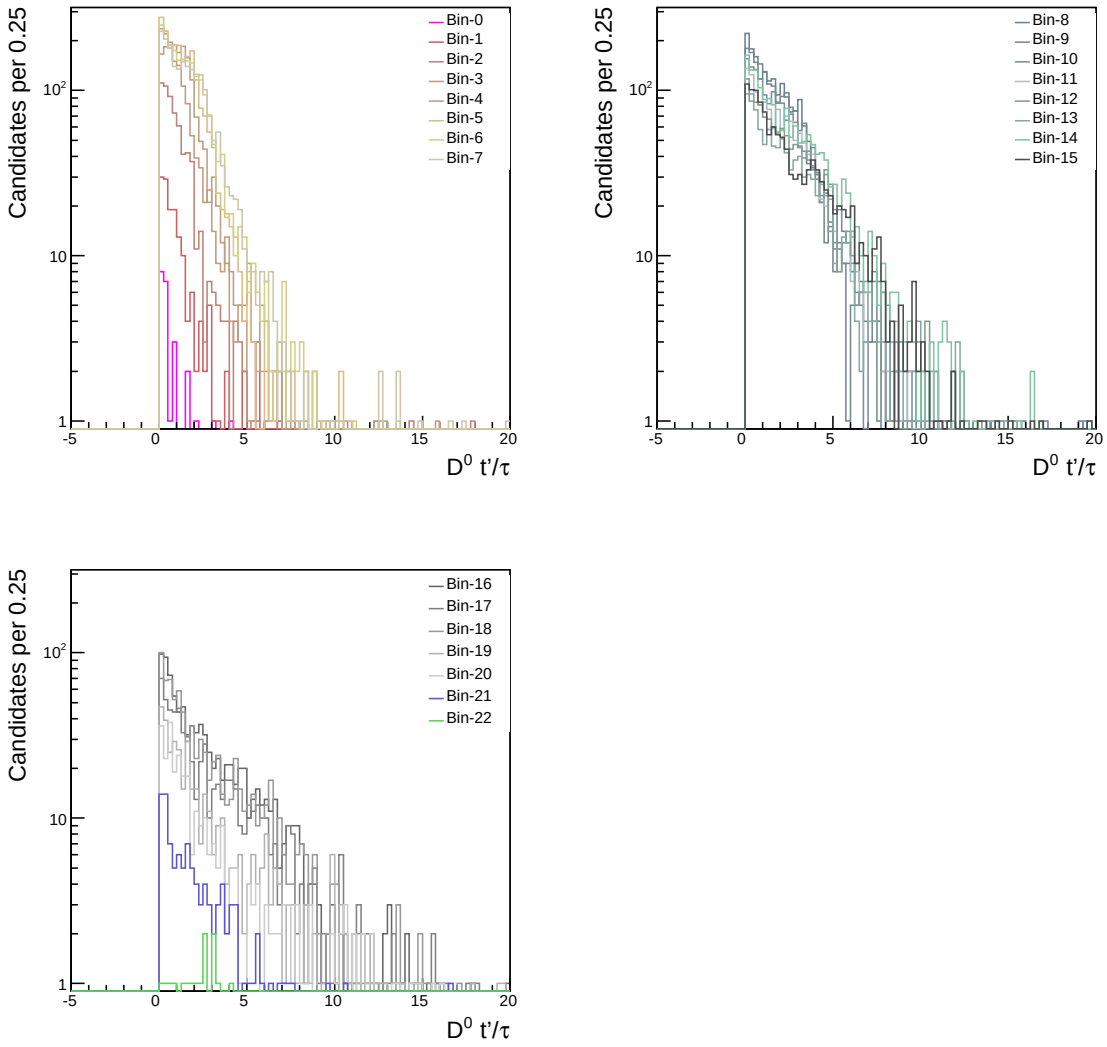

Figure 37: D^0 true t/τ distribution from a $B \to DX$ MC shown for $|d_0(D^0)| < 60$ μm and all time bins in logarithmic scale

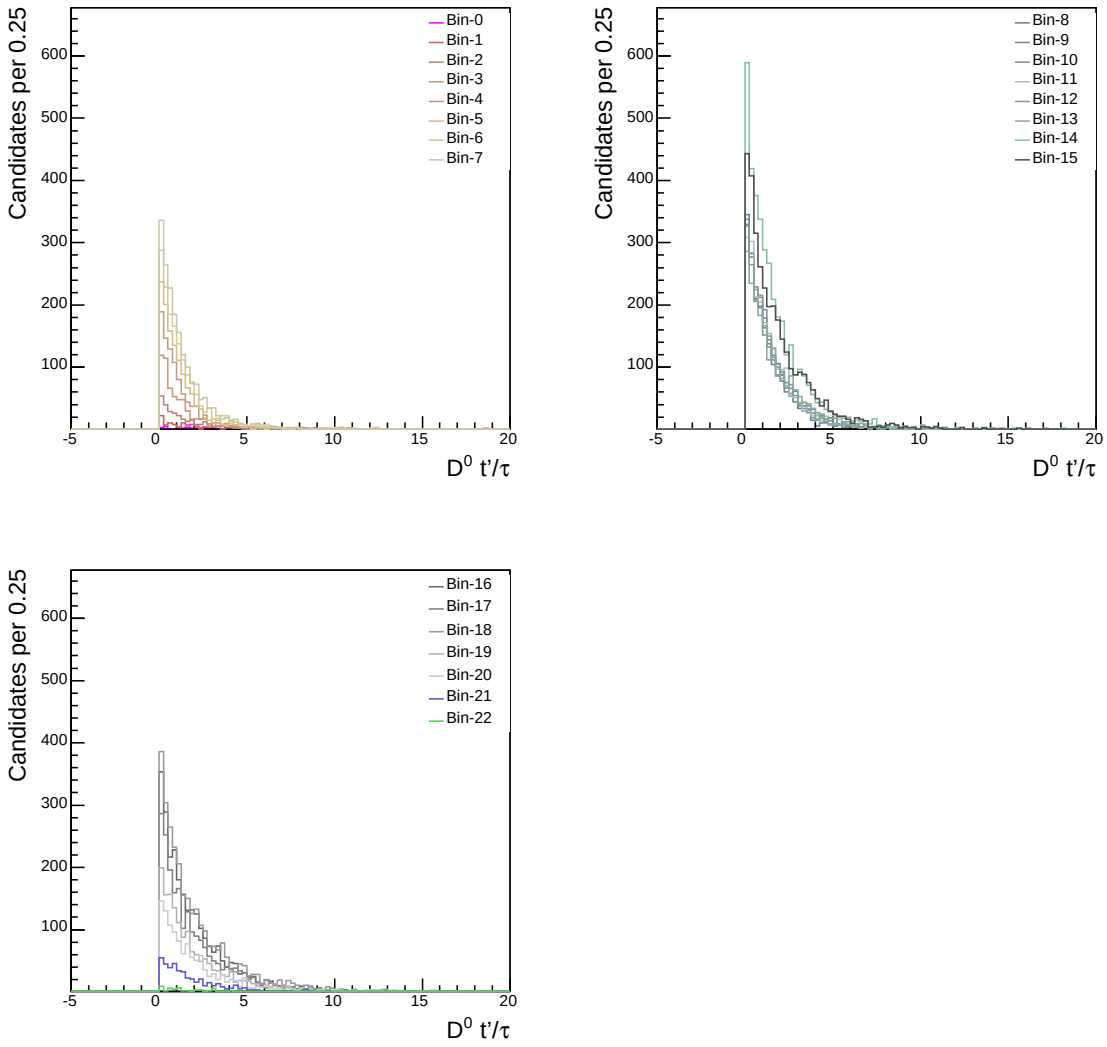

Figure 38: D^0 true t/τ distribution from a $B \to DX$ MC shown for $60 < |d_0(D^0)| < 500$ μm and all time bins in linear scale

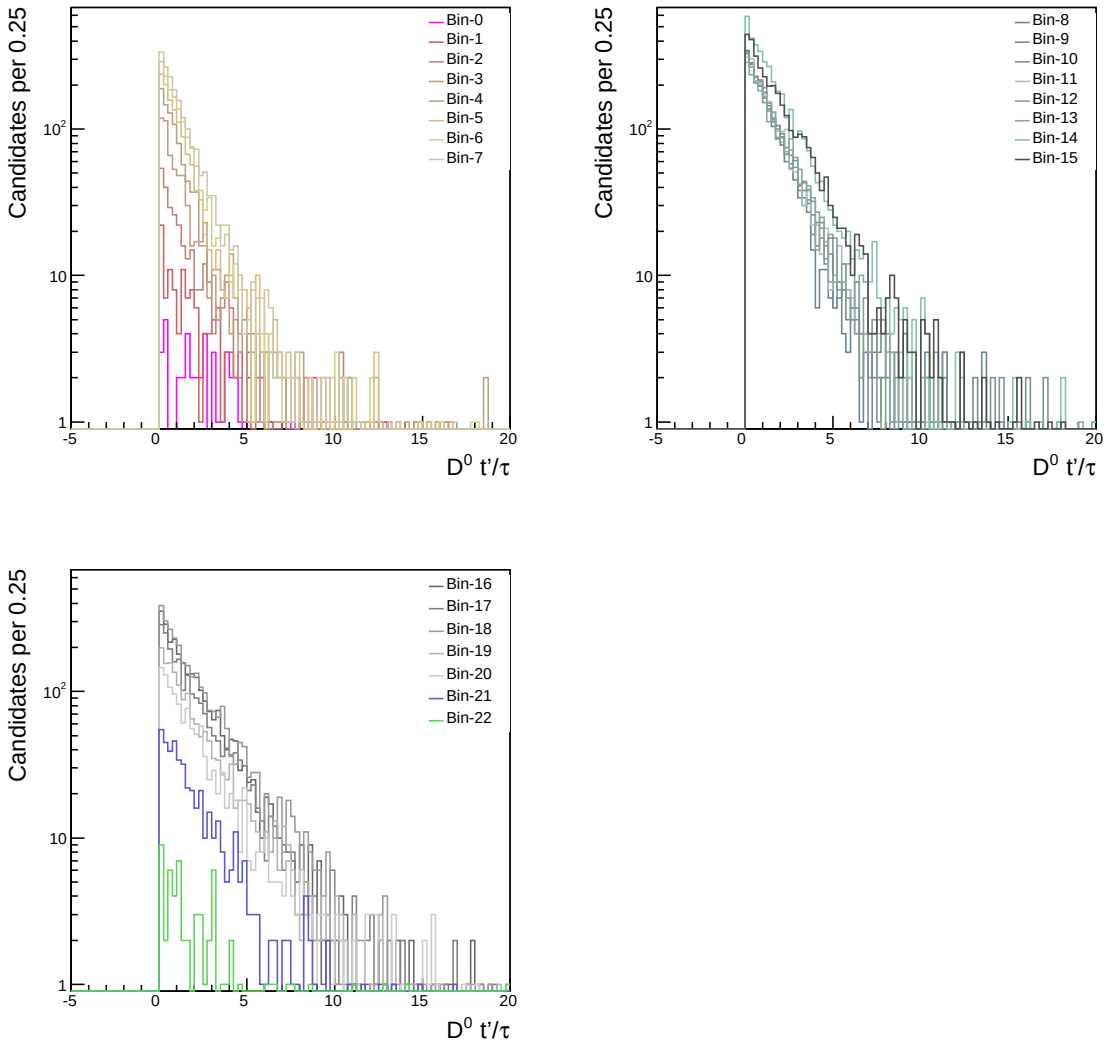

Figure 39: D^0 true t/τ distribution from a $B \to DX$ MC shown for $60 < |d_0(D^0)| < 500$ μm and all time bins in logarithmic scale

References

[1] Mark Mattson and Paul Karchin, *Analysis of $D^0 - \bar{D}^0$ Mixing in the $K\pi$ Channel*, CDF-Note 7116, 2006.

[2] CDF Collaboration, A. Abulencia *et al.*, *Measurement of the Ratio of Branching Fractions $\mathcal{B}(D^0 \to K^+\pi^-)/\mathcal{B}(D^0 \to K^-\pi^+)$ using the CDF II Detector*, Phys. Rev. D **74**, 031109 (R) (2006).

[3] Mark Mattson, Paul Karchin, and Nagesh Kulkarni, *Time Dependent Analysis of $D^0 - \bar{D}^0$ Mixing*, CDF-Note 8879, 2007.

[4] CDF Collaboration, T. Aaltonen *et al.*, *Evidence for D0-D0bar Mixing Using the CDF II Detector*, Phys. Rev. Lett. **100**, 121802 (2008).

[5] Nagesh Kulkarni, Paul Karchin, and Mark Mattson, *Analysis of $D^0 - \bar{D}^0$ Mixing Using the CDF II Detector*, CDF-Note 9806, 2009.

[6] BaBar Collaboration, B. Aubert *et al.*, *Search for $D^0 - \overline{D}^0$ Mixing and a Measurement of the Doubly Cabibbo-suppressed Decay Rate in $D^0 \to K\pi$ Decays*, Phys. Rev. Lett. **91**, 171801 (2003), hep-ex/0304007.

[7] Marko Starič, *Search for $D^0 - \overline{D}^0$ mixing at Belle and BaBar*, talk at XLII Rencontres de Moriond, La Thuile, Italy (13 March, 2007).

[8] BaBar Collaboration, Kevin Flood, *Evidence for $D^0 - \overline{D}^0$ Mixing*, talk at XLII Rencontres de Moriond, La Thuile, Italy (13 March, 2007).

[9] Belle Collaboration, M. Starič *et al.*, *Evidence for $D^0 - \overline{D}^0$ Mixing*, Phys. Rev. Lett. **98**, 211803 (2007).

[10] BaBar Collaboration, B. Aubert *et al.*, *Evidence for $D^0 - \overline{D}^0$ Mixing*, Phys. Rev. Lett. **98**, 211802 (2007).

[11] Belle Collaboration, K. Abe *et al.*, *Measurement of $D^0 - \overline{D}^0$ mixing in $D^0 \to K^0_s\pi^+\pi^-$ decays*, arXiv:0704.1000v1 (7 April, 2007).

[12] BABAR, B. Aubert et al., *Measurement of $D^0 - \bar{D}^0$ mixing from a time- dependent amplitude analysis of $D^0 \to K^+\pi^-\pi^0$ decays*, (2008), 0807.4544.

[13] CLEO, R. Godang et al., *Search for $D^0 - \bar{D}^0$ Mixing*, Phys. Rev. Lett. **84**, 5038 (2000), hep-ex/0001060.

[14] FOCUS, J. M. Link et al., *Measurement of the branching ratio of the decay D0 –¿ pi- mu+ nu relative to D0 –¿ K- mu+ nu*, Phys. Lett. **B607**, 51 (2005), hep-ex/0410068.

[15] Heavy Flavor Averaging Group, E. Barberio et al., *Averages of b−hadron and c−hadron Properties at the End of 2007*, (2008), 0808.1297.

[16] LHCb Collaboration, R. Aaij et al., *Observation of $D^0 - \overline{D}^0$ Oscillations*, Phys. Rev. Lett. **110**, 101802 (2013).

[17] F. Ruffini M. Morello, G. Punzi, *Measurement of Direct CP Violating Asymmetries in Charmless Decays of Strange Bottom Mesons and Bottom Baryons with 9.3 fb-1.*, CDF-Note 10726, 2012.

[18] http://www cdf.fnal.gov/htbin/twiki/bin/view/BStntuples/WebHome.

[19] Shin-Shan. Yu et al., *COT dE/dx Measurement and Corrections*, CDF-Note 6361, 2003.

[20] Saverio D'Auria et al., *Track-based calibration of the COT specific ionization*, CDF-Note 6932, 2004.

[21] CDF Statistics Committee Craig Blocker, *Uncertainties on Efficiencies*, CDF-Note 7168, 2004.

[22] S. D'Auria et al., *Relative Branching Fractions and CP-violating Decay Rate Asymmetries in Cabibbo Suppressed Decays of the D^0 Meson*, CDF-Note 6391, 2004.

[23] S. Donati et al., *Measurement of branching fractions and direct CP asymmetries of B0(s) to h+h'- decays in 1/fb*, CDF-Note 8464, 2008.